國立交通大學

電子物理系所

博 士 論 文

單分子電晶體內部之力學震盪
對電子傳輸的影響

The Influence of Nanomechanical Oscillations on
Electronic Transitions in Single-molecule Transistors

研 究 生：唐英瓚

指導教授：褚德三　教授

中 華 民 國 九 十 九 年 十一 月

單分子電晶體內部之力學震盪對電子傳輸的影響

The Influence of Nanomechanical Oscillations on Electronic Transitions in Single-molecule Transistors

研 究 生：唐英瓚　　Student：Ying-Tsan Tang

指導教授：褚德三　　Advisor：Der-San Chuu

國 立 交 通 大 學

電子物理系所

博 士 論 文

A Dissertation

Submitted to Department of Electrophysics

College of Science

National Chiao Tung University

in Partial Fulfillment of the Requirements

for the Degree of

Doctor of Philosophy

in

Electrophysics

Nov 2010

Hsinchu, Taiwan, Republic of China

中華民國九十九年十一月

單分子電晶體內部之力學震盪對電子傳輸的影響

學生：唐英瓚　　指導教授：褚德三

國立交通大學電子物理學系所博士班

摘　　要

由於微製成技術的進步,分子電子學在這幾年成為熱門的議題。當電子穿越低維尺度元件,如一維的奈米碳管(carbon nanotubes),零維的半導體量子點(semiconductor quantum dot)或分子聚合物(single molecules based on C60), 電流隨 bias 的增長呈現非線性關係, 傳統的歐姆定律不再適用。這時候,我們必須從能階量化角度研究這個問題。不同於傳統的半導體量子點(GaAs/AlGaAs)單純考慮能階量化，以分子當 SET 元件必須考慮 van der Walls 力造成的分子震盪, 該力可簡諧位勢用近，所以我們額外獲得聲子自由度。因為是 SET 元件，分子裡的電子與金屬導線裡的電洞形成靜電力，該力造成位勢的偏移。最後，聲子-聲子之間的 hoping 行為改變電子的傳輸性質。一般，聲子輔助傳輸分佈範圍很廣，即使在 bias-transport 區域(Coulomb Blockade)外也可以測到. 這些通道的數量可經由溫度, bias-voltage, EPI 強度來調節。在這份論文裡,我們分析了單分子電晶體裡的電流與雜訊受熱與 bias 的影響。在這個研究,我們使用非平衡態 Green function 的方法求得標準的 EPI 電流公式。經由電流的計算, 我們瞭解系統的電導如何受聲子的影響. 除此之外,我們也建立廣義的 EPI noise 公式, 其中包涵對導線裡 thermal fluctuation 與系統裡 shot noise 的描述, 也包涵了各級(e.g., sequential tunneling 與 co-tunneling) tunneling 的行為。更重要的,這個方法預測的結果與實驗很接近。

The Influence of Nanomechanical Oscillations on Electronic Transitions in Single-molecule Transistors

Student：Ying-Tsan Tang　　Advisor：Prof. Der-San Chuu

Department of Electrophysics
National Chiao Tung University

ABSTRACT

In recent years, molecular electronics has become one of the very popular topics due to the advances in micro-manufacturing technology. The current increases non-linearly with the increment of the voltage when electrons tunnel in low-dimensional devices, such as one-dinmensional carbon nanotubes, zero-dimensional semiconductor quantum dots or single molecules based on C60, Co-polymer. The conventional Ohm's law is no longer applicable, and quantum mechanics has to be considered. Different from semiconductor quantum dots (GaAs/AlGaAs), in which only energy level quantization is taken into account, we need to deal with the effects of potential shift caused by van der Waals and static electric forces when using molecules as SETs The shift effects result in electron-vibron interactions, and these interactions will change the original tunneling rate of electrons. In our work, it is found that the correlation formed by electron-vibron is dependent on the temperature as well as external voltages. The results predict that the conductance will rise and blur as the voltage is increased. Meanwhile, an obvious conductivity gap occurs between the zeroth and the first phonon side-bands, implying that the phonon assisted state is a virtual state. Additionally, we also derive the generalized EPI noise formula and investigate the thermal fluctuation and shot noise behavior responding to the voltage. We find that at large voltages, the electrons will move randomly, returning to the classical behavior. The predictions coincide with the experimental results.

誌　　謝

我想要將這份研究獻給在最艱苦一年仍繼續鼓勵我做完研究的朋友與師長,感謝他們的耐心與愛心滋潤我25-32歲心靈的成長

Contents

List of Figures

CHAPTER I

INTRODUCTION

One of the main difference between SMTs and QDs is that SMTs have molecular structure and small mass, so oscillation tends to occur due to van der Waals forces and static electric forces. Brandes *et.al* [46] used Mater equation to study the non-linear current of double quantum dots in semiconductor. He concluded that non-linear mechanism stemmed from the interference of phonons. Because the phonons are easily destroyed by heat and structures, the DOS is assumed as ohmic loss distribution, and the phonons possess continuous modes. However, it is single mode in SMTs owing to the fact that van der Waals potential can be further approximated as single harmonic structure. Many scientists started to investigate in this field because of the advances in nanotechnology. Making thin films oscillation as molecules is no longer a critical issue. The following are the recent progress in this topic.

1.1 The Single-molecule Transistor

In recent years, it becomes more and more important to use a single-molecule transistor as conducting single electron transistors (SETs). In molecular electronics, due to the advance of nano-device technology. One special phenomenon is the discovery of the non-linear stair current. This phenomena, however, has been discovered widespread in a single molecule transistor, but not in the semiconductor quantum dot due to vibrational motion of the atoms. In the pioneering work by H. Park *et al,*[1] reported that the current increase presented the stair profile with the increment of bias voltage when the C60 molecule was connected to a gold wire, see Fig. 1. They deduced that the step behavior resulted from the vibrons assisting in the transport[1].

The vibrons originated from the quantization of the oscillating energy. In fact, when a C60 molecule is near the metal, it would be attracted weakly through van der Waals force. The trapping well could be roughly described by a harmonic potential, as seen from the

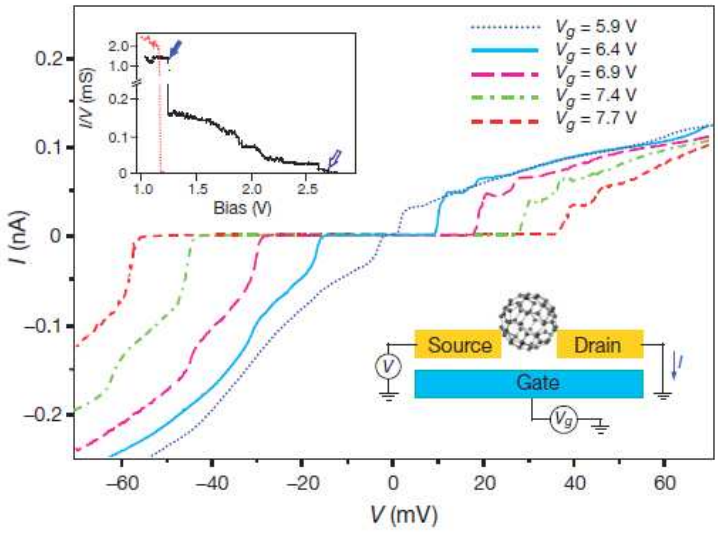

Figure 1: The current vs. the bias voltage obtained from C60 transistor at $T = 1.5K$. Reprinted from Ref.[1]

upper inset of Fig. 2a. This is a SET, as a consequence, electrons may leave from the metal surface to C60 (in the middle of Fig. 2b). The holes in the metal and the electrons in C60 would form a static electric field, and the C60 would be pulled to the metal, causing a position shift, as shown in the right inset of Fig.2b.

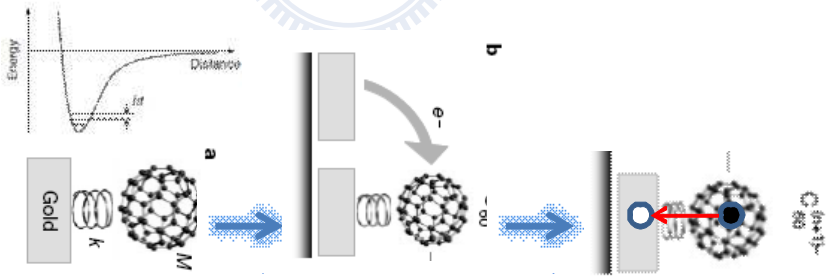

Figure 2: The mechanism for the C60-SMT. The van der Waals force and the static electric field play an essential role. Reprinted from Ref.[1]

1.1.1 Vibronic transitions: the Source of the Staircase Current

The Franck–Condon principle is a rule that explains the intensity of vibrational mode (vibron) transitions. Vibronic transitions are the simultaneous changes in electronic and

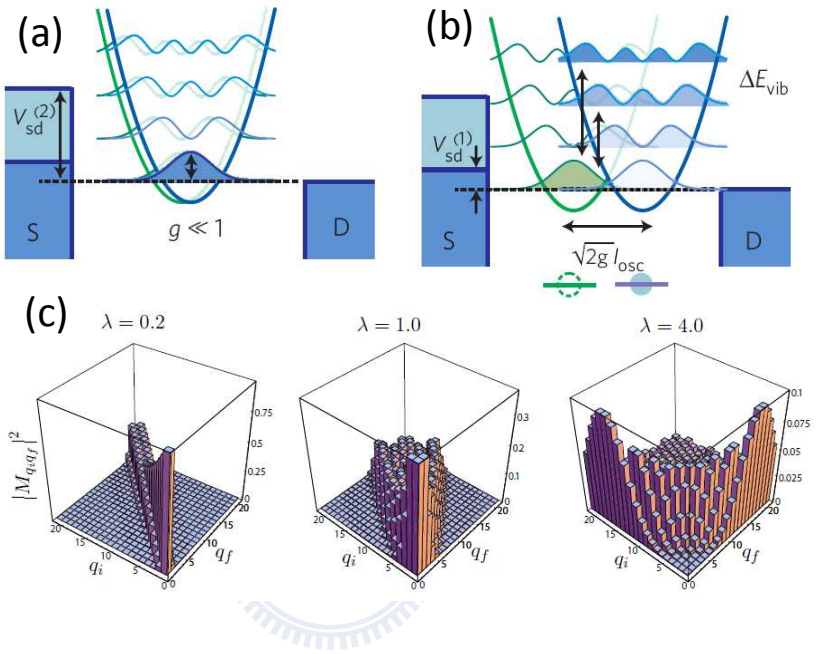

Figure 3: Schematic description of the displacement of the vibron potential for weak electron-vibron coupling (a) and strong electron-vibron coupling (b) The lower insets depict the electron-vibron coupling probability among different vibrational states in two potentials $|M_{n,m}|^2$, where the the coupling strength are given by $\lambda = 0.2$, 1.0 and 4.0, respectively. The diagonal term denotes the probability for emission/absorption of n bosons of frequency ω_0. n is positve for emission and negative for absorption. q_i denotes the quantized number before compressing the atom and q_f is that of compressed. Reprinted from Ref.[39] and Ref.[45].

vibrational energy levels of a molecule due to the absorption or emission of a vibron of appropriate energy. Because C60 was pulled to the metal due to forming the electron-hole electric field, causing a mechanical motion of C60. As a result, the overlap of two vibrational wave functions over a physical displacement, i.e. $\langle m| x |n\rangle$, highly renormalizes the electron tunneling rate of the SET (without vibronic transitions, the transition rate is determined by the Fermi's golden rule).

The profiles of the strong and the weak electron-vibron interaction are depicted in Fig. 3(a) and Fig. 3(b), respectively. Fig. 3(a) and Fig. 3(b) reveal the semi-classical diagram of Franck-Condon behavior. In the weak electron-vibron interaction case (see $g << 1$ in Fig. 3(a), where g represents the electron-vibron coupling strength), there is neither vertical shift of the potential nor horizontal shift of the position. $x \rightarrow 0$ and hence the off-diagonal vibronic transitions does not exist. Strong electron-vibron interaction leads to great potential deviation, and the energy level is accompanied changed, which results in less overlapping of low-energy vibrational states (see Fig. 3(b)). The less overlapping means a small amount of electrons may transport at low bias voltage, leading to the so-called "vibron blockade" (Franck-Condon blockade), as mentioned in Ref.[45][40][39]. On the contrary, the overlap of the vibrational wavefunctions at high energy region becomes larger, that is, the transmission between energy levels in this field is rather active and we expect to measure the current at large bias.

1.2 The Conductance Oscillation in the SMT

The physical quantities of interest, such as current, conductance and higher order correlation functions, e.g. noise, can be obtained as the spectral density (density of states) is solved. In experiments, the differential conductance has structure similar to the zero-bias spectral function.

1.2.1 Nanomechanical Oscillations in a single-C60 transistor

A single-C60 molecule is considered to have a single level of degeneracy. The vibrons may changed the single-level molecule into a multiple-level structure, as shown in Fig. 4. It can be seen that more and more vibron side-bands enter the transport window (the chemical

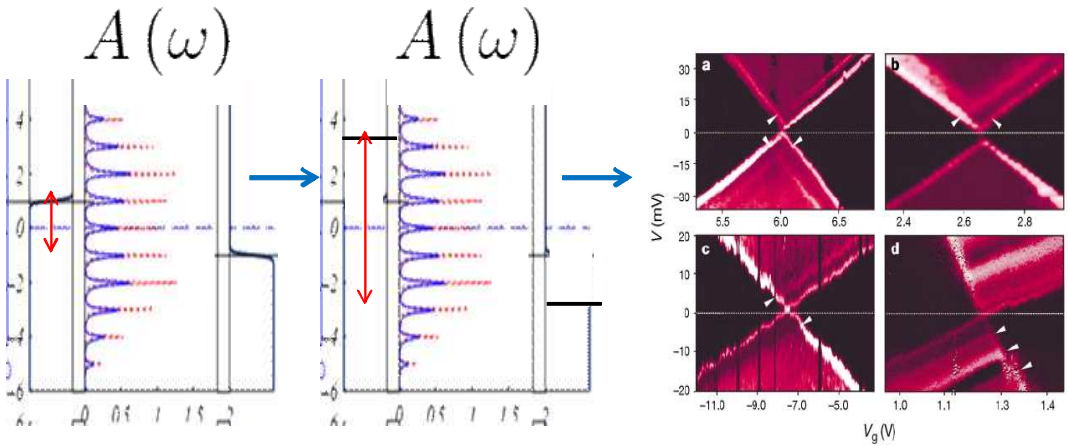

Figure 4: The density plot of the spectral function $A(\omega)$ at different bias, where the left denotes the small one and the right is the larger. The right figure shows the differential conductance as a function of the bias voltage and the gate voltage. The white triangle denotes the vibron sidebands. Reprinted from Ref.[1].

potential of the metal wire) as the bias is enhanced (the red arrow). As a result, the current abruptly increases when the chemical of the leads across the level energy of vibronic channel. Usually the hole states are distributed above the chemical potential of the leads and the electron states below. Therefore, it is expected to obtain a symmetric conductance map as the coupling of the molecule to the leads is symmetric. The right figure shows the 2D distribution of the conductance vs. the bias (vertical-axis) and the gate voltage (horizontal-axis) for four C60 transistors of various sizes. The white arrow indicates the occurrence of vibron side-band[1].

1.2.2 Coulomb blockade and the Kondo effect in single -atom transistors

In 2002, J. Park *et al.*[2] examined two related molecules containing a Co ion bonded to polypyridyl ligands to make a quantum dot and to observed the Kondo effect. In their work, a set of symmetric satellite Kondo peaks due to emission of the vibrons were observed as the bias matches multiples of the vibrational frequency. The model is given as follows. The left pictures in Fig. 6 show the 2D conductance for three devices of various sizes. In the black region (the blockade zone in Fig. 6a), Co2+ and Co3+ represent the molecular ground state and the excited state. In the transport bias window, the white line denotes

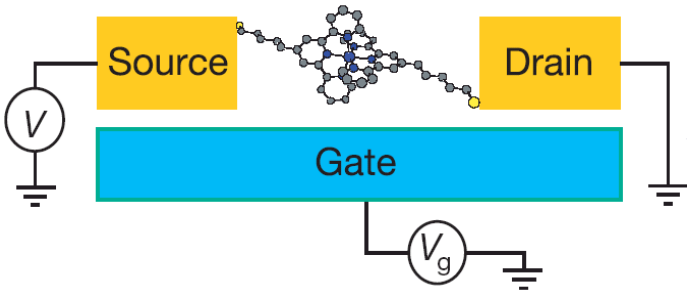

Figure 5: Preparation of the Co polymer transistors. Reprinted from Ref.[2].

the vibron-side band. Fig. 6(b) shows the level-splitting of ground state for the Co polymer when a magnetic field of $B = 6T$ is exerted in Fig. 6(a). The white triangle indicates the new energy levels after the magnetic field is turned on. This is the Zeeman splitting effect measured in the conductance. The splitting energy is linearly increased with the magnetic field (inset below Fig. 6(b)). At low temperature, the conductance peak starting from the Kondo effect is probed near $eV_b = 0$ in the Coulomb blockade region, as seen in Fig. 7(b). The right picture shows the differential conductance vs. the bias at $T = 1.5K$, where a maximum Kondo peak is found at $eV_b = 0$. As usual we may find maximum peak at $V_b = 0$. Due to the vibron assisting tunneling, we observe, furthermore, symmetric satellite maxima. The lower inset (c) shows that the conductance owns a logarithmic temperature dependence in the range of $T = 30$ to $T = 20K$. The lower-right figure (d): The splitting of the Kondo peak caused by a series of magnetic field.

1.2.3 Suspended Semiconductor Quantum Dot (Phonon Cavity)

Besides using molecules to confirm the phonon side-bands, E. M. Weig *et al.*[8]. designed a suspended quantum dot device embedded in a freestanding GaAs/AlGaAs membrane to verify the phonon blockade in the low bias region. There, the phonon of single frequency is applied by the suspended phonon cavity[31][32][33], as seen in Fig. 8. The conductance under different magnetic fields are shown on the RHS of Fig. 8. The right inset profiles the corresponding conductance vs. V_g at $V_b = 0$, where no conductance is found at Fig. 8(b). reflecting the phonon blockade. At higher temperature ($T = 350mK$), the conductance

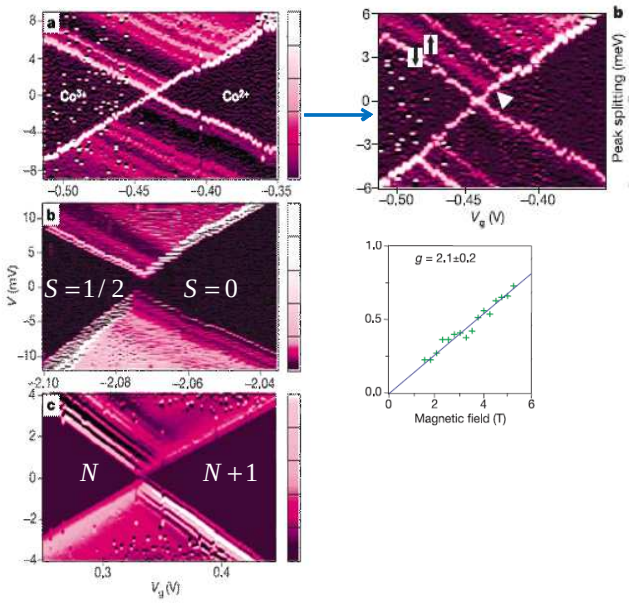

Figure 6: (a)Coulomb blockade and the Kondo effect in Co polymer transistors. The right figure (b) presents that the quantum dot with a magnetic field of $B = 6T$. The below inset denotes the Zeeman splitting as a function of the magnetic field. Reprinted from Ref.[2].

that phonon blockade starts to be decreased because of thermal broadening of the Fermi function helping hole states transport through the dot system.

1.2.4 Suspended Carbon Nanotube Quantum Dot

In 2006, S. Sapaz *et al.*[5] produced a suspended carbon nanotube quantum dot (CNT-QD), which was connected to metal wires and the step current was observed, as shown in Fig. 9. They deduced that the step current was from the longitudinal phonon waves in the carbon-nanotube. Besides, E. Onac *et al.*[6] adopted the same model and, furthermore, used a superconductor-insulator-superconductor device to measure the (a) current, (b) conductance, (c) noise and (d) differential noise. With current and noise, they calculated the Fano factor of the CNT-QD. They verify that in the Coulomb blockade regime, the inelastic co-tunneling yields a super-Poissonian noise, whereas poisson for the elastic co-tunneling. Fig. 27(a) shows the Fano factor according to $F = S/2e\langle I\rangle$, where $\langle I\rangle$ is the current given by Fig.10(c) and S is the noise shown in Fig.10(a).

In 2009, Leturcq *et al.*[39] took advantage of a suspended carbon nanotube (CNT) to

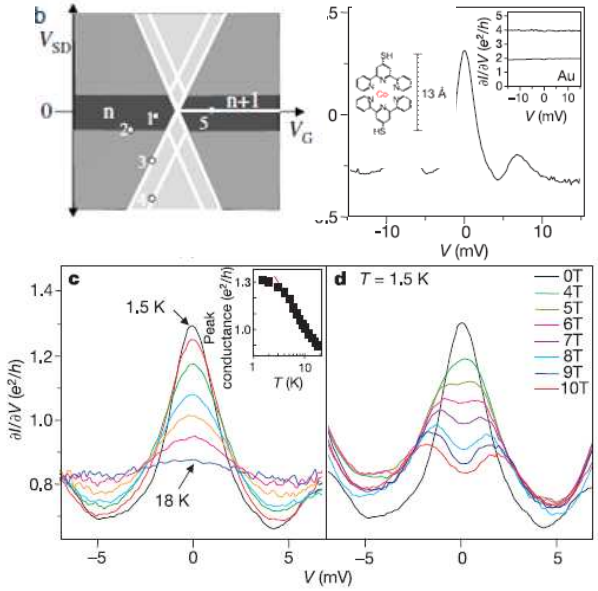

Figure 7: The Kondo effect in the Coulomb Blockade region (at $eV_b = 0$). Reprinted with permission from Ref.[2]

generate a vibrating quantum dot for the observation of strong electron-vibron coupling effects on the current, as seen in Fig. 12. They demonstrate the vibron frequency is governed by the longitudinal stretching vibrons in the CNT, and more importantly, they shows strong evidence of the vibron-blockade behavior at low-bias. In addition, they probed the conductance peaks in the blockade regions. At high temperature, the absorption of the vibron energy becomes active, and vibron-mediated states assist the electron transport, even at the coulomb blockade area. This nontrivial phenomena, however, not reported in previous studies of this kind, is believed to associate with the higher-order co-tunneling of vibrons, especially, when the strong elecron-vibron interaction is considered. On the other hand, to understand the electron-vibron interaction (EVI) again becomes an hot topic in recent years.

1.3 Theoretical Development of the Vibron-assisted Tunneling Problem

Theoretically, many efforts have been made to solve the electron transport the vibrating quantum dot or the SMT. Theoretical methods in this field include the scattering rate

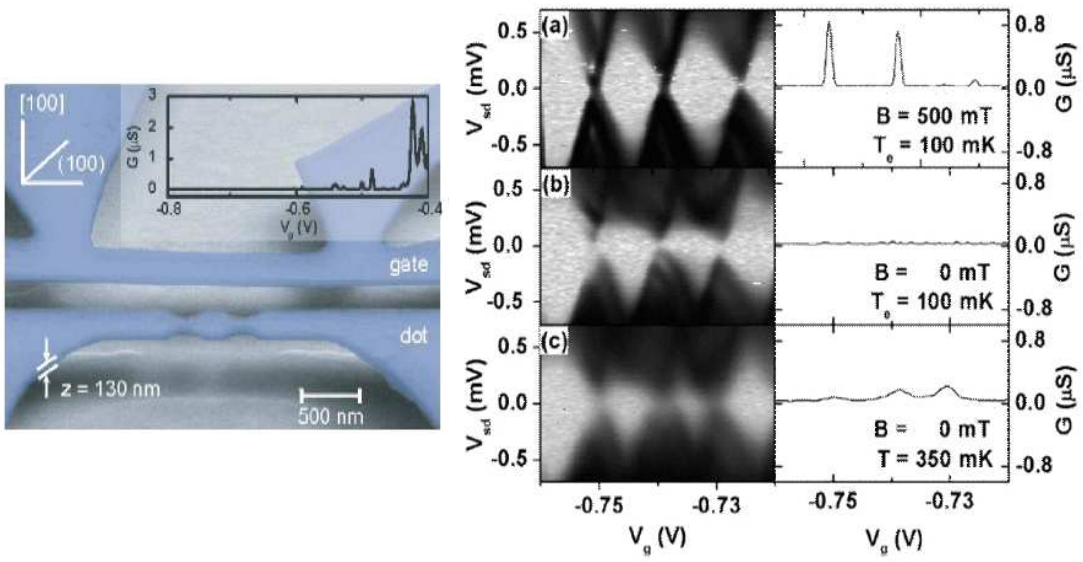

Figure 8: The left depicts the suspended quantum dot in a freestanding phonon cavity (130nm thin GaAs/AlGaAs) membrane. The right insets show conductance maps under $B = 500mT$ and $B = 0$. Inset (b) and (c) exhibit the conductance gap around $V_b = 0$ (linear response area). However, higer temperatue may reduce the suppress behavior. Reprinted from Ref.[8].

equation, the master equation and the non-equilibrium Green's function. The rate equation (RE)[37], the master equation[12][46][36] and the NEGF[14][15] have successfully explained many transport experiments. Each of these theoretical approaches has its own advantages and limitations. Among theses approaches, the RE may rapidly yield the equation of motion for every state by directly replacing the density $\rho(t')$ by $\rho(t)$ In the report by Brandes[46], they calculated the main current of double quantum dots via the RE and concluded that the non-linear electric current stemmed from the shake-up effects of the vibrons. However, different treatment of methods owes it convenience, however, the convenience is often based on the decoupling assumption. For example, the RE can be quickly solved only if we omitted the influence of self-energy, which causes the error message of the energy shift and the level broadening of the quantum dot. That is, the RE is an effective method for predicting that the hopping (correlation) time is much smaller than time spent in the quantum dot, i.e. valid for a weak-tunneling regime. To our knowledge, the non-equilibrium Green's function is the most convincing tool to solve quantum transport at finite bias because it contains

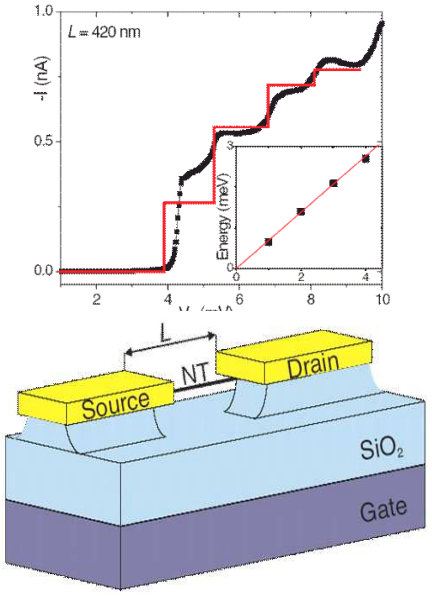

Figure 9: The upper figure presents the staircase current as a function of source-drain voltage at a fixed gate voltage. The lower inset depicts the experimental setup of a suspended carbon nanotube quantum dot (CNT-QD). Reprinted from Ref.[5]

both the hopping (correlation) and the self-energy of the interacting system. The early application of this technique on quantum transport were established by M. Wingreen and Y. Meir[15]. Later A. P. Jauho and his co-workers[14] extended this technique to other fields, like spin-dependent transport, superconductors and optical lattaice. For quantum transport, there is a basic current formula expressed as

$$J = \frac{e}{\hbar}\int d\omega \frac{\Gamma^L(\omega)\,\Gamma^R(\omega)}{\Gamma^L(\omega)+\Gamma^R(\omega)}\left[f_L(\omega)-f_R(\omega)\right]A(\omega)\,. \tag{1}$$

This formula, however, is well-defined in the EVI problem. Usually, th function $\Gamma(\omega)$ and $f(\omega)$ is related to the metal wire, can be solved by Fermi's golden rule and the Fermi–Dirac distribution. The problem lies in the determination of the function $A(\omega)$. Jauho *et.al*[11] solved this function by imposing the identical relation of $A(\omega) = 2\,\mathrm{Im}\,G^r(\omega)$, and they directly decoupled the total system's retarded Green's function as

$$G^{r,a}(t) \approx \widetilde{G}^{r,a}(t)\exp\left[-\Phi(t)\right], \tag{2}$$

$$\Phi(t) = \left(\frac{\lambda}{\omega_0}\right)^2\left[\left(1-e^{-i\omega_0 t}\right)(N_0+1)+\left(1-e^{i\omega_0 t}\right)N_0\right]. \tag{3}$$

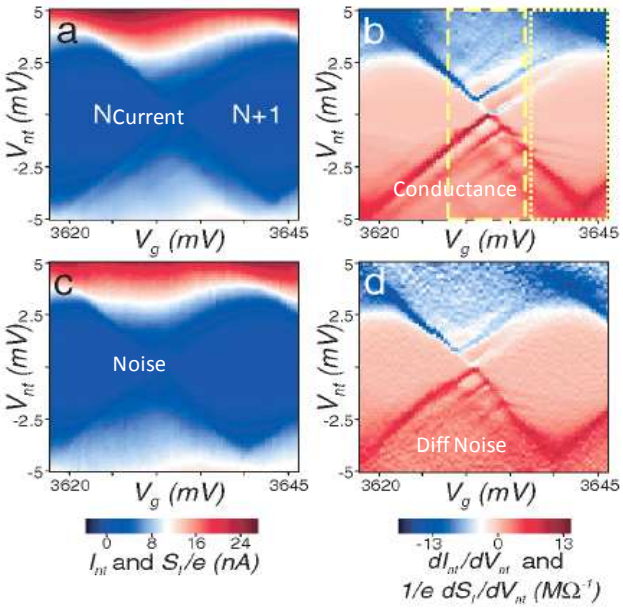

Figure 10: The density plot of (a) current, (b) conductance, (c) noise and (d) differential noise, where the vertical-axis is the bias and horizontal-axis is the gate voltage. Reprinted with permission from Ref.[6]

where the function $\widetilde{G}$ denotes the electron Green's function and $\exp\left[-\Phi\left(t\right)\right]$ is the vibron correlation. Later, Zhu and Balatsky extended this method to calculate the zero-frequency noise. At high temperature, this method gives the same tendency of the conductance as found in experiments, where the conductance peak does exists in the blockade area. However, this method fails at low temperature, that is, no conductance shall be found in this limit. The erroneous prediction arises from the ill treatment of electron-vibron decoupling. As a matter of fact, $G^a\left(t\right) = \left[G^r\left(t\right)\right]^*$ but $\Phi^*\left(t\right) = \Phi\left(-t\right) \neq \Phi\left(t\right)$, as a consequence, Eq.(2) is not appropriate for studying current–voltage characteristic of vibron assisted tunneling. Instead, it is convenient to start from function $G^{<,>}\left(t\right)$. Based on this, Chen and his co-workers solved this problem and quickly obtained the symmetric conductance, agreement with the experimental observations. However, in Chen's work, since an averaged field concept has been executed to simplify the EVI self-energy, they missed an important thermal broadening information from vibron Green's functions. In this thesis, we will examine the properties of the vibron correlation and address how to interpret the EVI transport question

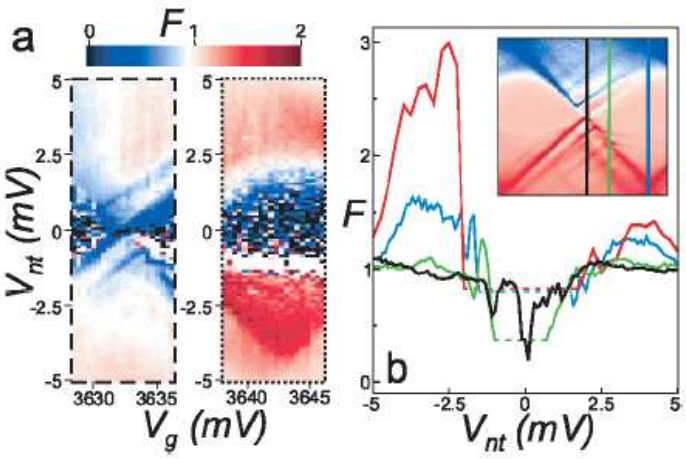

Figure 11: (a) The dashed line represents the transport bias window and the dot line is for the Coulomb blockade area. (b): Fano factor vs. the applied bias voltage at different gate voltages. Reprinted from Ref.[30]

in a more physical way. More importantly, a conductance gap between the chemical potential of the leads and the first vibron excited state, specifically, $e\,|V_b| > 2\omega_0$, is also examined.

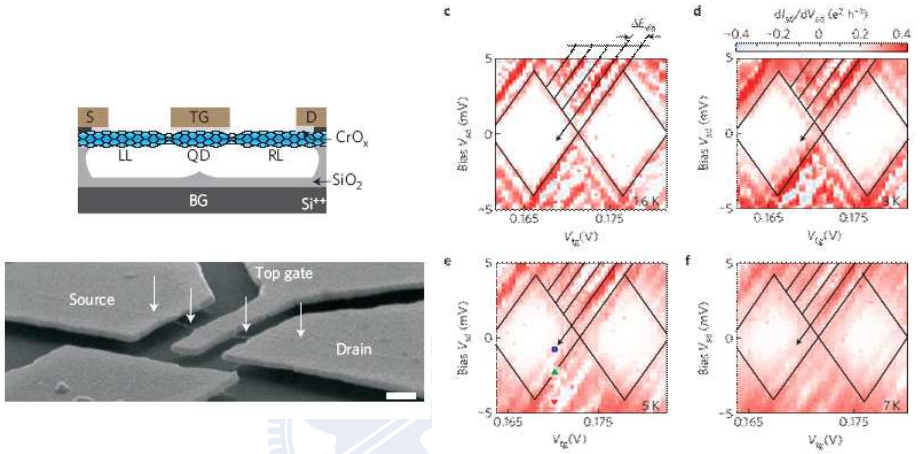

Figure 12: Left: The inset depicts the experimental setup of a CNT-QD, where S, D, and TG stands for the source, the drain, and the gate voltage. The quantum dots are located below the gate and in the left and right leads. The frequency is decided by the longitudinal stretching mode. Right: Franck-Condon blockade in suspended carbon nanotube QD, where higher temperature yields phonon side-bands appearing outside the bias transport area (Coulomb Blockade region). Reprinted from Ref.[39]

CHAPTER II

THEORY OF QUANTUM TRANSPORT

Our formalism is based on the nonequilibrium Keldysh Green's function method. The Keldysh Green's function is used to deal with the system coupled to a time-dependent external fields. This function describes how the system evolves with time from the initial state. Before the interaction is on, the system and the environment are at their equilibrium, and the their physical quantities can be described by the Matsubara Green's function. As the interaction is turned on, the transfer function of the system can be extended via the Dyson equation approach[14][16]. Next we briefly describe the mechanism behind the Keldysh Green's Function.

2.1 The Keldysh Green's Function

We consider a system under the Hamiltonian

$$\mathcal{H}(t) = H_S + H'(t).$$

The time-independent Hamiltonian H can be split into $H_S = H_0 + H_{intra}$, where H_{intra} denotes the interaction in the system H_S, such as the Coulomb repulsion. A quantum statistical expectation value of an field operator O at time t is given by

$$\langle O(t)\rangle = tr\left[\rho(t) O\right] = tr\left[\rho_0 O_{\mathcal{H}}(t)\right] = \langle O_{\mathcal{H}}(t)\rangle, \tag{4}$$

where $\rho(t) = U(t,t_0)\,\rho_0 U^{+}(t,t_0)$ and the quantity ρ_0 is the equilibrium density matrix given by

$$\rho_0 = \frac{e^{-\beta H_S}}{Tr\left[e^{-\beta H_S}\right]}.$$

Note here that $U(t,t_0) = \exp\left[-\frac{i}{\hbar}\int_{t'}^{t} dt\mathcal{H}(t)\right]$. At $t > t_0$,

$$\begin{aligned} O_{\mathcal{H}}(t) &= U(t,t_0)\, O U^{+}(t,t_0) \\ &= U_{H_S}(t,t_0)\, O_{H_S}(t)\, V_{H_S}^{+}(t,t_0), \end{aligned}$$

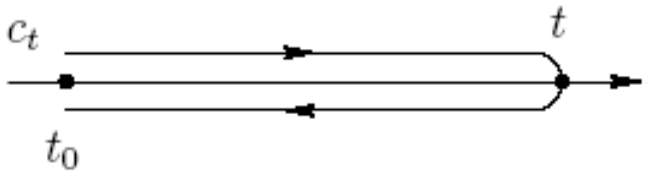

Figure 13: The contour time path c_t

where the unitary function $U_{H_S}(t,t_0)$ is given by

$$\begin{aligned} U_{H_S}(t,t') &= T\exp\left[-\frac{i}{\hbar}\int_{t'}^{t} dt H'_{H_S}(t)\right], \\ H'_{H_S}(t) &= e^{\frac{i}{\hbar}H_S(t-t_0)}H'(t)\,e^{-\frac{i}{\hbar}H_S(t-t_0)} \end{aligned}$$

Therefore, Eq.(4) can be rewritten as

$$\langle O(t)\rangle = tr\left\{\rho_0\exp\left[-\frac{i}{\hbar}\int_{c_t} dt' H'_{H_S}(t')\right]O_{H_S}(t)\right\}, \tag{5}$$

$O_{H_S}(t)$ is the time-dependent operator of the system, and the contour c_t is depicted in Fig. 13Since Eq.(5) is expreseed in terms of the equilibrium Hamiltonian H_{eq}, the contour-ordered Green's function plays a similar role as the equilibrium Green's function. Compared to the equilibrium Green's Function, we have two additional contour ordered Green's functions:

$$G(1,1') = \begin{cases} G^{<}(1,1') = -i\left\langle\psi_H(1)\,\psi_H^{+}(1')\right\rangle, \tau_1 < \tau_{1'} \\ G^{>}(1,1') = +i\left\langle\psi_H(1)\,\psi_H^{+}(1')\right\rangle, \tau_1 > \tau_{1'} \end{cases} \tag{6}$$

where $(1)\equiv(r_1,t_1)$. The detailed description of $G^{<}(1,1')$ is

$$\begin{aligned} G^{<}(1,1') &= -i\left\langle T_{c_1}\left\{e^{-\frac{i}{\hbar}\int_{c_1} dt' H'_I(t')}\psi_H(1)\right\}\cdot T_{c'_1}\left\{e^{-\frac{i}{\hbar}\int_{c'_1} dt' H'_I(t')}\psi_H^{+}(1')\right\}\right\rangle \\ &= -i\left\langle T_{c_1+c'_1}\left\{e^{-\frac{i}{\hbar}\int_{c_1+c'_1} dt' H'_I(t')}\psi_H(1)\,\psi_H^{+}(1')\right\}\right\rangle. \end{aligned} \tag{7}$$

It implies that the contour c_i stretches from t_0 and passes through t_1 and $t_{1'}$ and back to t_0, The last equality in Eq.(7) combines the contours $c_1+c'_1$, as plotted in Fig.14:

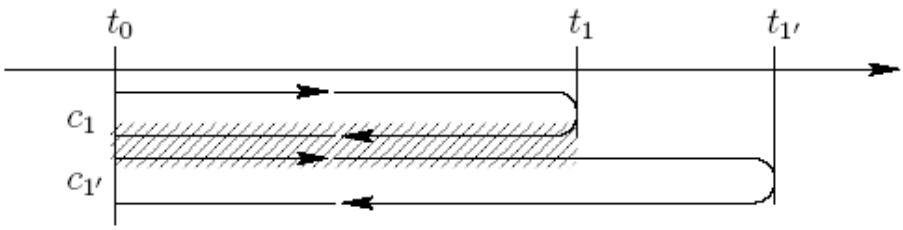

Figure 14: Parts of contour evolution operators canceling in Eq.(7). Reprinted from Ref.

2.1.1 Analytical Continuum

In general, the interaction complicates the evolving path in the contour-ordered Green's function. The procedure of converting this complex-time Green's function into a real-time one is called the analytic continuation or Langreth theorem, which is developed by Kadanoff, Baym[44] and Langreth.[17] The useful Langreth theorem is listed as follows:

Contour (Complex) Time	Real Time
$C(\tau,\tau')=\int_c d\tau_1$ $A(\tau,\tau_1)B(\tau_1,\tau')$	$C^{\lessgtr}(t,t')=\int dt_1\left[A^r(t,t_1)B^{\lessgtr}(t_1,t')\right.$ $\left.+A^{\lessgtr}(t,t_1)B^a(t_1,t')\right]$ $C^{r(a)}(t,t')=\int dt_1 A^{r(a)}(t,t_1)B^{r(a)}(t_1,t')$.
$D(\tau,\tau')=\int_{c1}d\tau_1\int_{c2}d\tau_2$ $A(\tau,\tau_1)B(\tau_1,\tau_2)C(\tau_2,\tau')$	$D^{\lessgtr}(t,t')=\int dt_1\int dt_2\left[A^r(t,t_1)B^r(t_1,t_2)\times\right.$ $C^{\lessgtr}(t_2,t')+A^r(t,t_1)B^{\lessgtr}(t_1,t_2)C^a(t_2,t')$. $\left.+A^{\lessgtr}(t,t_1)B^a(t_1,t_2)C^a(t_2,t')\right]$ $D^{r(a)}(t,t')=\int dt_1\int dt_2 A^{r(a)}(t,t_1)\cdot$ $B^{r(a)}(t_1,t_2)C^{r(a)}(t_2,t')$.
$C(\tau,\tau')=A(\tau,\tau')B(\tau,\tau')$	$C^{\lessgtr}(t,t')=A^{\lessgtr}(t,t')B^{\lessgtr}(t,t')$. $C^{r(a)}(t,t')=A^{<}(t,t')B^{r(a)}(t,t')$ $+A^{r(a)}(t,t')B^{<}(t,t')$ $+A^{r(a)}(t,t')B^{r(a)}(t,t')$. $=\pm\theta(\pm t\mp t')\cdot$ $[A^{>}(t,t')B^{>}(t,t')-A^{<}(t,t')B^{<}(t,t')]$
$D(\tau,\tau')=A(\tau,\tau')B(\tau',\tau)$	$D^{\lessgtr}(t,t')=A^{\lessgtr}(t,t')B^{\lessgtr}(t',t)$. $D^{r(a)}(t,t')=A^{\lessgtr}(t,t')B^{a(r)}(t',t)$ $+A^{r(a)}(t,t')B^{\lessgtr}(t',t)$

2.2 The Single Molecular Transistor

Here we begin with a description of the system of interest, that is, the single-molecule transistor. The experimental setup of this vibrating single-molecule transistor is shown in Fig. 15. Here the spin degree of freedom and the influence of Coulomb interaction are omitted. The model Hamiltonian of the C60 and the metal wires reads

$$H_{leads} = \sum_{k\alpha}\varepsilon_{k\alpha}c^{+}_{k\alpha}c_{k\alpha} \quad (8)$$

$$H_{dot(c60)} = \varepsilon_d d^{+}d, \quad (9)$$

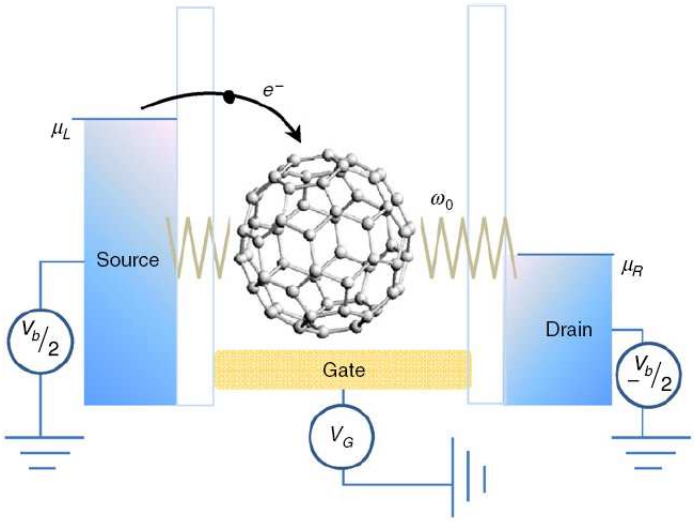

Figure 15: The experimental setup of a vibrating single-molecule transistor (C60). The dot level is cotrolled by the gate voltage and the transport window is tuned by the bias voltage in the terminal.

When the C60 molecule is connected to a gold wire, the van der Waals potential energy appears. This potential energy may be described as the harmonic potential,

$$\begin{aligned} H_{ph} &= \frac{p_0^2}{2m_0} + \frac{1}{2} m_0 \omega_0^2 x_0^2 \\ &= \omega_0 b^+ b. \end{aligned} \tag{10}$$

We consider an electron-hole electric force will depart in the direction from the source to C60. As the electron is added to the molecule, the hole in the wire then attracts the electron in C60, forming a constant electric field and pulling C60 towards the source wire. This behavior is described by

$$\begin{aligned} H_{db} &= qEx_0 d^+ d \\ &= \lambda \left(b^+ + b\right) d^+ d, \lambda = qE/\sqrt{2m\omega_0}. \end{aligned} \tag{11}$$

It is worth noting that the electric field causes the original harmonic potential to shift x_0, but it does not change the harmonic potential much. In the second quantization picture, Eq.(11) interprets an electron in the transport process, where λ reflects the EVI coupling strength. The system will emit (or absorb) a vibron at the same time. However, it only emits vibrons at zero temperature.

Basically, there are interactions among the QD system, the wire, and the vibrons. For convenience, two of them are usually dealt with as one quasi-particle. In previous studies, a quasi-particle polaron may result from the combination of vibron and QD. Here, we first combine the vibron and the non-interacting wire, and then perform the EOM expansion on the coupling of QD and the wire. In this case, the model is simplified as the coupling of multi-channel leads and a QD system with simple energy levels. That is to say, the electrons jump to the QD system from the chemical potentials and then to the wire.

2.3 The Current and the Spectral function

In this section, we derive the standard EVI current formula through the SMT.

2.3.1 Discrete Spectrum: The Anderson-Holstein Model

The electron transport between the leads and the central region is considered as shown in Fig. 15. In our study only one level of the dot system is considered, and electrons vibrate at a single frequency ω_0. The EVI system is studied theoretically through a non-perturbative canonical transformation $\overline{H} = e^S H e^{-S}$ with $S = (\lambda/\omega_0)\, d^+ d\, (b^+ - b)$ (the detailed derivation is shown in Appendix A). Under this unitary transformation, the Hamiltonian now reads:

$$\overline{H}_T = \overline{H}_{cen} + \overline{H}_{lead} + \overline{H}_T,$$

$$\overline{H}_{cen} \equiv \overline{\varepsilon}_0 \left(V_g\right) d^+ d + \omega_0 b^+ b, \tag{12}$$

$$\overline{H}_{lead} = \sum_{k_\alpha, \alpha \in L,R} \varepsilon_{k_\alpha} c^+_{k_\alpha} c_{k_\alpha}, \tag{13}$$

$$\overline{H}_t = \sum_{k_\alpha, \alpha \in L,R} V_{k_\alpha} c^+_{k_\alpha} dX + h.c, \tag{14}$$

where

$$X \equiv \exp\left[-\frac{\lambda}{\omega_0}\left(b^+ + b\right)\right], \tag{15}$$

The operators d^+ (d) and $c^+_{k_\alpha}$ (c_{k_α}) represent the creation (annihilation) operators of electron in the QD (or SMT) and the α lead, respectively. The operator b^+ (b) is the creation (annihilation) operator of the vibron. $\overline{\varepsilon}_0 \equiv \varepsilon_0 \left(V_g\right) - \Delta$ is the dot level energy controlled

by the gate voltage, with the canonical energy shift $\Delta = \lambda^2/\omega_0$. The coupling strength of EVI is denoted by λ and the tunneling matrix element between the QD (or SMT) and the α lead is defined as V_{k_α}. Here ε_{k_α} is the energy of the electron in α lead, which remains unchanged because of the absence of vibron field in the α lead.

2.3.2 The Jauho's Current Formula (from the Perspective of the Quantum Dot)

The current from the left lead to the central region can be defined[11] as

$$J_L(t) = \frac{2e}{\hbar} \operatorname{Re} \sum_{k,\alpha \in L} V_{k\alpha,d} G^<_{d,k\alpha}(t,t') \mid_{t' \to t} \tag{16}$$

where the Green's function $G^<_{d,k\alpha}(t,t') \equiv i \left\langle c^+_{k\alpha}(t') X(t') d(t) \right\rangle$ together with its conjugate property are applied above. Note that the electron-hole interaction between the metal leads and the dot is mutual, both terminals are vibrating from the perspective of the quantum dot, hence $c^+_{k\alpha}$ and X evolves at the same time. $G_{d,k\alpha}(\tau,\tau')$ can be solved by

$$G_{d,k\alpha}(\tau,\tau') = \int_c dt_1 \widetilde{G}_{dd}(t,t_1) V^*_{k\alpha,d} g_{k\alpha}(t_1,t') \tag{17}$$

Performing the continuation rules[11] on $G_{d,k\alpha}(\tau,\tau')$ and substituting the resulting $G^<_{d,k\alpha}(t,t')$ into Eq.(16), we obtain:

$$\begin{aligned} J_L(t) = -\frac{2e}{\hbar} \operatorname{Im} \Bigg[\int_{-\infty}^{t} dt_1 \widetilde{G}^r_{dd}(t,t_1) \Sigma^<_{\alpha\epsilon L}(t_1,t) \\ + \widetilde{G}^<_{dd}(t,t_1) \Sigma^a_{\alpha\epsilon L}(t_1,t) \Bigg], \end{aligned} \tag{18}$$

The main task is to calculate the self-energy Σ_α.

2.3.3 Self-Energy

In frequency space, the appliance of the LT on the self-consistent Dyson equation of the electron Green's function in the QD (or SMT)[14][16] leads to $\widetilde{G}^{r,a}_{dd}(\omega) = \left[\omega - \overline{\varepsilon}_0 - \Sigma^{r,a}_T(\omega)\right]^{-1}$,

where the contour-ordered self-energy Σ_T induced by the tunneling process reads $\Sigma_T(\omega) = F^+(\omega) \widetilde{\Sigma}_T(\omega)$, they carry all the same time information on the lead electrons and vibrons.

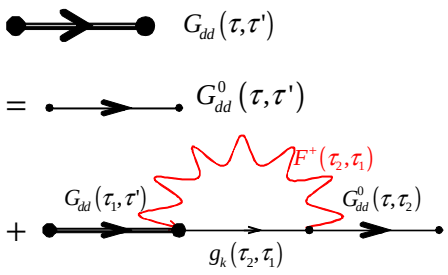

Figure 16: The diagrammatic representation of the perturbative expansion of the electron Green's function, where the electron-phonon interaction is depicted by the wave curve; the solid line denotes for the fermion line.

In Eq.(18), the partial part of the tunneling self-energy in the current formula can be found as

$$\Sigma^a_\alpha\left(t,t'\right)=-\theta\left(-t+t'\right)\sum_n\left[\Sigma^>_{\alpha,n}\left(t,t'\right)-\Sigma^<_{\alpha,n}\left(t,t'\right)\right]. \tag{19}$$

Here

$$\Sigma^{>,<}_{\alpha,n}=F^{+>,<}\cdot\sum_{k_\alpha}\left|V_{k\alpha}\right|^2 g^{>,<}_{k\alpha}.F^{+>}\left(t-t'\right)\equiv\left\langle X^+\left(t'\right)X\left(t\right)\right\rangle \tag{20}$$

and $F^{+<}\left(t-t'\right)\equiv\left\langle X\left(t\right)X^+\left(t'\right)\right\rangle$ are the greater and lesser vibron Green's functions, and $g^{<(>)}_{k\alpha}\left(t-t'\right)$ is the lesser (greater) Green's function for the free electron in the α lead. The Fourier transform of the self-energies in Eq.(19) lead to:

$$\begin{aligned}\Sigma^{r,a}_{\alpha,n}\left(\omega\right)&=\sum_{k\alpha}\left[p_n\frac{V^*_{k\alpha}V_{k\alpha}}{\omega+n\omega_0-\varepsilon_{k\alpha}\pm i\delta}f^<_\alpha\left(\varepsilon_{k\alpha}\right)\right.\\&\left.+p_{-n}\frac{V^*_{k\alpha}V_{k\alpha}}{\omega+n\omega_0-\varepsilon_{k\alpha}\pm i\delta}f^>_\alpha\left(\varepsilon_k\right)\right],\end{aligned} \tag{21}$$

$$\begin{aligned}\Sigma^{\gtrless}_{\alpha,n}\left(\omega\right)&=\sum_{k\alpha}V^*_{k\alpha}V_{k\alpha}p_{\mp n}g^{\gtrless}_{k\alpha}\left(\omega+n\omega_0\right)\\&=\mp i\sum_n p_{\mp n}\Gamma_\alpha\left(\omega+n\omega_0\right)f^{\gtrless}_\alpha\left(\omega+n\omega_0\right),\end{aligned} \tag{22}$$

where $f^<_\alpha\left(\varepsilon_{k\alpha}\right)$ and $f^>_\alpha\left(\varepsilon_{k\alpha}\right)$ are the electron and hole Fermi functions in the α lead. In this paper, $\Gamma_\alpha\left(\omega\right)=2\pi\sum_{k\alpha}\left|V_{k\alpha}\right|^2\delta\left(\omega-\varepsilon_{k\alpha}\right)$ represents the rate of a particle leaving the quantum dot system without the EVI. The factor p_n denotes the weighting function of the interactions between the electron and n vibrons, which is found as $p_n=e^{-2g\left(N_0+\frac{1}{2}\right)}e^{n\omega_0/2k_BT}I_n\left(2g\sqrt{N_0\left(N_0+1\right)}\right)$[16], where N_0 and I_n are the Bose function and the modified Bessel function.

Following Eq.(18), we obtain the EVI current formula, where the first term in the RHS of Eq.(18) explains the in-tunneling current J_{in}, where electrons entering the single-energy-level quantum dot system through the non-interacting wire with multi-channel. The second term in the RHS in Eq.(18) describes the out-tunneling current J_{out}, where the electron in the central region tunnels out of the central region via two channels, the transmission scheme is depicted in Fig.17.

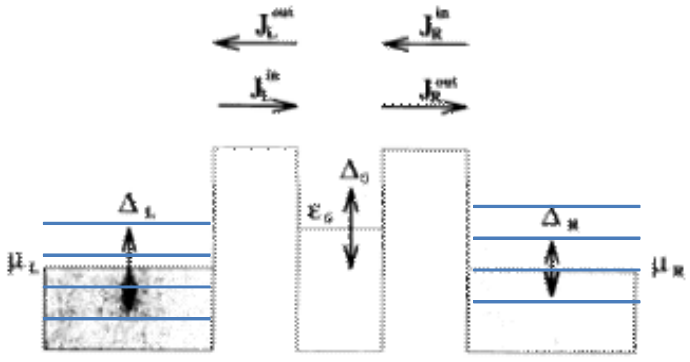

Figure 17: Jauho's transport picture. Reprinted with from Ref.[11]

Note here that the source wire emits vibrons when electrons transfer from one end to the other in a non-equilibrium system at low temperature. In addition, the quantum dot will couple with the multi-channel leads and forms step bandwidth (decay), which decides not only the lifetime of electron in the system but also the probability distribution. We have so far derived the diagrammatic formula and the Jauho's transport formula. Now we shall analyze the spectral function.

2.3.4 The Spectra Function $\widetilde{A}_d(\omega)$

From the definition of the spectral function $\widetilde{A}_d(\omega) = -2\,\mathrm{Im}\,\widetilde{G}^r_{dd}(\omega)$, we obtain:

$$\widetilde{A}_d(\omega) = \frac{\sum\limits_{n,\alpha}\left[p_n\Gamma_\alpha f^<_\alpha(\omega+n\omega_0) + p_{-n}\Gamma_\alpha f^>_\alpha(\omega+n\omega_0)\right]}{\left(\omega-\widetilde{\varepsilon}_0\right)^2 + \left[W(\omega)/2\right]^2}, \tag{23}$$

where $\widetilde{\varepsilon}_0 = \overline{\varepsilon}_0(V_g) - \mathrm{Re}\,\Sigma^r_T(\omega)$ denotes the renormalized level position, and $W(\omega) = -2\,\mathrm{Im}\,\Sigma^r_T(\omega)$ represents the life-time broadening (bandwidth) of the dot state. A comparison with the conventional JWM's formula in Ref.[14] assures that the life-time broadening

of a dot state $W(\omega)$ in Eq.(23) equals to the summation of out-tunneling rates between the leads and the system, i.e. Eq.(21); Eq.(18) is therefore self-consistent and meaningful. Note that $\widetilde{G}^{<}_{dd}(\omega)$ in Eq.(18) can be quickly solved via using the Keldysh equation $\widetilde{G}^{<}_{dd} = |G^{r}_{dd}|^2 \Sigma^{<}_{T}(\omega)$[11]. The remaining goal is to decide the retarded self-energy $\Sigma^{r}_{T}(\omega)$. To this end, $\sum_{k\alpha}$ is replaced by $\int d\omega \rho(\omega)$, and the Lorentz density of states with bandwidth E_C at the chemical potential μ_α is assumed[19][20]. With this auxiliary function, the integral becomes convergent, and the retarded self-energy of the electron in QD (SMT) reads

$$\begin{aligned}\mathrm{Re}\,\Sigma^{r}_{T}(\omega) = \sum_{n,\alpha}(p_n - p_{-n})\frac{\Gamma_\alpha(\omega+n\omega_0)}{2\pi}\left[\ln\left(\frac{E_C}{2\pi k_B T}\right)\right. \\ \left. -\mathrm{Re}\,\psi\left(\frac{1}{2}+i\frac{\omega+n\omega_0-\mu_\alpha}{2\pi k_B T}\right)\right], \qquad (24)\end{aligned}$$

$$\begin{aligned}\mathrm{Im}\,\Sigma^{r}_{T}(\omega) = \frac{1}{2\pi}\sum_{n,\alpha}\left[p_n\Gamma_\alpha(\omega+n\omega_0)\,f^{<}_{\alpha}(\omega+n\omega_0)\right. \\ \left. + p_{-n}\Gamma_\alpha(\omega+n\omega_0)\,f^{>}_{\alpha}(\omega+n\omega_0)\right]. \qquad (25)\end{aligned}$$

$\psi(z)$ is the digamma function with a complex argument. It can be seen from Eq.(24) that besides the energy shift Δ due to the canonical transformation, another energy shift $\mathrm{Re}\,\Sigma^{r}_{T}(\omega)$ is obtained from the vibron correlation function. In addition to the renormalization shift, we find that the life-time broadening of Eq.(25) from the LT is more complicated than that from the MFT[18], which is a constant. This is because, in non-equilibrium, the LT preserves the properties of electrons and holes in the leads via the vibron Green's functions.

2.3.5 The Physical Meaning of the Function $\widetilde{G}^{<}(\omega)$

Basically, the lesser Green's function is associated with the particle density[11]. This function can be solved via the continuous condition for the steady state, i.e. $\left\langle \dot{N} \right\rangle = \left\langle \partial\widetilde{G}^{<}/\partial t \right\rangle = 0$ (see appendix A) or solved with the Keldysh equation, i.e. $\widetilde{G}^{<}_{dd}(\omega) = \widetilde{G}^{r}_{dd}(\omega)\,\Sigma^{<}_{T}(\omega)\,\widetilde{G}^{a}_{dd}(\omega)$ (The relation of the particle conservation together with the Keldysh equation for $G^{<}(\omega)$ are proven in Appendix A). Consequently, the lesser/greater Green

function is found as

$$\widetilde{G}_{dd}^{\gtrless}(\omega)=\frac{\mp i\sum\limits_{n,\alpha}\left[p_{\mp n}\Gamma_{\alpha}\left(\omega+n\omega_{0}\right)f_{\alpha}^{\gtrless}\left(\omega+n\omega_{0}\right)\right]\cdot\widetilde{A}_{d}(\omega)}{\sum\limits_{n,\alpha}\left[p_{n}\Gamma_{\alpha}\left(\omega+n\omega_{0}\right)f_{\alpha}^{<}\left(\omega+n\omega_{0}\right)+p_{-n}\Gamma_{\alpha}\left(\omega+n\omega_{0}\right)f_{\alpha}^{>}\left(\omega+n\omega_{0}\right)\right]} \tag{26}$$

where $\widetilde{A}_{d}(\omega)$ is defined in Eq.(23) and the stationary probability for an empty state and an occupied state can be found as

$$P_{0}^{st}=\left\langle d(t)\,d^{+}\left(t'\right)\right\rangle_{t'\to t}=-\int\frac{d\omega}{2\pi i}\widetilde{G}_{dd}^{>}(\omega), \tag{27}$$

$$P_{1}^{st}=\left\langle d^{+}\left(t'\right)d(t)\right\rangle_{t'\to t}=\int\frac{d\omega}{2\pi i}\widetilde{G}_{dd}^{<}(\omega). \tag{28}$$

Comparing the expression of $P_{0(1)}^{st}$ with D(9) in Ref.[19], we see that the life-time broadening of the system is identical in all treatments there except that an EVI-assisted out-tunneling rate is maintained throughout our calculation. Nonetheless, owing to the relation of $\operatorname{Im}\widetilde{G}_{dd}^{<}-\operatorname{Im}\widetilde{G}_{dd}^{>}=\widetilde{A}_{d}(\omega)$, the normalization $P_{0}^{st}+P_{1}^{st}=\int\frac{d\omega}{2\pi}\widetilde{A}_{d}(\omega)=1$ is guaranteed in our calculation.

2.3.6 The Landauer-Büttiker Formula

The Landauer-Büttiker formula[23][24] can be used to describe the electron tunneling from one lead to another, and may be derived through the Green's function[11]: Using the identical relations of $\widetilde{G}^{r}-\widetilde{G}^{a}=\widetilde{G}^{>}-\widetilde{G}^{<}$ and $\Sigma^{r}-\Sigma^{a}=\Sigma^{>}-\Sigma^{<}$ on Eq.(18), an alternative expression of current is acquired as:

$$\begin{aligned}J_{\alpha}=\frac{e}{\hbar}\int\frac{d\omega}{2\pi}\sum_{n,n'}\Big[&\widetilde{T}_{nn'}^{\alpha\overline{\alpha}}(\omega)\,f_{\alpha}^{<}\left(\omega+n\omega_{0}\right)f_{\overline{\alpha}}^{>}\left(\omega-n'\omega_{0}\right)\\&-\widetilde{T}_{n'n}^{\overline{\alpha}\alpha}(\omega)\,f_{\alpha}^{>}\left(\omega-n\omega_{0}\right)f_{\overline{\alpha}}^{<}\left(\omega+n'\omega_{0}\right)\Big],\end{aligned} \tag{29}$$

where the tunneling function $\widetilde{T}_{nn'}^{\alpha\overline{\alpha}}$ is defined as

$$\widetilde{T}_{nn'}^{\alpha\overline{\alpha}}(\omega)=p_{n}p_{n'}\frac{\Gamma^{\alpha}\left(\omega+n\omega_{0}\right)\Gamma^{\overline{\alpha}}\left(\omega-n'\omega_{0}\right)}{W(\omega)}\widetilde{A}_{d}(\omega), \tag{30}$$

Eq.(29) and Eq.(30) are the central formulas for studying the joint effect due to the vibron-assisted tunneling rate. Moreover, Eq.(29) provides a clearer picture of EVI transport

than Eq.(18) does, that is, the electron departs from the n-th (electron) state in the α-lead (source), tunnels through the dot, and arrives at the n'-th (hole) state in the $\overline{\alpha}$-lead (drain). In general, the electron states are located below the chemical potential and the hole states above. Fig. 18(a) shows a graphical illustration for this description for a low-lying level position $\overline{\varepsilon}_0 = -\omega_0$ (left), medium level $\overline{\varepsilon}_0 = 0$ (central), and higher level $\overline{\varepsilon}_0 = \omega_0$ (right), where the bias is at $eV_b = 2\omega_0$, and the red arrows indicate the significant channels for particles passing through the dot.

From Eq.(30), we see that $T^{\alpha\overline{\alpha}}_{nn'}$ is expressed in terms of the tunneling function, tunneling rates, and weight factors on both terminals p_n and $p_{n'}$ due to the EVI effect. At zero temperature, the weight factor p_n is zero for $n < 0$[18], the Fermi function goes towards a step function, and the transport window for each channel, i.e. $\theta(\mu_\alpha - \omega - n\omega_0)\,\theta(\omega - n'\omega_0 - \mu_{\overline{\alpha}})$, in Eq.(29) is given by $\varepsilon^F_{\alpha,-n} - \varepsilon^F_{\overline{\alpha},n'} = \mu_\alpha - \mu_{\overline{\alpha}} - (n+n')\,\omega_0$. At low temperature, the particle transport practices are within μ_L and μ_R. However, at high temperature, p_{-n} is non-zero, and hence the vibron-mediated states outside the transport window also participate. Therefore, the current in this field is probable.[39]

An analogous transport scheme[12],[14],[11],[9],[13],[18],[28],[38], has been presented in previous publications although the background physics is different. For example, in Refs. [9] and [18] the n-th vibron-mediated state exists in the QD (or SMT) because the vibron field is treated as being involved in the evolution of the dot, so the vibron sidebands come from the SMT electrons and holes. Note that the quantized number is labeled from the energy of the dot, not from the chemical potential of the leads. Furthermore, Dong *et al.*[28]performed a mapping technique to reach a Landauer-Büttiker formula similar to the one in Eq.(29). However, since the vibron correlation is not involved in the tunneling self-energy, this technique results in a bias-independent bandwidth in the tunneling function, no matter what approximation is adopted. It is worth mentioning that the results obtained by Braig and Flensberg[38] through the RE are similar to those of ours. In fact, the report by Braig and Flensberg was to obtain the current through the RE method, which only contained the lowest-order term, i.e., the sequential tunneling current.

2.4 The Bias-dependent Tunneling Rate and the Differential Conductance

In this section, we start to numerically study the stationary properties of the spectral function, current and the its conductance through a single molecule system based on Eq.(23), Eq.(29) and Eq.(30). For simplicity, here and in the following we ignore the energy dependence of $\Gamma^{\alpha}(\omega)$ (wide band approximation).

2.4.1 The Bias-dependent Tunneling Rate

First we examine the spectral function. According to Eq.(23) one could anticipate that $\widetilde{A}_d(\omega)$ approximately behaves as a Lorentzian function with maximum value at $\widetilde{\varepsilon}_0$ and the lifetime broadening is given by $W(\omega)$ (see Fig.19(a)).

Usually this broadening function is equivalent to a tunneling rate from Fermi golden rule[25] so that we obtain $\Gamma_{out} = W(\omega)$. This identical relation can also be verified in Eq.(21). When increasing the bias voltage, the amplitude of spectral function is suppressed as shown in Fig.19(a), which means that in the presence of EVI, the tunneling rate is strongly associated with an increased transport window. Since the quantum fluctuation mainly takes place near the surface of continuum states, one focuses on the energy change near the chemical potential. Fig.19(b) depicts the total transmission rate of the particle in the system as a function of the bias voltage with a LT method (blue curve) and with a MFA method (red line), respectively.[18] We find that the out-tunneling rate $\Gamma_{out}(\omega = eV_b/2)$ shows a staircase curve along the increase of eV_b whereas the MFA method produces a flat line, irrelevant to the bias voltage. This is an important difference between the LT and the MFA. In LT results, Γ_{out} increases abruptly in the neighborhood of $eV_b = n\omega_0$. The abrupt increment results from the opening an additional channel for particle transport through the system when the bias voltage exceeds the required tunneling energy. The plateau maintains till the nth channel fully enters the transport window, where the plateau is generated around $eV_b = (n+1)\omega_0/2$. Note that the result of LT calculation is in agreement with that obtained by the MFA as one sets $e|V_b| < \omega_0$. In this restriction the tunneling rate is reduced to $\Gamma_{out} = p_0\left(\Gamma^L + \Gamma^R\right)$, and spectral function together with the current formula

are given by

$$\widetilde{A}_0(\omega) = p_0\left(\Gamma^L + \Gamma^R\right) / \left\{(\omega - \overline{\varepsilon}_0)^2 + \left[p_0\left(\Gamma^L + \Gamma^R\right)/2\right]^2\right\}, \tag{31}$$

and

$$J_0 = \frac{e}{\hbar}\int \frac{d\omega}{2\pi}\frac{\Gamma^L\Gamma^R}{\Gamma^L + \Gamma^R} p_0 A_0(\omega)\left[f_\alpha^<(\omega) - f_{\overline{\alpha}}^<(\omega)\right]. \tag{32}$$

This is consistent with earlier study with MFA theory because only the channel with $n \to 0$ in the lead is allowed for particle transport through the system.

2.4.2 The Spectral Function $A^{(tot)}(\omega)$

In addition to comparing the tunneling rate, we now inspect the difference between spectrum function with different approaches. For comparison, one needs to replace $\Gamma_n^{\alpha\lessgtr}(\omega + n\omega_0) \to \Gamma_n^{\alpha\lessgtr}(\omega)$ in the integrand of Eq.(49) and redefine $A^{(tot)}(\omega) \equiv \sum_{n=-\infty}^{\infty} p_n \widetilde{A}_d(\omega - n\omega_0)$ for the system spectral function. In this way, we have
a non-interacting lead and an interacting system. This system could now be regarded as an EVI quasi-particle (a spectrum function with multiple satellite peaks).

Fig.20 depicts the spectral function for two different renormalized level position ($\overline{\varepsilon}_0 = \pm 4\omega_0$) with $eV_b = 0.04\omega_0$. We see that no peaks appear in the left side of the level position and the LT spectral function is always in the form of skewed distribution (see Fig.20(a)) with a tail in the large energy rather than a mirror symmetry function (see Fig.20(b)) in MFA theory, i.e,

$$A(\omega = \overline{\varepsilon}_0 - \triangle\omega, \overline{\varepsilon}_0 = 4\omega_0, eV_b) = A(\omega = \overline{\varepsilon}_0 + \triangle\omega, \overline{\varepsilon}_0 = -4\omega_0, -eV_b)$$

.[18] Due to the fact that the spectral function in Eq.(23) satisfies the a identical mirror symmetry relation as MFA, the skewed distribution of the spectral function $A^{(tot)}$ can be traced back to the fact that no available vibron states for absorption before tunneling at low temperature.[28] Note that in Fig.20(a) the variation of $\overline{\varepsilon}_0$ only modulates the magnitude of spectrum function but without changing its skewness. This is different from the MFA spectra in which an electron or hole picture can be readily achieved by shifting the level position of the system. Note that the current formula can be expressed in terms of the

product of $A^{(tot)}(\omega)$ and a bare tunneling rate with weight p_n, which is analogy to the expression in earlier researches.[9][18][21]

2.4.3 Differential Conductance

Taking derivative of Eq.(29) with respect to the bias voltage, the differential conductances can be expressed as:

$$G = G_{lead} + G_{dot}, \tag{33}$$

$$G_{lead} = \frac{e}{\hbar}\int \frac{d\omega}{2\pi}\sum_{n,n'} T^{\alpha\overline{\alpha}}_{nn'}(\omega)\, F_{nn'}(\omega), \tag{34}$$

$$G_{dot} = -\frac{e}{\hbar}\int \frac{d\omega}{2\pi}\sum_{n,n'} \frac{\partial T^{\alpha\overline{\alpha}}_{nn'}(\omega)}{\partial V_b} f_{nn'}(\omega), \tag{35}$$

$$f_{nn'}(\omega) = f^{<}_{\alpha}(\omega + n\omega_0)\, f^{>}_{\overline{\alpha}}\left(\omega - n'\omega_0\right) - f^{<}_{\overline{\alpha}}(\omega + n\omega_0)\, f^{>}_{\alpha}\left(\omega - n'\omega_0\right), \tag{36}$$

where the wide-bad limit is considered, and G_{lead} and G_{dot} respectively reflect the conductance in the leads and in the QD (or SMT) system. $J_\alpha(\omega)$ is the current density, $f_{nn'}(\omega)$ determines the effective transport window and $F_{nn'}(\omega)\,(=\partial f_{nn'}(\omega)/\partial V_b)$ denotes a thermal broadening function in the leads[27],

$$F_{nn'}(\omega) = \beta\sum_{\eta\in\pm 1}\left\{\frac{f^{>}_R(\eta\omega - n'\omega_0)}{8\cosh^2\left[\frac{\beta}{2}(\omega + \eta n\omega_0 - \mu_L)\right]} + \frac{f^{<}_L(\eta\omega - n\omega_0)}{8\cosh^2\left[\frac{\beta}{2}(\omega - \eta n'\omega_0 - \mu_R)\right]}\right\}. \tag{37}$$

For $eV_b > 0$, $F_{nn'}(\omega)$ shows multiple peaks at $\omega = \varepsilon^F_{\alpha,-n}\,(=\mu_\alpha - n\omega_0)$ and $\omega = \varepsilon^F_{\overline{\alpha},n}\,(=\mu_{\overline{\alpha}} + n\omega_0)$,where n and $n' = 0, 1, 2$ and so on. Substituting Eq.(37) back into Eq.(34), it is found that G_{lead} reaches its maximum when the dot level $(\widetilde{\varepsilon}_0(V_g))$ matches those peaks. Therefore, when drawing G_{lead} vs. V_g, the satellite peaks of differential conductance are at $V_g = \varepsilon^F_{\alpha,-n}$ and $\varepsilon^F_{\overline{\alpha},n}$, symmetrically distributed with respect to $V_g = 0$.

Figure 2(A) depicts the vibron-assisted tunneling process under a new transport scheme for a low-lying level position $\overline{\varepsilon}_0 = -\omega_0$ (left), medium level $\overline{\varepsilon}_0 = 0$ (central), and higher level

$\overline{\varepsilon}_0 = \omega_0$ (right), where the bias is at $eV_b = 2\omega_0$, and the red arrows indicate the significant channels for particles passing through the dot. The differential conductance for each path is plotted in Fig. 2(B), where the quantum pair (n, n') means that the particle transports from the nth vibron-mediated state in the α lead to the n'th vibron-mediated state in the $\overline{\alpha}$ lead. An analogous transport scheme has been presented in previous publications of the rate equation method[12][13], although the background physics is different. For example, the nth vibron-mediated state exists in the QD (or SMT) because the vibron field is treated to involve in the evolution of the dot. The quantized number is labeled from the energy of the dot, not from the chemical potential of the leads. Furthermore, Dong *et al.*[28] performed a mapping technique to reach the Landauer-Büttiker formula similar to the one in Eq.(29). However, since the vibron correlation is not involved in the tunneling self-energy, this technique results in a bias-independent bandwidth in the tunneling function, no matter what approximation is adopted.

2.4.4 The Influence of the EVI Energy Shift

According to Eq.(35), the conductivity probed in the dot can be further divided into two parts,

$$G_{dot}^{s(l)} = -\frac{e}{\hbar}\int \frac{d\omega}{2\pi} J_\alpha(\omega)\, K_{s(l)}(\omega)\,, \tag{38}$$

where G_{dot}^{s} and G_{dot}^{l} respectively characterize the conductance induced by the energy shift and the bandwidth of the dot level, and $K_s(\omega)$ and $K_l(\omega)$ are solved as

$$K_s(\omega) = -\left\{ \begin{array}{c} \mathrm{Re}\, G^r(\omega) \cdot \left[\sum\limits_{n,\alpha\in L,R} (p_n - p_{-n})\, \Gamma^\alpha\, (-1)^{\delta_{L,\alpha}} \right. \\ \left. \beta\, \mathrm{Im}\, \psi_1\left(\frac{1}{2} + i\frac{\beta}{2\pi}(\omega + n\omega_0 - \mu_\alpha)\right)\right] + \end{array} \right\}, \tag{39}$$

$$K_l(\omega) = A_d(\omega)\, \overline{K}_l(\omega)\,, \tag{40}$$

$$\overline{K}_l(\omega) = \partial W(\omega)/\partial V_b = \beta \sum_{n,\alpha\in L,R} \frac{(p_n - p_{-n})\, \Gamma^\alpha\, (-1)^{\delta_{L,\alpha}}}{16\cosh^2\left[\frac{\beta}{2}(\omega + n\omega_0 - \mu_\alpha)\right]}.$$

A comparison between G_{dot}^{s} and G_{dot}^{l} in Fig.21 gives that G_{dot}^{l} is always negative while G_{dot}^{s} is positive at the quantized levels of vibron-mediated states ($eV_g = n\omega_0$). In addition, G_{dot}^{s}

also exhibits an energy-shift dependence near the quantized level, as depicted in the inset of Fig.21. This is due to the consideration of the EVI-renormalized energy shift during particle transport. Compared with G^s_{dot} in Fig.22, the energy-shift dependence becomes more apparent (dot line) as the electron-electron coupling is increased ($\Gamma_L = \Gamma_R = 0.6\omega_0$), whereas it is reduced when increasing the intensity of the EVI. This is because of the existence of e^{-g} in the weighting factor p_n.

2.4.5 The Mean-field Approximation

In this section we investigate an experimentally observable feature induced by the vibron-assisted tunneling rate, the conductance gap[1] (cg). Compared to Fig.23(a), Fig.23(b) suggests that a gap always exists between the edge of conductance (chemical potential, $n = 0$) and the first vibron-mediated state ($n = 1$); however, no conductance gap appears in the MFT calculation. In the MFT, the current can be understood as an effective particle propagating in an average field between the multi-channel leads, where the spectral function of the dressed electron in the dot is given by $\widetilde{A}_d(\omega) = \widetilde{\Gamma}/[(\omega - \overline{\varepsilon}_0)^2 + \widetilde{\Gamma}^2]$ with $\widetilde{\Gamma} = (\Gamma_L + \Gamma_R)\langle X\rangle^2/2$, which is independent of the bias, analogous to the model without EVI. Taking $\widetilde{A}_d(\omega)$ into Eq.(33) to Eq.(36), we obtain $G = G_{lead}$, and hence the conductance peak represents the vacant vibron-mediated states in the wire. In general, the bandwidth is the decay rate, i.e., the out-tunneling rate. At dynamic equilibrium, the total out-tunneling rate is supposed to balance the sum of the in-tunneling rate so as to satisfy the continuity rule. Nevertheless, in the MFT the in-tunneling rate is bias-related while the out-tunneling rate is a constant, which signifies that some information, such as electrical properties, will be lost during the transport.

Fig.24(d) gives the profile of G_{lead} and G_{dot} vs. eV_g at $eV_b = 2.5\omega_0$. We can see that G_{dot} presents a similar peak-structure as G_{lead}, but with negative amplitude. In order to analyze those peaks, we can perform the weak-coupling limit[14].

2.4.6 The Weak Electron–Electron Coupling Limit

This assumption means that the lead-dot coupling is much smaller than the electron-vibron coupling. In other words, the electron life-time is far larger than the vibron relaxation time. The occupied state of vibron will not respond to the change of dot or lead. So the evolution of vibron can be described by the zero-order vibron correlation. That is to say, the DOS of vibron exhibits many delta peaks, reflecting the numbers of vibrons absorbed or emitted at various levels. But this is not the practical case for the time dimension of electron relaxation could be close to that of vibron. The effects of electrons on vibrons is more than the delta-peak distribution of energy level. We must consider the level-broadening effect on the vibron energy levels. This non-equilibrium process destroy the original statistical distribution and new behavior is generated, such as the vibron blockade, which has been a very important topic in recent years.

Taking the weak coupling, that is, the spectral function in Eq.(23) taking the form of $\widetilde{A}_d(\omega) = 2\pi\delta(\omega - \overline{\varepsilon}_0)$, on Eq.(34), Eq.(35) and Eq.(29), which gives

$$G_{lead} = \frac{e}{\hbar}\frac{\Gamma^{\alpha}\Gamma^{\overline{\alpha}}}{W(\overline{\varepsilon}_0)}\sum_{n,n'} p_n p_{n'} f'_{nn'}(\overline{\varepsilon}_0), \tag{41}$$

$$G^{(l)}_{dot} = -\frac{e}{\hbar}J(\overline{\varepsilon}_0)W'(\overline{\varepsilon}_0), \tag{42}$$

$$J(\overline{\varepsilon}_0) = \frac{e}{\hbar}\frac{\Gamma^{\alpha}\Gamma^{\overline{\alpha}}}{W(\overline{\varepsilon}_0)}\sum_{n,n'} p_n p_{n'} f_{nn'}(\overline{\varepsilon}_0) \tag{43}$$

G^{s}_{dot} does not exist since $\mathrm{Re}\,\Sigma^{r}_{T}(\omega)$ approaches zero at small Γ. This is a good approximation because Eq.(41), Eq.(42) and Eq.(43) satisfies the definition of $G = \partial J(\overline{\varepsilon}_0)/\partial V_b$. Moreover, when rewriting $p_{-n} = p_n e^{-\beta n\omega_0}$ in $W(\overline{\varepsilon}_0)$ and $f_{nn'}(\overline{\varepsilon}_0)$, and performing some algebra, we readily reach the same current expression for a single resonant model as reported by Braig and Flensberg[38]. This is because the appliance of the RE, a method used to describe the quantum transport as the correlations in the system is much shorter than electron transfer time, is equivalent to the expression of $\widetilde{A}_d(\omega) = 2\pi\delta(\omega - \overline{\varepsilon}_0)$ in NEGF[40][21].

2.4.7 The Origin of the Conductance Gap

Here, we investigate the source of conductance gap. At zero temperature, the summation of Eq.(41) and Eq.(42) leads to:

$$\begin{aligned} G &= G_{dot} + G_{lead} \\ &= \frac{e}{\hbar}\frac{\Gamma^L\Gamma^R e^{-2g}}{W^2_{T=0}\left(\overline{\varepsilon}_0\right)}\sum_{n,n'}\frac{g^{n+n'}}{n!n'!}\left[W'_{T=0}\left(\overline{\varepsilon}_0\right)f_{nn'}\left(\overline{\varepsilon}_0\right) + W_{T=0}\left(\overline{\varepsilon}_0\right)f'_{nn'}\left(\overline{\varepsilon}_0\right)\right], \end{aligned} \tag{44}$$

where $W_{T=0}$ and $f_{nn'}$ consist of multiple step functions, and $W'_{T=0}\left(\overline{\varepsilon}_0\right)$ and $f'_{nn'}\left(\overline{\varepsilon}_0\right)$ comprise delta functions. In the MFT, $W_{T=0}\left(\overline{\varepsilon}_0\right) = \widetilde{\Gamma}$, which is a constant such that $W'_{T=0}\left(\overline{\varepsilon}_0\right) = 0$ and $G = G_{lead}$. Consequently, Eq.(44) is directly proportional to the thermal broadening function $f'_{nn'}\left(\overline{\varepsilon}_0\right)$, and results in a multiple peak structure, as depicted in Fig.24(c). At $eV_g/\omega_0 = 0.75$, three available channels $(0,0)$, $(0,1)$, and $(0,2)$ contribute to the tunneling current (see the left inset of Fig.24(c)). However, for the LT method, $W'_{T=0}\left(\overline{\varepsilon}_0\right)$ is non-zero at $eV_g/\omega_0 = 0.75$. Taking those quantum pair into Eq.(44), it reveals that G_{dot} and G_{lead} are are of the same order and cancel each other out (see Fig.24(d)), suggesting that the existence of vibron-assisted tunneling rate would greatly scale down the current and leads to a conductance gap in this field. The current-voltage characteristics in the right inset of Fig.24(d) reflect this phenomenon. From the viewpoint of physics, this means that an virtual state is generated in this energy field. It is the first time that such the conductivity gap is examined theoretically in the quantum dot system.

2.4.8 The Rate Equation (the Master Equation)

In this case, the behavior of a electron was described by the semi-classical sequential tunneling when the life-time for the electron to stay in the system is much bigger than the tunneling time. Then the equation of motion for the system affected by surroundings can be described by the RE. Referring to the work done by S. Brag and K. Flensberg[38], the occupancy of the dot are defined by:the stationary probability for an empty state and an

occupied state can be found as

$$P_0^{st} = \left\langle d\left(t\right) d^{+}\left(t'\right)\right\rangle_{t'\to t} = -\int \frac{d\omega}{2\pi i}\widetilde{G}_{dd}^{>}\left(\omega\right), \tag{45}$$

$$P_1^{st} = \left\langle d^{+}\left(t'\right) d\left(t\right)\right\rangle_{t'\to t} = \int \frac{d\omega}{2\pi i}\widetilde{G}_{dd}^{<}\left(\omega\right). \tag{46}$$

Owing to the fact that

$$e\frac{\partial}{\partial t} P_{0(1)}^{st} = \mp\left[J_L + J_R\right], \tag{47}$$

and $J_\alpha\left(t\right)$ is solved as

$$\begin{aligned} J_L\left(t\right) = -\frac{2e}{\hbar}\,\mathrm{Im}\Bigg[&\int_{-\infty}^{t} dt_1 \widetilde{G}_{dd}^{r}\left(t,t_1\right)\Sigma_{\alpha\epsilon L}^{<}\left(t_1,t\right) \\ &+ \widetilde{G}_{dd}^{<}\left(t,t_1\right)\Sigma_{\alpha\epsilon L}^{a}\left(t_1,t\right)\Bigg], \end{aligned} \tag{48}$$

$$\begin{aligned} &= \frac{2e}{\hbar}\Bigg[\int_{-\infty}^{t} dt_1 \widetilde{G}_{dd}^{>}\left(t,t_1\right)\Sigma_{L}^{<}\left(t_1,t\right) \\ &- \widetilde{G}_{dd}^{<}\left(t,t_1\right)\Sigma_{L}^{>}\left(t_1,t\right)\Bigg]. \end{aligned} \tag{49}$$

Substituting Eq.(49) into Eq.(47), we readily obtain the RE given by:

$$\begin{aligned} \frac{\partial}{\partial t} P_0^{st} &= i\Bigg[\int \frac{d\omega}{2\pi}\widetilde{G}_{dd}^{<}\left(\omega\right)\cdot\sum_{n,\alpha} p_n \Gamma_\alpha^{>}\left(\omega + n\omega_0\right) \\ &\quad - \widetilde{G}_{dd}^{>}\left(\omega\right)\cdot\sum_{n,\alpha} p_{-n}\Gamma_\alpha^{<}\left(\omega + n\omega_0\right)\Bigg] = 0, \end{aligned} \tag{50}$$

$$\begin{aligned} \frac{\partial}{\partial t} P_1^{st} &= i\Bigg[\int \frac{d\omega}{2\pi}\widetilde{G}_{dd}^{>}\left(\omega\right)\cdot\sum_{n,\alpha} p_{-n} \Gamma_\alpha^{<}\left(\omega + n\omega_0\right) \\ &\quad - \widetilde{G}_{dd}^{<}\left(\omega\right)\cdot\sum_{n,\alpha} p_{n}\Gamma_\alpha^{>}\left(\omega + n\omega_0\right)\Bigg] = 0, \end{aligned} \tag{51}$$

with

$$\Gamma_\alpha^{\lessgtr}\left(\omega\right) \equiv \Gamma_\alpha\left(\omega + n\omega_0\right) f_\alpha^{\lessgtr}\left(\omega + n\omega_0\right) \tag{52}$$

We can see that no corresponding P_0^{st} and P_1^{st} in the RHS of Eq.(50) and Eq.(51). In order to solve this problem, we consider a special case that a particle's relaxation time is much longer than its correlation time, as a consequence, the spectral function of the quantum dot reads

$$\widetilde{A}_d \approx 2\pi\left(\omega - \varepsilon_d\right).$$

and the kinetics becomes semi-classical (sequential tunneling). The corresponding occupancy density is therefore given by

$$\widetilde{G}_{dd}^{\lessgtr}(\omega) \to \pm 2\pi i \delta(\omega - \varepsilon_d) P_{1(0)}^{st} \tag{53}$$

Taking Eq.(53) back into Eq.(50) and Eq.(51), we obtain

$$\begin{pmatrix} -\sum_{n,\alpha} p_{-n}\Gamma_\alpha^{<}(\varepsilon_d + n\omega_0) & \sum_{n,\alpha} p_n \Gamma_\alpha^{>}(\varepsilon_d + n\omega_0) \\ \sum_{n,\alpha} p_{-n}\Gamma_\alpha^{<}(\varepsilon_d + n\omega_0) & -\sum_{n,\alpha} p_n \Gamma_\alpha^{>}(\varepsilon_d + n\omega_0) \end{pmatrix} \begin{pmatrix} P_0^{st} \\ P_1^{st} \end{pmatrix} = 0, \tag{54}$$

forming the well-known Rate equation. Here the occupancy$P_{1(0)}^{st}$ can be solved with

$$P_{1(0)}^{st} = \frac{\sum\limits_{n,\alpha} p_{\mp n}\Gamma_\alpha^{<}(\varepsilon_d + n\omega_0)}{\sum\limits_{n,\alpha}\left[p_n\Gamma_\alpha^{<}(\omega + n\omega_0) + p_{-n}\Gamma_\alpha^{>}(\omega + n\omega_0)\right]}. \tag{55}$$

In conclusion, a generalized RE can be recovered from the JWM's formula. However, if one wanted to acquire $P_{1(0)}^{st}$ from $\widetilde{G}^{<,>}(\omega)$, it is necessary to let $\widetilde{A}_d(\omega)$ to be a delta function. On the other hand, electrons have a great period of transport time in the system, far more than the time when they pass through the barrier.

To sum up, we can understand that NEGF reflects the transition rate and relaxation rate of systems, but it has limits in calculating EPI current. During the last decade, many theoretical works have studied the EPI current with the NEGF method. However, some of their results disagree with experiments. For example, at zero temperature, they acquired the phonon side-band conductance in the Coulomb blockade region. It results from the EVI correlation being decomposed using high-temperature approximation. As another example, a gap exists between the chemical potential and the first phonon excited state. The bandwidth of conductance will blur as the bias is increased. Although Chen *et.al* proposed MFT theory to fix the conductance at low temperature, the second issue remains unsolved. Rate equation clearly illustrates the changes in systems, it can only apply for weak interaction and sequential tunneling. The bandwidth of conductance reflects the thermal information of the wire for the resonant tunneling only takes place near the chemical potential. It's insufficient to describe the change of the quantum system, like the blurred behavior of the conductance at large bias area. To sum up, the NEGF with the LT is the most well-rounded

approach to tackle nonequilibrium problems, especially the nonequilibrium mechanism is determined by the bias. Besides the above-mentioned advantages as mentioned in the RE, the NEGF further shows the renormalization of energy levels. This result is coincident with experiments as well.

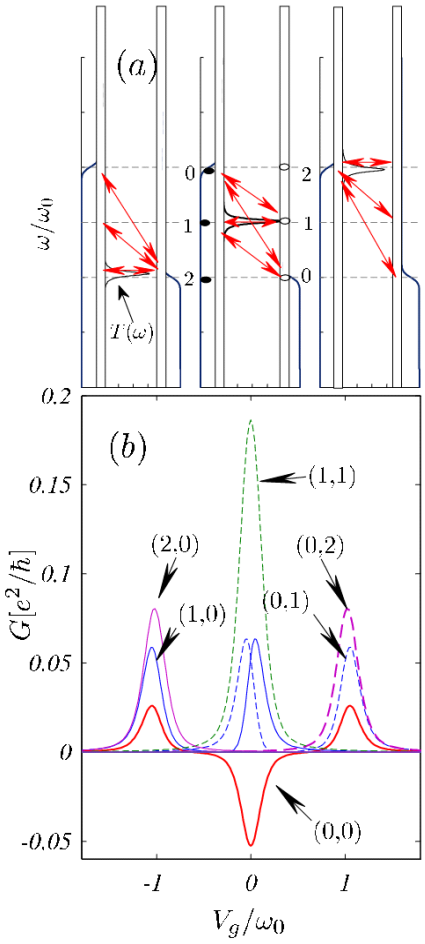

Figure 18: (a) A schematic description of the transport channels and tunneling coefficient at different gate voltages. Here • represents the electron state (labeled from the chemical potentail of the left lead μ_L) and ∘ for the hole state (from the chemical potential of the right lead μ_R). The red arrow denotes the transport path. (b) The differential conductance for each channel, where the quantum pair (n, n') means that the particle transports from the nth phonon-mediated state in the α lead (electron state •) to the n'th phonon-mediated state in the $\overline{\alpha}$ lead (hole state ∘). The parameters of the system are $\Gamma_L = \Gamma_R = 0.2\omega_0$, $k_BT = 0.05\omega_0$, $\lambda = 1.5\omega_0$, $\mu_L = -\mu_R = \omega_0$ and the Lorentz cut-off is $E_C = 100$ in the integral calculation[20].

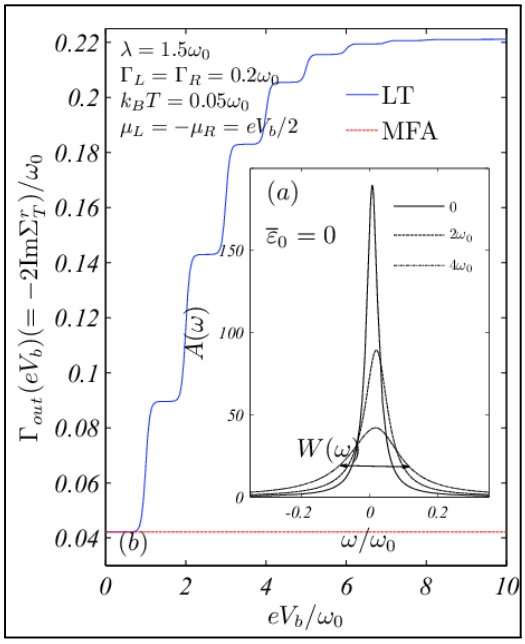

Figure 19: (a) The out-tunneling rate $\Gamma^{\alpha}_{out}(\omega = V_b/2)$ vs. bias voltage. (b) The maps of differential conductance as a function of gate and bias voltage is calculated with MFA's approach and (c) is worked with Langreth theorem.

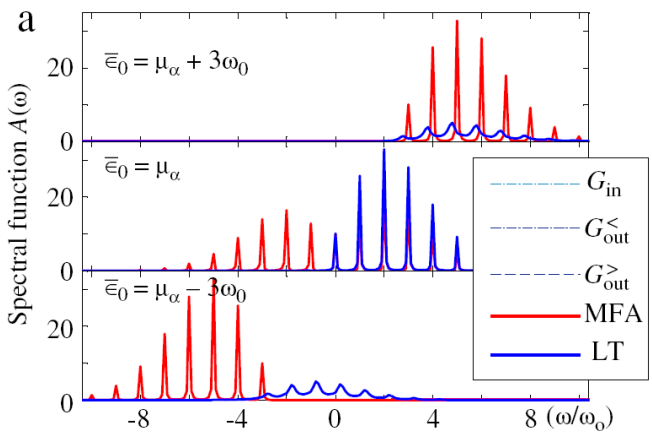

Figure 20: (a) The spectral function of the strong EPI system v.s. energy ω for different energy levels for $\widetilde{\varepsilon}_0$. The chemical potential in the leads are fixed at $\mu_L = -\mu_R = 0.1\omega_0$. The parameters used are $\Gamma_L = \Gamma_R = 0.4\omega_0$, $k_BT = 0.05\omega_0$, $\lambda = 1.6\omega_0$.

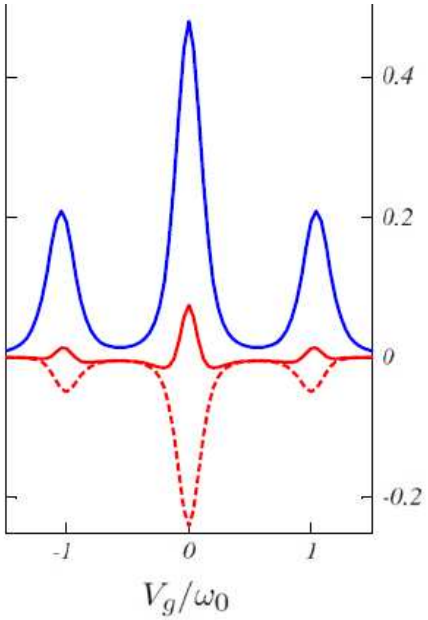

Figure 21: Differential conductance in the leads G_{lead} (blue line) and in the dot $G^{s,l}_{lead}$ (red lines), where G^{s}_{dot} (solid line) is induced by the EPI renormalization), and G^{l}_{dot} (dot line) is caused by the level broadening .

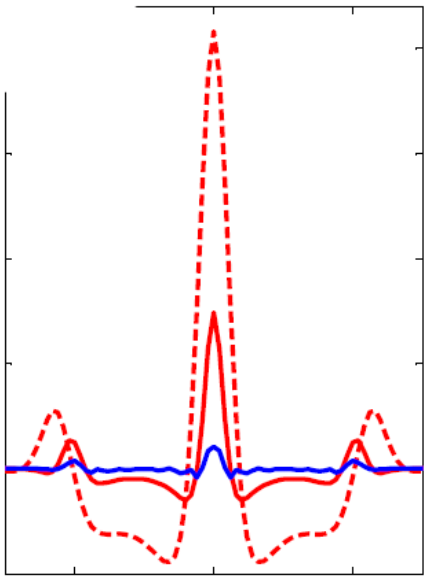

Figure 22: The conductance G^{s}_{dot} becomes sibnificant at strong electron-electron coupling (red dot line, $\Gamma_L = \Gamma_R = 0.6\omega_0$) while it is highly supressed at strong electron-phonon coupling (blue line, $\lambda = 2\omega_0$).

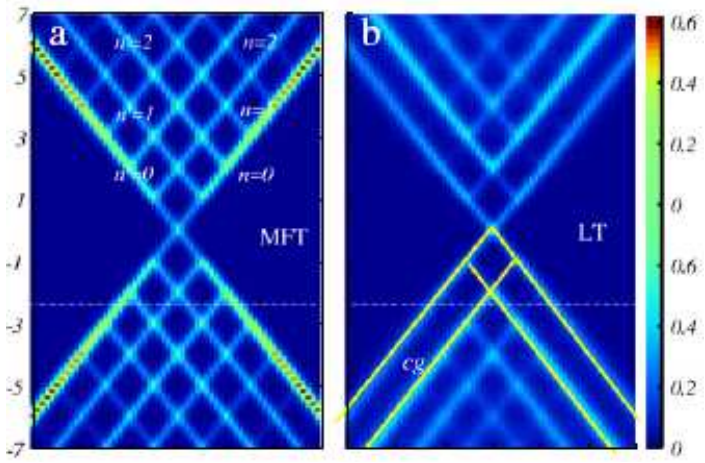

Figure 23: The conductance map vs. the gate voltage V_g and the bias voltage V_b, where (a) is solved with the MFT method and (b) with the LT method. In figure (b), a gap always exists between the edge of conductance (chemical potential, $n = 0$) and the first phonon-mediated state ($n = 1$).

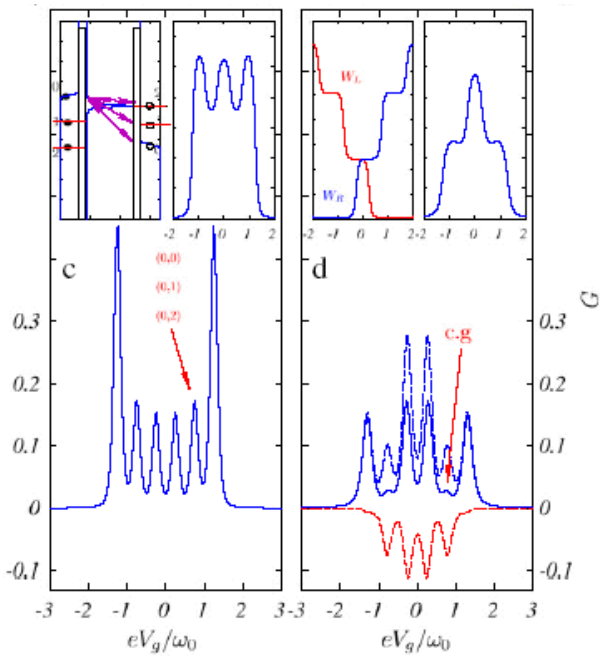

Figure 24: Note that the parameters are the same in Fig. 2 and Fig. 3. The differnetial conductance as a fnction of the gate voltage is plotted at $eV_b = 2.5\omega_0$. Left inset: The schematic description of particle transport through the dot at $eV_g = 0.75\omega_0$. There exist three channels for particle transport, $(0,0)$, $(0,1)$, and $(0,2)$. Right inset: The MFT-PAT current.

CHAPTER III

THE LOW-FREQUENCY NOISE

3.1 Experimental Motivation and Recent Progress

The electrical current through a device always fluctuates around the average value due to the discreteness of the charge carriers, as shown in Fig. 25. As a matter of fact, these deviation contains the system's correlation function. One of the ways to read the correlation is to calculate the current-current correlation function via the Fourier transform.

The average current $\langle I\rangle$ is defined by $\langle I\rangle = \lim_T \frac{1}{T}\int_{-T/2}^{T/2} dtI\left(t\right)$,where I is the current operator and T is the time interval. $I\left(t\right)$ and $\langle I\rangle$ form an identical relation $I\left(t\right) = \langle I\rangle + \delta I\left(t\right)$, where δI denotes the deviation current caused by the transfer particle.

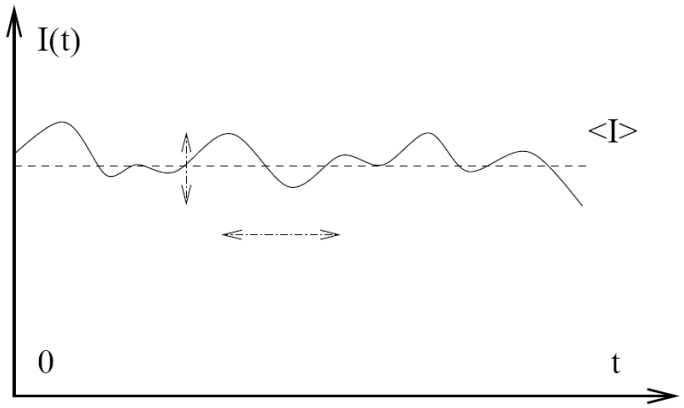

Figure 25: Current flucuation around the average current $\langle I\rangle$. Reprinted from Ref.

In 1918,Walter Schottky took advantage of a vacuum tube and discovered the shot noise. Since nothing existed in the vacuum tube, he deduced the nose relation of $S = 2q\langle I\rangle$ consists, with q denoting the charge. This is the traditional shot noise, $S = S_P$. Nonetheless, not all carriers carry single charge, for example, the free carriers in superconductor are with two charges (cooper-pair), and in quantum Hall effect, the carrier possesses one third of an electron charge. The unit charge cannot be probed via the average current, but it can be

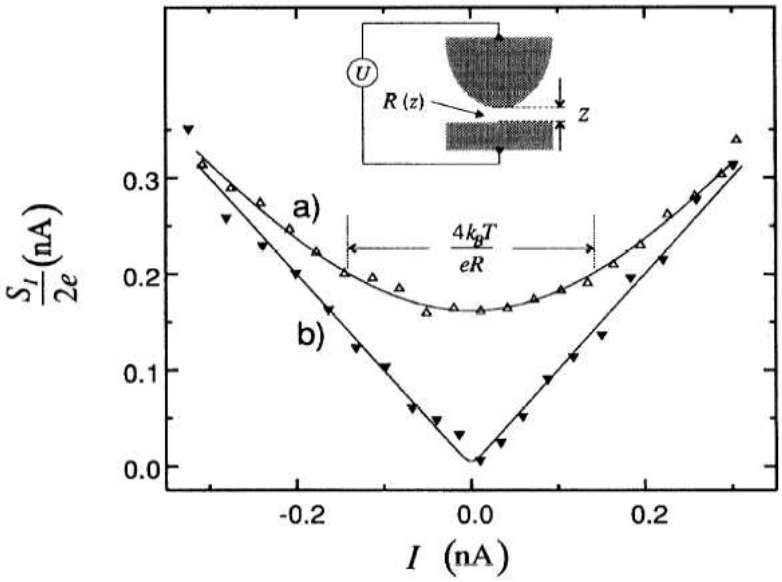

Figure 26: The shot noise normalized by 2e as a function of the current. The inset depicts the experimental setup with the STM tip and a single tunneling barrier to Au-metal. Reprinted from Ref.[41]

obtained from the shot noise.

In contrast to the equilibrium thermal noise, shot noise dominates the current correlation in large bias condition, besides, shot noise provides additional information about transport properties, not available in conventional conductance, such as the loss of phase coherence and the Pauli exclusion principals in mesoscopic system. Fig.26 depicts the noise as a function of the current (or bias). The solid line shows the theoretical prediction and the dot reveals for the experimental data. It can be seen that (a) at high temperature ($T = 300K$), and the thermal noise can be described by the well-known Johnson-Nyquist formula.(b) at low temperature, the shot noise governs the current correlation, where the correlation comes from the interaction among carriers, e.g. Pauli exclusion principle or the Coulomb interaction. However, since Birk *et al.*[41] apply Au-metal in the central region, the transfer process is completely random. There is no correlation inside, and the shot noise is directly proportional to the average current (or the bias). Sometimes it is useful to define

a dimensionless quantity, as known as Fano factor, $F \equiv S(\omega \to 0)/S_P$, to probe the deviation from the uncorrelated Poisson noise, with $S_P = 2e\langle I \rangle$. When $F = 1$, it suggests that the motion of transporting electron is completely random (uncorrelated). While $F < 1$, it has correlation inside.

In 2006, E. Onac *et al.*[30] took advantage of a suspended carbon nanotube (CNT) and s SIS to measure a vibrating quantum dot for the observation of strong electron-vibron coupling effects on the current, as depicted in Fig. 27. With current and noise, they calculated the Fano factor of the CNT-QD.

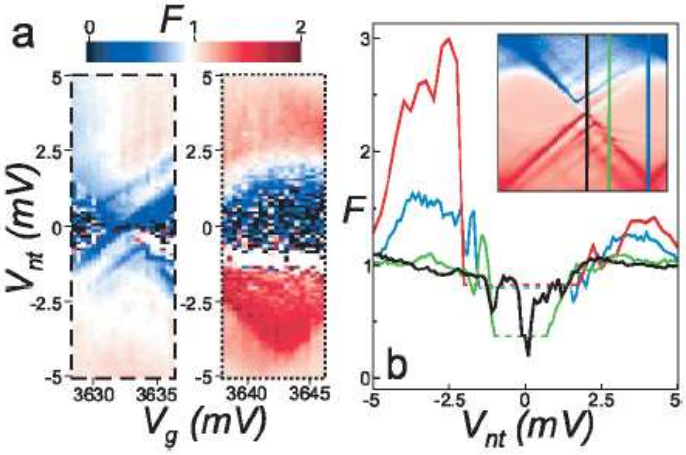

Figure 27: (a) The the dashed rectangle shows the Fano factor inside transport bias window. The dotted rectangle is for the Coulomb blockade. (b) Fano factor versus the applied bias at different gate voltages. Reprinted from Ref.[30].

Fig. 27(b) presents the Fano factor vs.V_b at different gate voltages V_g. When the gate voltage is located within the range of the chemical potential (transport bias window), the transport is dominated by the sequential tunneling, meanwhile, F is less than one (sub-Poissonian). At large bias, the interference of the channels becomes significant, and electron motion becomes random, as a consequence, F approaches unity. In the Coulomb blockage region, the sequential tunneling is suppressed, and the higher-order tunneling process, e.g. the elastic co-tunneling and inelastic co-tunneling become active. Note that the elastic co-tunneling does not change the ground state of the dot system, thus the electron motion is uncorrleated, so $F = 1$. However, inelastic co-tunneling yields the change of states, two

channels takes part in quantum transport, and thus the Fano factor is beyond unity. At $F = 1$, the electron relaxation is from high energy level to a lower one and then leaves the system. As for $F > 1$, the electrons directly depart from high levels as a bundle. Meanwhile, the relaxation among levels remains, and induces the sequential tunneling. After the occurrence of the sequential tunneling, the Fano factor starts to be less than three..

3.2 Motivation for Noise Calculation

In 2000, Q. F. Sun and J. Wang[29] studied the shot noise of a quantum dot in the presence of a microwave field. They concluded the following results: First, At zero temperature, the shot noise noise can be measured even the current is zero, as illustrated in Fig. 28(b). They deduced the zero-bias noise is supplied by the assistance of the photons. Second, the zero-bias differential noise as a function of the gate voltage shows an anti-symmetric structure and exhibits satellite PSD at multiple energy of the photon frequency, as shown in Fig. 28(a). In practice, the above description conflicts with the experimental observations, as shown in Fig. [5], where a suspended carbon nanotube quantum dot (CNT-QD) is considered. At $T = 20mK$, only emission of photons are allowed, and conductance peaks is forbidden to take place within the Coulomb blockade, as shown in Fig. 29(b). Besides, at $V_b = 0$, the current is very weak, and the noise shall approach zero. Therefore, to investigate the differences between theoretical and experimental methods becomes the key goal of this research.

3.3 Theoretical Calculation of Zero-Frequency Noise

To our knowledge, there are two theoretical formulations that are used to explore the quantum transport in nanoscale systems, i.e. Rate equation method (RE) and the non-equilibrium Keldysh Green's function (NEGF). In contrast to the weak perturbation method for the electron-electron coupling in Rate equation, the NEGF provides a general physical condition for particle transport through a non-equilibrium system, valid from the small

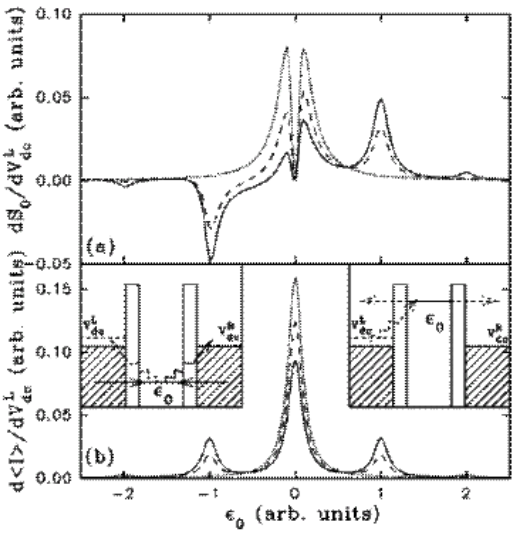

Figure 28: The plot of the differential conductance and differential noise vs. V_g for an photon-assisted tunneling model. Reprinted from Ref.[29]

bias to the large bias in the leads, where the influence of EVI is explicitly considered when applying the small polaron canonical transformation on the vibrating quantum dot system. The relevant Green's function can be solved via the Dyson equation and the Langreth rule. Among the NEGF approach, there are two different physical picture that are used to interpret the vibron-assisted process. Firstly, a concept of effective one-body tunneling scheme (with no fluctuations inside) is imposed to interpret the particle scattering in the QD system, i.e. replacing the electron-vibron interaction to a an average field. In practice, the relevant transport quantities such as current and the differential noise were discussed and reported by Chen *et al*[18], while the current correlation is not yet exposed before. In this work, we employ the mean-field approach to examine the zero-frequency noise, and then compare with an exact analytical solution to that solved by the analytic continuation. Basically, the EVI not only breaks the symmetry properties of electrons and holes in the quantum dot system, but also yields a significant staircase phenomenon on the tunneling rate as well as on the bandwidth of a single state for the central system. The main difference between the MFT approach and LT are: The EVI correlation is regarded as scalar, and therefore the vibron correlation will not couple to the Fermi function of the leads, irrelevant to the chemical potential difference. This resulting correlation gives the 0th quantized state

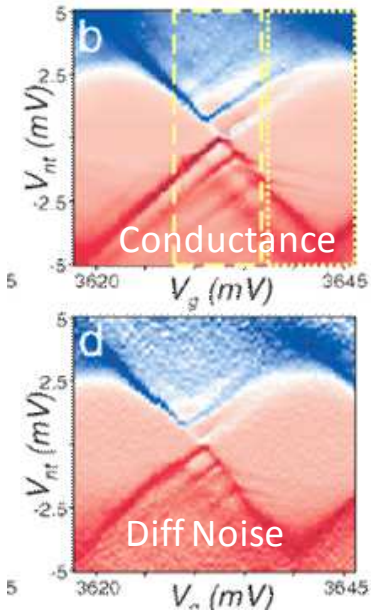

Figure 29: The upper shows $G = dI/dV_b$ vs. V_g (gate volatge) and V_b (bias voltage, vertical axis). The lower density plot reveals the differential noise dS/dV_b. Reprinted from Ref.

of the LT method, proving that the LT treatment is beyond than previous researches of this kind. Note that in this paper, we ignore higher order tunneling process from heating of vibration or mutual influence within the sub-electronic and sub-vibronic subsystems,[22] we focus only on the lowest order electron-vibron interaction. Besides we neglect the spin degree of freedom and the influence of Coulomb interaction.

3.3.1 The JWM Transport Formula (from the perspective of the metal wire)

The current from the left lead to the central region can be defined by:

$$J_L(t) = \frac{2e}{\hbar} \mathrm{Re} \sum_{k,\alpha \in L} V_{k\alpha,d} G^{<}_{d,k\alpha}(t,t') \,|_{t' \to t} \,, \tag{56}$$

where the Green's function $G^{<}_{d,k\alpha}(t,t') \equiv i \left\langle c^{+}_{k\alpha}(t') X(t) d(t) \right\rangle$. The first-order expansion of Dyson series on $G_{d,k\alpha}$ gives

$$G_{d,k\alpha}(\tau,\tau') = \int d\tau_1 \widetilde{G}_{dd}(\tau,\tau_1) F^{+}(\tau,\tau_1) V^{*}_{k\alpha} g_{k\alpha}(\tau_1,\tau') \,. \tag{57}$$

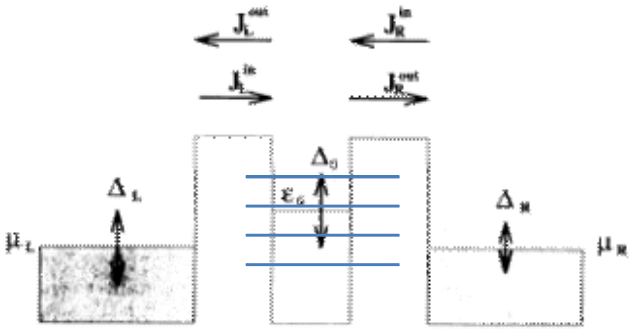

Figure 30: The vibrating quantum dot model. Here the equilibrium vibronic is coupled to the QD system. Reprinted from Ref.[11]

Performing the continuation rules[11] on $G_{d,k\alpha}(\tau,\tau')$ and substituting the resulting $G^{<}_{d,k\alpha}(t,t')$ into Eq.(56), the steady current is written as:

$$J_L(t) = -\frac{2e}{\hbar}\,\mathrm{Im}\left[\int_{-\infty}^{t} dt_1 G^{r}_{dd}(t,t_1)\,\widetilde{\Sigma}^{<}_{\alpha\epsilon L}(t_1,t) + G^{<}_{dd}(t,t_1)\,\widetilde{\Sigma}^{a}_{\alpha\epsilon L}(t_1,t)\right], \tag{58}$$

where $\widetilde{\Sigma}^{>,<}_{\alpha}(t,t_1) = \sum_{\alpha}|V_{k\alpha}|^2\, g^{>,<}_{k\alpha}(\tau_1,\tau_2)$, and $G^{\lessgtr}_{dd}(t,t_1)$ are defined as:

$$G^{\lessgtr}_{dd}(t,t_1) \equiv F^{+\lessgtr}(t,t')\,\widetilde{G}^{\lessgtr}_{dd}(t,t'), \tag{59}$$

where $F^{+>}(t-t') \equiv \langle X^{+}(t')\,X(t)\rangle$ and $F^{+<}(t-t') \equiv \langle X(t)\,X^{+}(t')\rangle$ denote the greater and lesser vibron Green's functions, and the lesser (greater) Green's function for a free electron in the α lead is denoted by $g^{<(>)}_{k\alpha}(t-t')$. Moreover, the (self-consistent) Dyson expansion of the electron Green's function $\widetilde{G}_{dd}$ is found as:[14][16]

$$\widetilde{G}_{dd}(\tau,\tau') = \widetilde{G}^{(0)}_{dd}(\tau,\tau') + \int_{c1} d\tau_1 \int_{c2} d\tau_2\, \widetilde{G}^{(0)}_{dd}(\tau,\tau_1)\,\Sigma_T(\tau_1,\tau_2)\,\widetilde{G}_{dd}(\tau_2,\tau'), \tag{60}$$

where the contour-ordered self-energy reads

$$\begin{aligned}\Sigma_T(\tau_1,\tau_2) &= \sum_{k\alpha\in L,R}|V_{k\alpha}|^2\, g_{k\alpha}(\tau_1,\tau_2)\left\langle T_c X^{+}(\tau_1)\,X(\tau_2)\right\rangle \\ &= F^{+}(\tau_1-\tau_2)\,\widetilde{\Sigma}_T(\tau_1-\tau_2).\end{aligned} \tag{61}$$

The self-energy contains all correlations about lead electrons and the vibrons. $F^{+}(\tau_1-\tau_2)\equiv\langle T_c X^{+}(\tau)X(\tau')\rangle$ is the vibron Green's function and

$$\widetilde{\Sigma}_T(\tau_1-\tau_2)=\textstyle\sum_{k\alpha\in L,R}|V_{k\alpha}|^2 g_{k\alpha}(\tau_1,\tau_2) \tag{62}$$

is the self-energy due to the electron coupling. The retarded (advanced) self-energy can be easily found as

$$\begin{aligned}\Sigma_T^{r,a}(t,t') &= \pm\sum_{k_\alpha}|V_{k\alpha}|^2\,\theta(\pm t\mp t')\\ &\quad\cdot\left[F^{+>}(t-t')\,g_{k\alpha}^{>}(t-t')-F^{+<}(t-t')\,g_{k\alpha}^{<}(t-t')\right]\\ &= \pm\theta(\pm t\mp t')\left[\Sigma_{\alpha,n}^{>}(t,t')-\Sigma_{\alpha,n}^{<}(t,t')\right].\end{aligned} \tag{63}$$

The Fourier transform further gives the retarded and the lesser self-energies

$$\Sigma_\alpha^{r,<}(\omega)=\sum_n\Sigma_{\alpha,n}^{r,<}(\omega), \tag{64}$$

$$\begin{aligned}\Sigma_{\alpha,n}^{r}(\omega) &= \sum_{k\alpha}\left[p_n\frac{V_{k\alpha}^{*}V_{k\alpha}}{\omega+n\omega_0-\varepsilon_{k\alpha}+i\delta}f_\alpha^{<}(\varepsilon_{k\alpha})\right.\\ &\quad\left.\cdot+p_{-n}\frac{V_{k\alpha}^{*}V_{k\alpha}}{\omega+n\omega_0-\varepsilon_{k\alpha}+i\delta}f_\alpha^{>}(\varepsilon_k)\right],\end{aligned} \tag{65}$$

$$\begin{aligned}\Sigma_{\alpha,n}^{\gtrless}(\omega) &= \sum_{k\alpha}V_{k\alpha}^{*}V_{k\alpha}p_{\mp n}g_{k\alpha}^{\gtrless}(\omega+n\omega_0)\\ &= \mp i\sum_n p_{\mp n}\Gamma_\alpha(\omega+n\omega_0)\,f_\alpha^{\gtrless}(\omega+n\omega_0),\end{aligned} \tag{66}$$

where $f_\alpha^{<,>}(\varepsilon_{k\alpha})$ denotes the electron and the hole Fermi functions in the α lead, and $\Gamma_\alpha(\omega)=2\pi\sum_{k\alpha}|V_{k\alpha}|^2\,\delta(\omega-\varepsilon_{k\alpha})$ shows the tunneling rate without EVI. Also, the Fourier transform of Eq.(59) leads to

$$G_{dd}^{\gtrless}(\omega)=\sum_n p_{\mp n}\widetilde{G}_{dd}^{\gtrless}(\omega+n\omega_0). \tag{67}$$

The weighting factor p_n, which indicates the probability of the electron interacting with n vibrons, is

$$p_n=e^{-2g\left(N_0+\frac{1}{2}\right)}e^{n\omega_0/2k_BT}I_n\left(2g\sqrt{N_0(N_0+1)}\right), \tag{68}$$

where $g=(\lambda/\omega_0)^2$, N_0 is the Bose function, and I_n is the modified Bessel function. As to $\widetilde{G}^{\gtrless}(\omega)$ in Eq.(67), this propagator can be evaluated using the Keldysh formulation[14],

that is,

$$\widetilde{G}_{dd}^{\gtrless}(\omega) = \Sigma_d^{\gtrless}(\omega)\left|\widetilde{G}_{dd}^{r}(\omega)\right|^2 \tag{69}$$
$$= \mp i\sum_{n,\alpha} p_{\mp n}\Gamma_\alpha^{\gtrless}(\omega - n\omega_0)\left|\widetilde{G}_{dd}^{r}(\omega)\right|^2,$$

$$\widetilde{G}_{dd}^{r,a}(\omega) = \left[\omega - \overline{\varepsilon}_0 - \Sigma_T^{r,a}(\omega)\right]^{-1}, \tag{70}$$

where $\Gamma_\alpha^{\gtrless}(\omega) = \Gamma^\alpha(\omega) f_\alpha^{\gtrless}(\omega)$ and $\widetilde{G}_{dd}^{r,a}$ is derived from Eq.(60).

Eq.(18) can be recast into the effective expression derived by Wingreen and Meir[15], where the current is expressed as the product of the transport window and the tunneling function. Performing some algebra on Eq.(18), we get:

$$J_\alpha = \frac{ie}{h}\int d\omega\left[f_\alpha^{<}(\omega) - f_{\overline{\alpha}}^{<}(\omega)\right]T(\omega), \tag{71}$$

$$T(\omega) = \frac{\Gamma^L(\omega)\Gamma^R(\omega)}{\Gamma^L(\omega)+\Gamma^R(\omega)}A(\omega), \tag{72}$$

$$A(\omega) = i\sum_n p_n\left[\widetilde{G}_{dd}^{>}(\omega - n\omega_0) - \widetilde{G}_{dd}^{<}(\omega + n\omega_0)\right], \tag{73}$$

where $T(\omega)$ ($A(\omega)$) denotes the EVI tunneling (spectral) function for the vibrating QD (or SMT). Substituting the results of Eq.(69) back into Eq.(72), the EVI tunneling function $T(\omega)$ is written as

$$T(\omega) = \frac{\Gamma^L(\omega)\Gamma^R(\omega)}{\Gamma^L(\omega)+\Gamma^R(\omega)}\cdot \tag{74}$$
$$\sum_{n,n'=-\infty,\alpha}^{\infty}\frac{p_{-n}p_{n'}\Gamma_\alpha^{>}[\omega + (n+n')\omega_0] + p_n p_{-n'}\Gamma_\alpha^{<}[\omega + (n+n')\omega_0]}{[\omega + n\omega_0 - \widetilde{\varepsilon}_0(\omega + n\omega_0)]^2 + [W(\omega + n\omega_0)/2]^2},$$

where $\widetilde{\varepsilon}_0 = \overline{\varepsilon}_0(V_g) - \mathrm{Re}\,\Sigma_T^r(\omega)$ denotes the renormalized level position of the quantum dot state. $W(\omega) = -2\,\mathrm{Im}\,\Sigma_d^r(\omega)$ represents the life-time broadening (bandwidth).[19] it is worth mentioning that $T(\omega)$ possesses some symmetries such as $T(\omega, V_g, V_b) = T(\omega, V_g, -V_b)$, and

$$T(\omega = \widetilde{\varepsilon}_0 - \Delta\omega, -V_g, V_b) = T(\omega = \widetilde{\varepsilon}_0 + \Delta\omega, V_g, V_b).$$

3.3.2 Zero-Frequency Noise formula

Now we proceed to calculate the noise. Generally, the noise is the current correlation defined as $S_{\alpha\alpha'}(t,t') \equiv \langle\{\delta I_\alpha(t), \delta I_{\alpha'}(t')\}\rangle = \langle\{I_\alpha(t), I_{\alpha'}(t')\}\rangle - 2J_\alpha^2$, where $\delta I_\alpha(t) =$

$I_\alpha(t) - \langle I_\alpha(t)\rangle$ together with the stationary fact of $J_\alpha = \langle I_\alpha(t)\rangle = \langle I_{\alpha'}(t')\rangle$ are performed for previous description. Substituting the current operator of Eq.(56) into the definition of noise and taking the Fourier transform $S_{\alpha\alpha'}(\varepsilon) = \int_{-\infty}^{\infty} d(t-t')\, e^{i\varepsilon(t-t')} S_{\alpha\alpha'}(t-t')$ with $\varepsilon \to 0$[22][14][26], we obtain the current correlation from the zero-frequency noise (see Appendix E).

$$\begin{aligned} S_{\alpha\alpha'}(\varepsilon \to 0) &= \frac{2e^2}{h}\int d\omega \left\{ G^{>}_{dd}(\omega)\,\Sigma^{<}_{L}(\omega) + G^{<}_{dd}(\omega)\,\Sigma^{>}_{L}(\omega) \right. \\ &\quad \left. -2\Sigma^{<}_{L}(\omega)\,\Sigma^{>}_{L}(\omega)\,|G^{r}_{dd}|^2(\omega) - I^2_L(\omega) \right\}. \end{aligned} \tag{75}$$

In steady state, $\langle J\rangle = J_L = -J_R$, and the summation of current in Eq.(18), $J_L + J_R = 0$, ensures the relation $G^{\lessgtr}_{dd}(\omega) = \pm i \frac{\Gamma^{\lessgtr}_L(\omega)+\Gamma^{\lessgtr}_R(\omega)}{\Gamma_L(\omega)\Gamma_R(\omega)} T(\omega)$. Combining this relation and the integrand in Eq.(58), Eq.(75) is rewritten as

$$\begin{aligned} S = \frac{2e^2}{h}\int d\omega \left\{ \left[f^{<}_L(\omega)\, f^{>}_L(\omega) + f^{<}_R(\omega)\, f^{>}_R(\omega) \right] T(\omega) \right. \\ \left. + \left[f^{<}_L(\omega) - f^{<}_R(\omega) \right]^2 T(\omega)\left[1 - T(\omega)\right] \right\}. \end{aligned} \tag{76}$$

3.3.3 Thermal Noise and Shot Noise

The advantage of Eq.(76) is that all the EVI effects are kept in the dot system $T(\omega)$, not in the leads. Besides, the first term, which vanishes at zero temperature, means the thermal noise S_{th}. As the bias voltage is smaller than $k_B\mathcal{T}$, i.e. the equilibrium system, the second term (shot noise) disappears, and the equilibrium noise is $S_{th} = 4k_B\mathcal{T}G_T$, aka the Johnson-Nyquist formula. Here, the differential conductance is defined as $G_T = \frac{2e^2}{h}\int d\omega F_{th}(\omega)\, T(\omega)$, and

$$F_{th}(\omega) = \frac{1}{4k_B\mathcal{T}} \sum_{\alpha} \sec h^2 \left(\frac{\omega - \mu_\alpha}{2k_B\mathcal{T}} \right)$$

is referred to the thermal broadening function in the leads[27]. Considering the inverse case of $e|V_b| > k_B\mathcal{T}$, the second term of Eq.(76) dominates the non-equilibrium noise, which is basically proportional to the average current and inversely proportional to $1 - T(\omega)$, saying that the fluctuation of the electrical current due to the discreteness of the charge carriers

in mesoscopic devices behaves the fluctuation of the occupation number. If the particles randomly transmitted, i.e. uncorrected, then the shot noise is $S_P = 2e\langle I\rangle$, this is the shot noise which was firstly proposed by Schottky and was observed in vacuum diodes.

At zero temperature, the Fermi functions goes forward the step functions, and the weighting factors are given by $p_n = e^{-g}g^n/n!$ for $n \geqq 0$ and $p_n = 0$ for $n < 0$. Applying these rules on Eq.(76) leads to

$$S = \frac{2e^2}{h}\int_{\mu_R}^{\mu_L}\frac{d\omega}{2\pi}T(\omega)\left[1-T(\omega)\right], \tag{77}$$

$$\begin{aligned} T(\omega) &= \frac{\Gamma^L\Gamma^R}{\Gamma^L+\Gamma^R}e^{-2g}\sum_{n,n',\alpha}\frac{g^{(n+n')}}{n!n'!}\cdot \\ &\left\{\frac{\Gamma^\alpha\theta\left[\omega-(n+n')\omega_0-\mu_\alpha\right]}{\left[\omega-n\omega_0-\widetilde{\varepsilon}_0(\omega-n\omega_0)\right]^2+W^2_{\mathcal{T}=0}(\omega-n\omega_0)/4}\right. \\ &\left.+\frac{\Gamma^\alpha\theta\left[\mu_\alpha-\omega-(n+n')\omega_0\right]}{\left[\omega+n\omega_0-\widetilde{\varepsilon}_0(\omega+n\omega_0)\right]^2+W^2_{\mathcal{T}=0}(\omega+n\omega_0)/4}\right\}, \end{aligned} \tag{78}$$

where the life-time broadening is given by

$$W_{\mathcal{T}=0}(\omega) = e^{-g}\sum_{n,\alpha}\frac{g^n}{n!}\Gamma^\alpha\left[\theta(\omega-n\omega_0-\mu_\alpha)+\theta(\mu_\alpha-\omega-n\omega_0)\right], \tag{79}$$

different from previous studies with a mean-field approximation. For simplicity, we ignored the energy dependence of Γ^α (wide-band approximation) here and in the following. Furthermore, it can be checked that Eq.(76) also satisfies the symmetric relations such as $S(V_g,V_b) = S(V_g,-V_b)$, and $S(V_g,V_b) = S(-V_g,V_b)$. Next we study the stationary properties of the tunneling function, the current, and its zero-frequency noise according to Eq.(74), Eq.(71) and Eq.(76).

In general, there exist two sources of correlations in the mesoscopic device: The first is the Pauli principal for the non-interacting electrons, and the other is the EVI effect stemming from the vibrons, both effects are revealed in Eq.(78). Before study this tunneling coefficient, first of all, it is convenient to assume that the energy level of the QD is aligned with the chemical potential of leads. When applying an external bias to the leads, it is expected that the chemical potential in the leads would asymmetrically deviate from the level energy of the dot, that is, $\mu_{L(R)} = \overline{\varepsilon}_0(V_g=0) \pm eV_b/2$ and $\overline{\varepsilon}_0(V_g=0) = \frac{\mu_L+\mu_R}{2}$. The

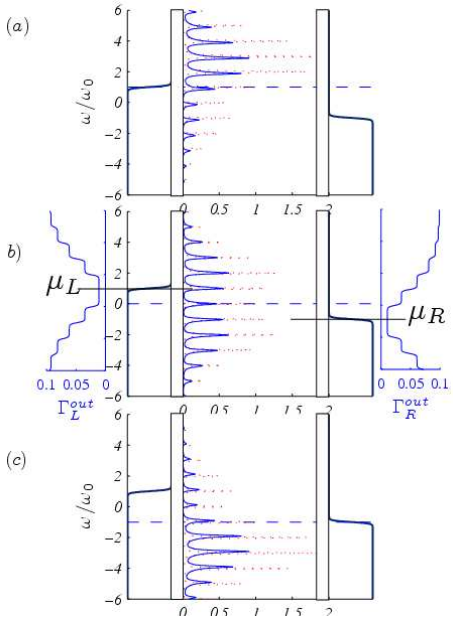

Figure 31: The density plot of the tunneling function. The left (right) inset in the middle figure depicts the distribution of the left (rigth) out-tunneling rate $\Gamma^{out}_{L(R)}$.

tunneling probabilities are depicted for high- and low-lying levels at $\overline{\varepsilon}_0 = \omega_0$ and $\overline{\varepsilon}_0 = -\omega_0$ in Fig. 31(a)(c) and for medium level at $\overline{\varepsilon}_0 = 0$ in Fig. 31(b), with the bias $eV_b = 2\omega_0$ and the tunneling rate $\Gamma_L = \Gamma_R = 0.4\omega_0$.

Fig. 31shows that the amplitude of tunneling function are distributed asymmetrically with respect to $\overline{\varepsilon}_0(\pm V_g)$ symmetrically for $\overline{\varepsilon}_0(eV_g = 0)$, implying the broken symmetry between electrons and holes in the QD (or SMT)[18]. In addition, it is found that the satellite peaks in the LT tunneling function are nonuniformly broaden, and its amplitude is much smaller than the MFT one[18]. This is because a staircase change of the vibron-assisted tunneling rate has been considered as the particle tunneling through the junction. Owing to the vibron emission and absorption, the statistical probabilities of finding n vibrons in occupied states and available states are different, breaking the electron-hole symmetry in the QD (or SMT). Generally, the electron states are located below the chemical potential of the leads, while the hole states are above. Such a non-uniform tunneling phenomenon results in a step-like tunneling rate (W_α) in energy space, with the symmetric centers at

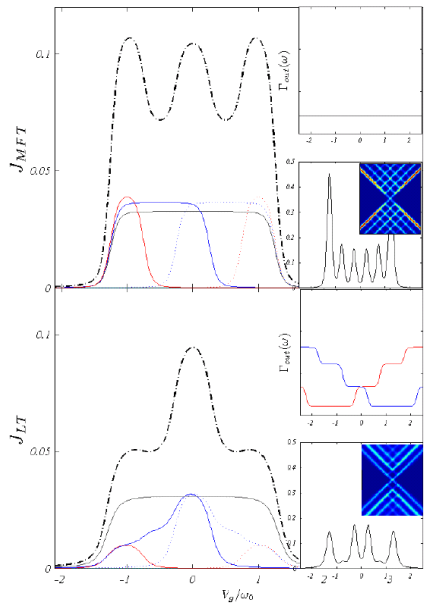

Figure 32: The current profile as a function of the gate voltage. The upper is wih the MFT method and the lower with the LT method. The upper inset in each figure denotes the total out-tunneling rate (or the level-broadening), where the blue (red) curve denotes for the left (right) out-tunneling rate. The lower inset depicts the corresponding differential conductance. The density plot of the conducatnce is accompnied attached.

μ_L and μ_R. The left (right) profile in Fig. 31(b) exhibits the vibron-assisted tunneling rate from the vibrating QD (or SMT) to the α lead, where the solid curve stands for the LT method, and the dashed line for the MFT one.[18] Note that the MFT tunneling rate remains constant, which coincides with the 0th vibron mode of the LT one, no matter whether the bias voltage is changed or not. This owes to the fact that the average-field approximation, i.e. $V_{k\alpha}X \to V_{k\alpha}\langle X\rangle$, is relevant to the time evolution of the vibron field, thus $F^{+><}(t-t') \to \langle X\rangle^2 = p_0$.

Fig. 32 shows the profile of the current as a function of the gate voltage. Compared to the MFT results (Up), we find that the LT current is strongly suppressed at $V_g/\omega_0 = \pm 0.75$ (Down). This can be understood as follows: In Eq.(18), the current is expressed as the tunneling function $T(\omega)$, multiplied by the transport window, $f_\alpha^<(\omega) - f_{\bar{\alpha}}^<(\omega)$. Basically, $T(\omega)$ is composed of $\widetilde{G}^>(\omega - n\omega_0)$ and $\widetilde{G}^<(\omega + n\omega_0)$, corresponding to the hole and electron occupation density, respectively. At zero temperature, $p_n = 0$ for $n < 0$, $f_\alpha^{\lessgtr}(\omega) \to \theta(\pm\mu_\alpha \mp \omega)$ and $\left|\widetilde{G}^r(\omega)\right|^2 = \widetilde{A}(\omega)/W_{\mathcal{T}=0}(\omega)$, and therefore the tunneling function $T(\omega)$ is expanded

as the summation of rectangular functions multiplied by the sideband peaks $A(\omega \pm n\omega_0)$. In the weak coupling limit, i.e. $A(\omega) \to 2\pi\delta(\omega)$, the current is found as:

$$\begin{aligned} J &= \frac{e}{\hbar}\frac{\Gamma^L\Gamma^R e^{-3g}}{\Gamma W_{\mathcal{T}=0}(\overline{\varepsilon}_0)} \sum_{n,n'=0}^{\infty} \frac{g^{(n+n')}\Gamma^\alpha}{n!n'!} \{[\theta(\mu_L - \overline{\varepsilon}_0 - n\omega_0) - \theta(\mu_R - \overline{\varepsilon}_0 - n\omega_0)] \\ &\quad \cdot \theta(\overline{\varepsilon}_0 - n'\omega_0 - \mu_\alpha) + [\theta(\mu_L - \overline{\varepsilon}_0 + n\omega_0) - \theta(\mu_R - \overline{\varepsilon}_0 + n\omega_0)] \\ &\quad \cdot \theta(\mu_\alpha - \overline{\varepsilon}_0 - n'\omega_0)\}, \end{aligned} \tag{80}$$

For the nth transport channel, electrons are allowed to transmit within $\mu_{\overline{\alpha}} < \omega < \mu_\alpha - n\omega_0$, and holes within $\mu_{\overline{\alpha}} + n\omega_0 < \omega < \mu_\alpha$. In addition, there exists a broadening function $W_{\mathcal{T}=0}(\overline{\varepsilon}_0)$ which renormalizes the current distribution (see Fig. 31(b2)). Note it stays the same ($W_{\mathcal{T}=0}(\overline{\varepsilon}_0) \to \Gamma$) in the MFT method. This effect results from the fact that the bias-associated information are included into the self-energy as the particle transport from the α lead to the $\overline{\alpha}$ lead, that is, the analytic continuation on Eq.(19). According to Eq.(79), $W^{-1}_{\mathcal{T}=0}(\overline{\varepsilon}_0)$ behaves as multiple decreasing steps at the resonant energies and symmetric about $eV_g = 0$, and hence the height of the electron (hole) current is suppressed along with the decrease (increase) of the gate voltage. Based on this, the peak-structure current at $eV_g/\omega_0 = \pm 0.75$ disappears, resulting in a remarkable conductance gap in Fig. 32(b).

3.3.4 Zero-frequency Noise

Now let we study the energy dependence of the shot noise. Fig. 33(a) to Fig. 33(d) shows the zero-frequency noise S vs V_g at various bias voltages, and the insets denote the differential noise. For comparison, we further plot the MFT noise as red dashed lines. For $eV_b/\omega_0 = 0.02$ (nearly zero dc bias), the current approaches zero. However, because the electrons tunneling through the QD can absorb or emit photons (here $n = 0$), the thermal noise changes significantly. It is noticed that no noise change occurs around $eV_g = n\omega_0$ ($n = \pm 1, \pm 2$, and so on) because the current stream is forbidden to flow. In other words, satellite peaks of the differential noise dS/dV_b do not occur in this area, as is shown in the inset of Fig. 34(a). These phenomena are different from previous theoretical predictions reported by Sun *et al.*[29] and Balatsky *et al.*[9] but agrees with the experimental observations[30] of the single resonant peak (see Fig. 28 and Fig. 29).

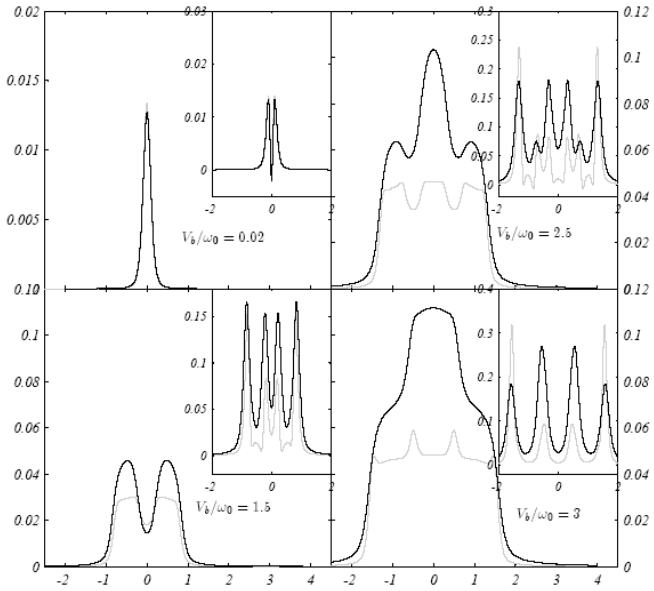

Figure 33: Zero-frequency noise vs. the gate voltage under four different bias voltage (form left to rgiht, $eV_b/\omega_0 = 0.02, 1.5, 2.5$ and 3). The insets denote the corresponding differential noise. The black line represents the LT method and the gray line for the MFT one. Noe that the shot noise is normalized by 2e

Fig. 34(a) depicts the detailed profiles for dS_{th}/dV_b (red curve) and dS_{ch}/dV_b (blue curve) vs. V_g, where the vibron-free case is labeled by dashed lines. Here, a sudden decline appears at $V_g = 0$ for the thermal noise because the PAT process is slightly forbidden by the Pauli exclusion principle[29].

3.3.5 Probing the EVI Coupling Strength

At $\mathcal{T} = 0$, the thermal noise vanishes, and a remarkable peak structure of dS_{ch}/dV_b is left, as seen in Fig. 34(a). This is different from the vibron-free case with a double-peak structure. Such behavior can be explained by the following: For $eV_b < \omega_0$, only the 0th channel makes the contribution, and the tunneling function of Eq.(78) reduces to

$$T_0(\omega) = \frac{\Gamma^L \Gamma^R e^{-g}}{(\omega - \overline{\varepsilon}_0)^2 + \left(\frac{\Gamma^L + \Gamma^R}{2} e^{-g}\right)^2}. \tag{81}$$

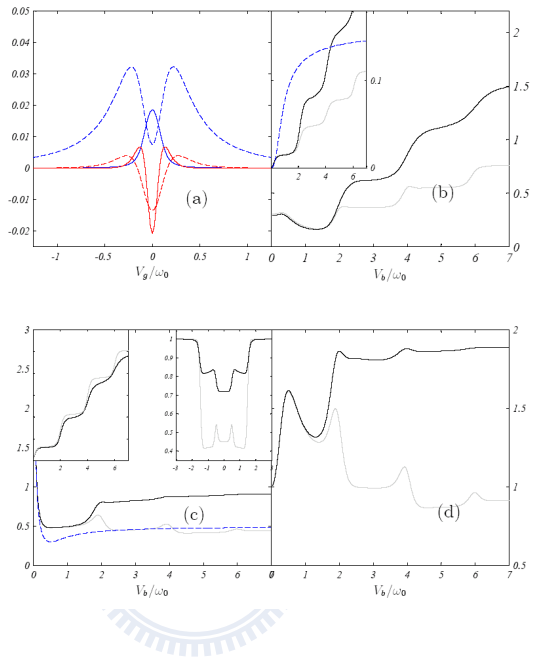

Figure 34: (a) dS_{th}/dV_b (red curve) and dS_{ch}/dV_b (blue curve) vs. V_g, the dashed lines denotes $\lambda = 0$ (no EPI) and the solid lines for $\lambda = 1.5\omega_0$. (b) The renormalized noise function S/S_0 vs. V_b, where S_0 is the noise without EPI. The black line denotes the LT method and the gray line as the MFT one. The inset reveals the original noise function S, an additional blue-dashed line is the noise without EPI. (c) The Fano factor vs. V_b. The left inset here denotes the corresponding noise and the right inset shows the Fano factor vs. V_g at $V_b = 6\omega_0$. (d) shows the renormalized factor (F/F_0) vs. V_b, we can see that they depart from each other at $V_b = 2\omega_0$.

Substituting Eq.(81) into Eq.(77) and taking the derivative over V_b, we obtain

$$\frac{dS}{dV_b} = \frac{2e^2}{h} \sum_{\alpha \in L,R} T_0\left(\mu_\alpha\right)\left[1 - T_0\left(\mu_\alpha\right)\right]. \tag{82}$$

In the equilibrium case, $\mu_L \approx \mu_R = \overline{\varepsilon}_0\left(V_g = 0\right)$, and a double-peak structure of Eq.(82) exists when $T_0\left(\overline{\varepsilon}_0\right) > 1/2$, that is,

$$\left(\Gamma^L + \Gamma^R\right)^2 e^{-\left(\frac{\lambda}{\omega_0}\right)^2} - 8\Gamma^L\Gamma^R < 0. \tag{83}$$

On the other hand, for the symmetric electron coupling $\Gamma^L = \Gamma^R = \Gamma$, the single peak structure of dS/dV_b appears as $\lambda > 0.83\omega_0$. This is useful in verifying the coupling strength of the EVI in the experiments.

Next, we examine the noise for $eV_b > \omega_0$. As shown from Fig. 32(b) to Fig. 32(d), large bias voltages yield a staircase noise with the steps occurring at the resonant energies and symmetric about $eV_g = 0$. This is in contrary to the MFT results, where the heights of the noise are close, analogous to that observed in current.

Thermal noise becomes significant with finite temperature. Performing the weak coupling limit on the first term of Eq.(76), we obtain

$$\begin{aligned} S_{th} &= \frac{2e^2}{h}\frac{\Gamma^L\Gamma^R}{\Gamma^2 W\left(\overline{\varepsilon}_0\right)} \sum_{n,n',\alpha,\alpha'} p_n p_{n'} \left\{ F_{th}\left(\overline{\varepsilon}_0 + n\omega_0 - \mu_\alpha\right)\Gamma^{>}_{\alpha'}\left(\overline{\varepsilon}_0 - n'\omega_0\right) \right. \\ &\left. + F_{th}\left(\overline{\varepsilon}_0 - n\omega_0 - \mu_\alpha\right)\Gamma^{<}_{\alpha'}\left(\overline{\varepsilon}_0 + n'\omega_0\right) \right\}, \end{aligned} \tag{84}$$

which exhibits peaks at $eV_g = \pm eV_b/2 \mp n\omega_0$, as shown in Fig. 32(d). Note that these peaks are not apparent in the LT curve because the LT shot noise is much larger than its thermal noise. As one plots S_{th} vs. V_b, we find that thermal broadening peaks occurs at $eV_b = 2n\omega_0$. Nonetheless, due to the staircase structure of the vibron-assoicated tunneling rate $W\left(\overline{\varepsilon}_0\right)$, LT thermal noise decays faster than the MFT one along with the increasing bias, as shown in Fig. 32(b). In the large bias limit, e.g. $\mu_L \gg \mu_R$, $f^{<}_L = f^{>}_R = 1$, $f^{>}_L = f^{<}_R = 0$, the thermal noise vanishes and the shot noise are found as

$$S = 2e\left\langle I\right\rangle \left\{ 1 - \frac{2\Gamma^L\Gamma^R}{\Gamma} \sum_{n,n'=-\infty}^{\infty} \frac{\left(p^L_n\gamma^L + p_{-n}\gamma^R\right)\left(p_{n'}\gamma^L + p_{-n'}\gamma^R\right)}{\left(\gamma^L + \gamma^R\right)\left[\left(\gamma^L + \gamma^R\right)^2 + \left(n - n'\right)^2\omega_0^2\right]} \right\},. \tag{85}$$

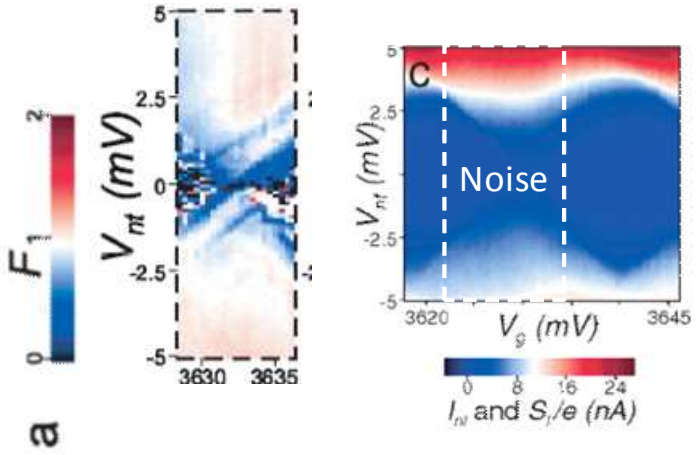

Figure 35: The density plot of the Fano factor as studied in a CNT-QD. Reprinted from Ref.[5].

where $\gamma^\alpha \to e^{-g}\Gamma^\alpha$ for the MFT method and $\gamma^\alpha \to \Gamma^\alpha$ for the LT one. It is noticeable that both approach result in the same current expression in large bias limit, that is, $\langle I\rangle = \frac{e}{\hbar}\frac{\Gamma^L\Gamma^R}{\Gamma}$ (see also in the left inset of Fig. 34(c)), but not for the shot noise (see the inset in Fig. 34 (b)), which implies that the shot noise gives additional and complementary information on the current-voltage characteristic. Substituting $\langle I\rangle$ and Eq.(85) back into the definition of the Fano factor and considering the primary correlation of $n = n'$, the Fano factors become $F_{MFT} \approx 1 - \frac{2\Gamma^L\Gamma^R}{\Gamma^2}e^g \sum_{n=-\infty}^{\infty}\left(p_n\Gamma^L + p_{-n}\Gamma^R\right)^2$ and $F_{LT} \approx 1 - \frac{2\Gamma^L\Gamma^R}{\Gamma^2}\sum_{n=-\infty}^{\infty}\left(p_n\Gamma^L + p_{-n}\Gamma^R\right)^2$, respectively. Apparently, F_{LT} shows the higher value than F_{MFT} due to the absence of e^g. In the absence of EVI effect ($\lambda \to 0$), Eq.(85) reduces to $S_0 = 2e\langle I\rangle\left(1 - 2\Gamma^L\Gamma^R/\left(\Gamma^L + \Gamma^R\right)^2\right)$, and we obtain $F = 0.5$ for the symmetric electron-electron coupling. This is in agreement with that observed in experiments[5], as shown in Fig. 35.

CHAPTER IV

SUMMARY AND FUTURE WORKS

By applying the small polaron transformation and the non-equilibrium Green's function (NEGF) technique, we examine the joint effects due to the vibron-assisted tunneling rate. We conclude that:

(1) As the vibrons coupled to the electron tunneling process, the relevant vibron correlation will break the electron-hole symmetry in the non-interacting terminals, making the tunneling rate change in a quantized feature of the vibration frequency.

(2) The electrons through a SMT can be remodeled into to a single-level quantum dot coupling to multi-channel leads, and the current is described as a sum of all tunneling flux via various channels.

(3) The conductance gap between the chemical potential of the leads and the first vibron excited state is in agreement with recent experimental results and is recognized as an occurrence of a virtual state.

(4) We can reproduce our results to that worked with the rate equation method, only if we replaced the single particle spectral function as delta function. That is, the NEGF approach gives more general information than the RE method, such as the energy shift and the level broadening.

(5) At high temperature, the holes may occupy higher energy levels above the chemical potential due to the absorption of vibrons, and thus we can measure conductance peaks in the Coulomb blockade region, in agreement with the recent CNT-QD experiments.

(6) When coupling to the vibrational modes, the zero-frequency noise still can be decomposed into the standard formation of thermal noise (Johnson–Nyquist noise) and the

shot noise, the same with that without EVI.

(7) In contrast to previous theoretical works of this kind with an anti-symmetric structure in noise and conductance, we obtain symmetric results, both in differential conductance and differential noise, fulfilling with recent CNT-QD experiments.

(8) We demonstrate that the differential noise could be a feasible tool for probing the EVI coupling strength.

(9) The first vibron excited state changes the noise, which is proportional to λ^4, not previous prediction λ^2. This is in agreement with the First principal calculation.

Finally, we have to admit that, in comparison with recent theoretical work done by Felix von Oppen's group, our method is insufficient to interpret the Franck-Condon blockade at low bias. Usually this behavior takes places in the strong electron-vibron interaction area. The lacking of suppression in our calculation is due to the usage of the equilibrium vibron assumption through the whole calculation. In the weak EVI, our results matches the experiments, including the conductance gap between the chemical potential od the leads and the position of the vibron sidebands. However, as the EVI is increased, the theoretical and experimental results are far from each other. We believe the difference lies on the assumption of the equilibrium vibron bath is insufficient to interpret the influence of vibrational motion of the atoms. In fact, it makes sense that the time scale of the vibron relaxation is comparable to the flow of the electrons into and out of the molecule. In the NEGF's calculation, the shorter life-time of the vibrons means more explicit calculation of the self-energy in vibron Green's function. We will briefly describe the numerical recipe of this project in the Appendix F.

In conclusion, we hope that this new transport scheme together with the noise formula could provide useful insights into the quantum transport field, and more studies, such as non-equilibrium vibrons bath, can be explored, allowing a systematic description of interesting physical effects in the future.

REFERENCES

[1] H. Park, J. Park, A. K. L. Lim, and E. H. Anderson, A. P. Alivisatos, and P. L. McEuen, Nature **407,** 57 (2000).

[2] J. Park, A. N. Pasupathy, J. I. Goldsmith, C. Chang, Y. Yaish, J. R. Petta, M. Rinkoski, J. P. Sethna, H. D. Abruña, P. McEuen and D. C. Ralph, Nature **417,** 722 (2002).

[3] L. H. Yu and D. Natelson, Nano Lett. **4**, 79(2004).

[4] S. Sapmaz, P. Jarillo-Herrero, J. Kong, C. Dekker, L.P. Kouwenhoven, and H.S.J. van der Zant, Phys. Rev. B **71**, 153402 (2005).

[5] S. Sapmaz, P. Jarillo-Herrero, Y.M. Blanter, C. Dekker, and H.S.J. van der Zant, Phys. Rev. Lett. **96**, 026801 (2006).

[6] E. Onac, F. Balestro, B. Trauzettel, C. F. J. Lodewijk, and L. P. Kouwenhoven, Phys. Rev. Lett. **96**, 026803 (2006).

[7] R. Leturcq, C. Stampfer, K. Inderbitzin, L. Durrer, C. Hierold, E. Mariani, M.G. Schultz, F. von Oppen, and K. Ensslin, Nature Physics **5**, 327 - 331 (2009).

[8] E.M. Weig, R. H. Blick, T. Brandes, J. Kirschbaum, W. Wegscheider, M. Bichler, and J.P. Kotthaus, Phys. Rev. Lett. **92**, 046804.

[9] J.-X. Zhu and A.V. Balatsky, Phys, Rev. B **67**, 165326 (2003).

[10] M. Galperin, A. Nitzan, and M. A. Ratner, Phys, Rev. B **73**, 045314 (2006).

[11] A.P. Jauho, N.S. Wingreen and Y. Meir, Phys. Rev. B **50**, 5528 (1994).

[12] A. Mitra, I. Aleiner, and A. J. Millis, Phys. Rev. B **69**, 245302 (2004).

[13] A. Zazunov, D. Feinberg, and T. Martin, Phys. Rev. B **73**, 115405 (2006); A. Zazunov and T. Martin, ibid. 76, 033417 (2007).

[14] H. Haug and A.P. Jauho, Quantum Kinetics in Transport and Optics of Semiconductors (Springer; 2nd edition, 2007).

[15] Y. Meir and N. S. Wingreen, Phys. Rev. Lett. **68**, 2512 (1992).

[16] G. D. Mahan, Many Particle Physics (Plenum, New York, 1981), Sec. 5.5B.

[17] D. C. Langreth and P. Nordlander, Phys. Rev. B **43**, 2541–2557 (1991).

[18] Z. Z. Chen, R. Lu and B.F. Zhu, Phys. Rev. B **71**, 165324 (2005).

[19] J. König, J. Schmid, H. Schoeller, and G. Schön, Phys. Rev. B **54**, 16820 (1996).

[20] J. König, H. Schoeller, and G. Schön, Phys. Rev. Lett. **76**, 1715 - 1718 (1996).

[21] M. Esposito and M. Galperin, Phys. Rev. B **79**, 205303 (2009).

[22] M. Galperin, A. Nitzan, and M. A. Ratner, Phys. Rev. B **76**, 035301 (2007).

[23] R. Landauer, Philos. Mag. **21**, 863 (1970).

[24] M. Büttiker, Phys. Rev. Lett. **57**, 1761 (1986).

[25] T. Kubis, C. Yeh, and P. Vogl, A. Benz, G. Fasching, and C. Deutsch, Phys. Rev. B **79**, 195323 (2009). T. Kubis and P. Vogl, J. Comput. Electron. **6**, 183 (2007).

[26] F. M. Souza, A.P. Jauho, and J. C. Egues, Phys, Rev. B **78**. 155303 (2008).

[27] S. Datta, Electronic Transport in Mesoscopic Systems (Cambridge University Press, 1997).

[28] B. Dong, H. L. Cui, and X. L. Lei, Phys, Rev. B**69**, 205315 (2004).

[29] Q. F. Sun, J. Wang, and T. H. Lin, Phys. Rev. B **61**: 13032 (2000).

[30] E. Onac, F. Balestro, B. Trauzettel, C. F. J. Lodewijk, and L. P. Kouwenhoven, Phys. Rev. Lett. **96**, 026803 (2006).

[31] R. H. Blick et al., Phys. Rev. B 62, 17 103 (2000).

[32] J. Kirschbaum et al., Appl. Phys. Lett. 81, 280 (2002).

[33] E.M. Höberger, T. Krämer, W. Wegscheider, and R. H. Blick, Appl. Phys. Lett. 82, 4160 (2003).

[34] I. G. Lang and Y. A. Firsov, Kinetic theory of semiconductors with low mobility, Sov.Phys. JETP 16, 1301 (1963).

[35] T. Brandes, B. Kramer, Phys. Rev. Lett. 83 (1999) 3021–3024.

[36] R. Aguado, T. Brandes, Phys. Rev. Lett. 92 (2004) 206601.

[37] S.A. Gurvitz, Ya.S. Prager, Phys. Rev. B 53 (1996) 15932–15943.

[38] S. Braig, K. Flensberg, Phys. Rev. B 68 (2003) 205324.

[39] R. Leturcq, C. Stampfer, K. Inderbitzin, L. Durrer, C. Hierold, E. Mariani,M.G. Schultz, F. von Oppen, K. Ensslin, Nat. Phys. 5 (2009) 327–331.

[40] J. Koch, Felix von Oppen, and A. V. Andreev, Phys. Rev. B 74, 205438 (2006).

[41] H. Birk, M. J. M. de Jong, and C. Schöenberger, Phys. Rev. Lett. 75, 1610–1613 (1995).

[42] Q.-F. Sun and Hong Guo, Phys, Rev. B **66**, 155308 (2002).

[43] K. C. Lin and D. S. Chuu, Phys. Rev. B **72**, 125314 (2005).

[44] L. P. Kadanoff, G. Baym: Quantum Statistical Mechanics (Benjamin, New York, 1962).

[45] Jens Koch and Felix von Oppen, Phys. Rev. B **72**, 113308 (2005).

[46] T. Brandes and B. Kramer, Phys. Rev. Lett. **83**, 3021–3024 (1999)

APPENDIX A

CALCULATION OF OCCUPATION DENSITY $G^{<}(\omega)$

A.1 Conservation Rule

In this appendix,we present the detailed derivation for $\widetilde{G}_{dd}^{<}(\omega)$ in Eq.(26). We follow the derivation proposed by Sun and Guo[42][43]. In the stationary limit, the occupation number operator of the system is zero, i.e., $\left\langle \dot{N}_d \right\rangle (t) = 0$, where $N_d = d^{+}d$ and $\left[\overline{H}_{cen(lead)}, N_d\right] = 0$. Using the equation-of-motion[11][14], we readily find

$$\begin{aligned} \frac{\partial}{\partial t}\left\langle N_d \right\rangle (t) &= J_L(t) + J_R(t) \\ &= \sum_{k\alpha \in L,R} \left[V_{k\alpha} G_{d,k\alpha}^{<}(t,t') - V_{k\alpha}^{*} G_{k\alpha,d}^{<}(t,t') \right]_{t' \to t}. \end{aligned} \tag{86}$$

The lesser Green's function can be derived using the S-matrix expansion and Langreth theorem. Here the contour-ordered Green's function can be obtained from Eq.(57). By using the analytic continuum[11][14][17] we get

$$\begin{aligned} G_{d,k\alpha}^{<}(t,t') = V_{k\alpha}^{*} \int dt_1 \Big\{ & \widetilde{G}_{dd}^{r}(t,t_1) \left[g_{k\alpha}(t_1,t') F^{+}(t_1,t') \right]^{<} \\ & + \widetilde{G}_{dd}^{<}(t,t_1) \left[g_{k\alpha}(t_1,t') F^{+}(t_1,t') \right]^{a} \Big\}, \end{aligned} \tag{87}$$

$$\begin{aligned} G_{k\alpha,d}^{<}(t,t') = V_{k\alpha} \int dt_1 \Big\{ & \left[g_{k\alpha}(t,t_1) F^{+}(t,t_1) \right]^{r} \widetilde{G}_{dd}^{<}(t_1,t') \\ & + \left[g_{k\alpha}(t,t_1) F^{+}(t,t_1) \right]^{<} \widetilde{G}_{dd}^{a}(t_1,t') \Big\}. \end{aligned} \tag{88}$$

Substituting Eq.(87) and Eq.(88) into Eq.(86) and then applying the Fourier transform, we obtain

$$\begin{aligned} & \int \frac{d\omega}{2\pi} \left[\widetilde{G}_{dd}^{r}(\omega) \textstyle\sum_{\alpha} \Sigma_{\alpha,n}^{<}(\omega) + \widetilde{G}_{dd}^{<}(\omega) \sum_{\alpha} \Sigma_{\alpha,n}^{a}(\omega) \right] \\ & = \int \frac{d\omega}{2\pi} \left[\textstyle\sum_{\alpha} \Sigma_{\alpha,n}^{r}(\omega) \widetilde{G}_{dd}^{<}(\omega) + \sum_{\alpha} \Sigma_{\alpha,n}^{<}(\omega) \widetilde{G}_{dd}^{a}(\omega) \right]. \end{aligned} \tag{89}$$

Eq.(89) has a particular solution when the left and right integrands are equivalent. By substituting $\Sigma_{\alpha,n}^{r,<}(\omega)$ (see Eq.(21) and Eq.(22)) into Eq.(89) and doing some simple algebra,

the lesser Green function is found as

$$\widetilde{G}_{dd}^{<}(\omega)=\frac{\mp i\sum\limits_{n,\alpha}p_{\mp n}\Gamma_{\alpha}(\omega+n\omega_{0})f_{\alpha}^{<}(\omega+n\omega_{0})\widetilde{A}_{d}(\omega)}{\sum\limits_{n,\alpha}\left[p_{n}\Gamma_{\alpha}(\omega+n\omega_{0})f_{\alpha}^{<}(\omega+n\omega_{0})+p_{-n}\Gamma_{\alpha}(\omega+n\omega_{0})f_{\alpha}^{>}(\omega+n\omega_{0})\right]}. \tag{90}$$

A.2 The Keldysh Formulation for EVI System

Using Langreth theorem on the Dyson equation of Eq.(60) for G_{dd} and performing the Fourier transform $G(\omega)=\int dte^{i\omega\tau}G(\tau)$, Eq.(60) leads to

$$\widetilde{G}_{dd}^{<}=\widetilde{G}_{dd}^{(0)<}+\widetilde{G}_{dd}^{(0)r}\Sigma_{T}^{r}\widetilde{G}_{dd}^{<}+\widetilde{G}_{dd}^{(0)r}\Sigma_{T}^{<}\widetilde{G}_{dd}^{<}+\widetilde{G}_{dd}^{(0)<}\Sigma_{T}^{a}\widetilde{G}_{dd}^{a}. \tag{91}$$

Eq.(91) can be written as

$$\begin{aligned}\widetilde{G}_{dd}^{<}&=\left[\widetilde{G}_{dd}^{(0)<}\left(1+\Sigma_{T}^{a}\widetilde{G}_{dd}^{a}\right)+\widetilde{G}_{dd}^{(0)r}\Sigma_{T}^{<}\widetilde{G}_{dd}^{a}\right]\left[1-\widetilde{G}_{dd}^{(0)r}\Sigma_{T}^{r}\right]^{-1}\\&=\widetilde{G}_{dd}^{(0)<}\left(1+\Sigma_{T}^{a}\widetilde{G}_{dd}^{a}\right)\left[1+\widetilde{G}_{dd}^{(0)r}\Sigma_{T}^{r}+\left(\widetilde{G}_{dd}^{(0)r}\Sigma_{T}^{r}\right)^{2}+...\right]+\\&\widetilde{G}_{dd}^{a}\Sigma_{T}^{<}\widetilde{G}_{dd}^{(0)r}\left[1+\widetilde{G}_{dd}^{(0)r}\Sigma_{T}^{r}+\left(\widetilde{G}_{dd}^{(0)r}\Sigma_{T}^{r}\right)^{2}+...\right].\end{aligned} \tag{92}$$

Regrouping the first infinity iteration into $\widetilde{G}_{dd}^{r}\Sigma_{T}^{r}$ and combing the second bracket together with $\widetilde{G}_{dd}^{(0)r}$ as $\widetilde{G}_{dd}^{r}$, Eq.(91) can be written in the form of

$$\widetilde{G}_{dd}^{<}=\left(1+\widetilde{G}_{dd}^{r}\Sigma_{T}^{r}\right)\widetilde{G}_{dd}^{(0)<}\left(1+\widetilde{G}_{dd}^{a}\Sigma_{T}^{a}\right)+\widetilde{G}_{dd}^{r}\Sigma_{T}^{<}\widetilde{G}_{dd}^{a}. \tag{93}$$

Due to $\widetilde{G}_{dd}^{(0)<}(\omega)=2\pi i f_{d}^{<}(\omega)\delta(\omega-\omega_{d})$ we obtain a formal Keldysh equation:

$$\widetilde{G}_{dd}^{<}=\widetilde{G}_{dd}^{r}\Sigma_{T}^{<}\widetilde{G}_{dd}^{a}, \tag{94}$$

where $\Sigma_{T}^{<}(\omega)$ is introduced in Eq.(61) and $\widetilde{G}_{dd}^{r,a}$ can be solved with the Dyson equation. Note that Eq.(94) is identical to Eq.(90), showing that our calculation for the occupation $G^{<}$ is self-consistent. When considering the imaginary part of $\widetilde{G}_{dd}^{<}(\omega)$, Eq.(94) gives the exact equivalent expression to Eq.(26).

APPENDIX B

LANG-FIRSOV TRANSFORMATION OF THE SMT

The SMT setup is described in Eq.(8)~Eq.(11). We want to eliminate the coupling between electrons and vibrons, i.e. Eq.(11). This can be explicitly removed by the canonical transformation $S = \frac{\lambda}{\omega_0} n_d \left(b^+ - b\right)$[34], where $n_d = d^+ d$. Based on the Baker-Campbell-Hausdorff formula[16], we have

$$e^S O e^{-S} = O + [S, O] + \frac{1}{2!}[S, [S, O]] + \frac{1}{3!}[S, [S, [S, O]]] + ... \tag{95}$$

The appliance of this transformation on the relevant operators leads to

$$\overline{d} = d e^{\frac{\lambda}{\omega_0}\left(b^+ - b\right)}, \tag{96}$$

$$\overline{n}_d = n_d, \tag{97}$$

$$\overline{b} = b - \frac{\lambda}{\omega_0} n_d, \tag{98}$$

$$\overline{c}_{k\alpha} = c_{k\alpha}. \tag{99}$$

Here the relations of $[n_d, d]_m = (-1)^m d$ and $[b^+ - b, b] = -1$ have been used. As a consequence, the Hamiltonian can be diagonalized as:

$$\overline{H} = \overline{H}_{cen} + \overline{H}_{lead} + \overline{H}_T,$$

$$\overline{H}_{cen} \equiv \overline{\varepsilon}_0 \left(V_g\right) d^+ d + \omega_0 b^+ b, \tag{100}$$

$$\overline{H}_{lead} = \sum_{k_\alpha, \alpha \in L,R} \varepsilon_{k_\alpha} c^+_{k_\alpha} c_{k_\alpha}, \tag{101}$$

$$\overline{H}_T = \sum_{k_\alpha, \alpha \in L,R} V_{k_\alpha} c^+_{k_\alpha} dX + h.c, \tag{102}$$

where $\overline{\varepsilon}_0 = \varepsilon_0 - \frac{\lambda^2}{\omega_0}$ and the function X represents a shift operator, given by

$$X \equiv \exp\left[\frac{\lambda}{\omega_0}\left(b^+ - b\right)\right]. \tag{103}$$

For the time-dependent displacement function, we have

$$\begin{aligned} X(t) &= e^{i\omega_0 b^+ bt} X e^{-i\omega_0 b^+ bt} \\ &= e^{-\left(\frac{\lambda}{\omega_0}\right)^2/2} \cdot e^{i\omega_0 b^+ bt} \exp\left[\frac{\lambda}{\omega_0}\left(-b^+ + b\right)\right] e^{-i\omega_0 b^+ bt}. \end{aligned} \tag{104}$$

As the Feynman's disentangling theorem is applied, that is, $e^{A+B} = e^A e^B e^{-[A,B]/2}$, Eq.(104) can be further written as

$$X(t) = e^{-\left(\frac{\lambda}{\omega_0}\right)^2/2} \cdot \left(e^{i\omega_0 b^+ bt} e^{-\frac{\lambda}{\omega_0} b^+} e^{-i\omega_0 b^+ bt}\right) \cdot \left(e^{i\omega_0 b^+ bt} e^{\frac{\lambda}{\omega_0} b} e^{-i\omega_0 b^+ bt}\right), \tag{105}$$

where

$$\begin{aligned} e^{i\omega_0 b^+ bt} e^{-\frac{\lambda}{\omega_0} b^+} e^{-i\omega_0 b^+ bt} &= \sum_{n=0} \frac{\left(-\frac{\lambda}{\omega_0}\right)^n}{n!} b^n e^{-i\omega_0 nt} \\ &= e^{-\frac{\lambda}{\omega_0} b e^{-i\omega_0 t}}, \end{aligned} \tag{106}$$

and

$$e^{i\omega_0 b^+ bt} e^{\frac{\lambda}{\omega_0} b} e^{-i\omega_0 b^+ bt} = e^{\frac{\lambda}{\omega_0} b e^{-i\omega_0 t}}. \tag{107}$$

Taking these back into Eq.(105), we have

$$\begin{aligned} X(t) &= e^{-\left(\frac{\lambda}{\omega_0}\right)^2/2} \cdot e^{-\frac{\lambda}{\omega_0} b e^{-i\omega_0 t}} \cdot e^{\frac{\lambda}{\omega_0} b e^{-i\omega_0 t}} \\ &= e^{-\left(\frac{\lambda}{\omega_0}\right)^2/2} \cdot \exp\left[-\frac{\lambda}{\omega_0}\left(b^+ e^{i\omega_0 t} - b e^{-i\omega_0 t}\right)\right] \end{aligned} \tag{108}$$

and its conjugate is

$$X^+(t) = e^{-\left(\frac{\lambda}{\omega_0}\right)^2/2} \cdot \exp\left[-\frac{\lambda}{\omega_0}\left(b e^{-i\omega_0 t} - b^+ e^{i\omega_0 t}\right)\right] \tag{109}$$

APPENDIX C

THE ELECTRON-VIBRON CORRELATION $F(T,T')$

For the calculation of the function $F(t,t')$, we need to introduce the function

$$F\left(t,t'\right)=\left\langle X\left(t\right)X^{+}\left(t'\right)\right\rangle =\frac{\sum_{n=0}^{\infty}\left\langle n\right|e^{-\beta\omega_{0}b^{+}b}X\left(t\right)X^{+}\left(t'\right)\left|n\right\rangle }{\sum_{n=0}^{\infty}\left\langle n\right|e^{-\beta\omega_{0}b^{+}b}\left|n\right\rangle } \tag{110}$$

where $|n\rangle=\left(b^{+}\right)^{n}|0\rangle/\sqrt{n!}$ is the bosonic state with n vibrons and the denominator part of Eq.(110) equals

$$\sum_{n=0}^{\infty}\left\langle n\right|e^{-\beta\omega_{0}b^{+}b}\left|n\right\rangle =\frac{1}{1-e^{-\beta\omega_{0}}}=e^{\beta\omega_{0}}/\left(e^{\beta\omega_{0}}-1\right)=e^{\beta\omega_{0}}N_{0}.$$

N_0 is the Bose-Einstein distribution. Now we take the time-dependent vibron operator $X(t)$ and $X^{+}(t')$ from Eq.(108) and Eq.(109), the function $F(t,t')$ then gives

$$\begin{aligned}F\left(t,t'\right) &= \frac{e^{-\beta\omega_{0}}}{N_{0}}\sum_{n=0}^{\infty}e^{-n\beta\omega_{0}}e^{-\left(\frac{\lambda}{\omega_{0}}\right)^{2}}\cdot \\ &\quad \left\langle n\right|\exp\left[-\frac{\lambda}{\omega_{0}}\left(b^{+}e^{i\omega_{0}t}-be^{-i\omega_{0}t}\right)\right]\exp\left[-\frac{\lambda}{\omega_{0}}\left(be^{-i\omega_{0}t'}-b^{+}e^{i\omega_{0}t'}\right)\right]\left|n\right\rangle \\ &= \frac{e^{-\beta\omega_{0}}}{N_{0}}\sum_{n=0}^{\infty}e^{-n\beta\omega_{0}}e^{-\left(\frac{\lambda}{\omega_{0}}\right)^{2}}\left\langle n\right|e^{-\frac{\lambda}{\omega_{0}}b^{+}e^{i\omega_{0}t}}e^{\frac{\lambda}{\omega_{0}}be^{-i\omega_{0}t}}e^{\frac{\lambda}{\omega_{0}}b^{+}e^{-i\omega_{0}t'}}e^{-\frac{\lambda}{\omega_{0}}be^{-i\omega_{0}t'}}\left|n\right\rangle .\end{aligned} \tag{111}$$

Next we have to switch b and b^{+} to make the destruction operators to the right. This can be done by performing

$$\begin{aligned}e^{\frac{\lambda}{\omega_{0}}be^{-i\omega_{0}t}}e^{\frac{\lambda}{\omega_{0}}b^{+}e^{-i\omega_{0}t'}} &= e^{\frac{\lambda}{\omega_{0}}b^{+}e^{-i\omega_{0}t'}}\left(e^{-\frac{\lambda}{\omega_{0}}b^{+}e^{-i\omega_{0}t'}}\cdot e^{\frac{\lambda}{\omega_{0}}be^{-i\omega_{0}t}}e^{\frac{\lambda}{\omega_{0}}b^{+}e^{-i\omega_{0}t'}}\right) \\ &= e^{\frac{\lambda}{\omega_{0}}b^{+}e^{-i\omega_{0}t'}}\cdot e^{\frac{\lambda}{\omega_{0}}be^{-i\omega_{0}t}}e^{-\left(\frac{\lambda}{\omega_{0}}\right)^{2}e^{-i\omega_{0}\left(t-t'\right)}}.\end{aligned} \tag{112}$$

As a result, b is shifted to the right and Eq.(111) can be written as

$$\begin{aligned}F\left(t,t'\right) &= \frac{e^{-\beta\omega_{0}}}{N_{0}}e^{-\left(\frac{\lambda}{\omega_{0}}\right)^{2}\left[1-e^{-i\omega_{0}\left(t-t'\right)}\right]}\sum_{n=0}^{\infty}e^{-n\beta\omega_{0}} \\ &\quad \left\langle n\right|\exp\left[\frac{\lambda}{\omega_{0}}b^{+}\left(e^{i\omega_{0}t'}-e^{i\omega_{0}t}\right)\right]\exp\left[-\frac{\lambda}{\omega_{0}}b\left(e^{-i\omega_{0}t'}-e^{-i\omega_{0}t}\right)\right]\left|n\right\rangle\end{aligned} \tag{113}$$

Owing to the fact that

$$b\left|n\right\rangle = \sqrt{n}\left|n-1\right\rangle, \tag{114}$$

$$b^2\left|n\right\rangle = \sqrt{n\left(n-1\right)}\left|n-2\right\rangle, \tag{115}$$

$$\cdots$$

$$b^m\left|n\right\rangle = \sqrt{\frac{n!}{(n-m)!}}\left|n-m\right\rangle, \tag{116}$$

therefore,

$$\exp\left[\frac{\lambda}{\omega_0}b\left(e^{-i\omega_0 t'}-e^{-i\omega_0 t}\right)\right]\left|n\right\rangle = \sum_{m=0}^{n}\frac{(-1)^m}{m!}\left[\frac{\lambda}{\omega_0}\left(e^{-i\omega_0 t'}-e^{-i\omega_0 t}\right)\right]^m\sqrt{\frac{n!}{(n-m)!}}\left|n-m\right\rangle \tag{117}$$

$$\left\langle n\right|\exp\left[-\frac{\lambda}{\omega_0}b^+\left(e^{i\omega_0 t'}-e^{i\omega_0 t}\right)\right] = \left\langle n-m\right|\sum_{m=0}^{n}\frac{1}{m!}\left[\frac{\lambda}{\omega_0}\left(e^{-i\omega_0 t'}-e^{-i\omega_0 t}\right)\right]^m\sqrt{\frac{n!}{(n-m)!}} \tag{118}$$

The combination of Eq.(117) and Eq.(118) leads to

$$\begin{aligned}
&\left\langle n\right|\exp\left[-\frac{\lambda}{\omega_0}b^+\left(e^{i\omega_0 t'}-e^{i\omega_0 t}\right)\right]\exp\left[-\frac{\lambda}{\omega_0}b\left(e^{-i\omega_0 t'}-e^{-i\omega_0 t}\right)\right]\left|n\right\rangle \qquad (119)\\
&= \sum_{m=0}^{n}\frac{(-1)^m}{m!}\frac{n!}{m!\,(n-m)!}\left[\frac{\lambda}{\omega_0}\left(e^{-i\omega_0 t'}-e^{-i\omega_0 t}\right)\right]^{2m}\\
&= L_n\left[\left(\frac{\lambda}{\omega_0}\right)^2\left(e^{-i\omega_0 t'}-e^{-i\omega_0 t}\right)^2\right],
\end{aligned}$$

where $L_n\left(z\right)$ is the Laguerre polynomials. As a consequence,

$$F\left(t,t'\right) = \frac{e^{-\beta\omega_0}}{N_0}e^{-\left(\frac{\lambda}{\omega_0}\right)^2\left[1-e^{-i\omega_0\left(t-t'\right)}\right]}\sum_{n=0}^{\infty}e^{-n\beta\omega_0}L_n\left[\left(\frac{\lambda}{\omega_0}\right)^2\left(e^{-i\omega_0 t'}-e^{-i\omega_0 t}\right)^2\right]. \tag{120}$$

With the identical relation of $\sum_{n=0}^{\infty}y^n L_n\left(x\right) = \left(1-y\right)^{-1}e^{\frac{xy}{y-1}}$ and the replacement of y by $e^{-\beta\omega_0}$, Eq.(120) can be simplified as

$$F\left(t,t'\right) = \exp\left\{-\left(\frac{\lambda}{\omega_0}\right)^2\left[\left(1-e^{-i\omega_0\left(t-t'\right)}\right)\left(N_0+1\right)+\left(1-e^{i\omega_0\left(t-t'\right)}\right)N_0\right]\right\}. \tag{121}$$

The Fourier transform of Eq.(121) then leads to

$$F\left(\omega\right) = \sum_{n=0}^{\infty}p_n\delta\left(\omega-n\omega_0\right), \tag{122}$$

$$p_n = e^{-\left(\frac{\lambda}{\omega_0}\right)^2\left(1+2N_0\right)}e^{n\omega_0/2k_BT}I_n\left(2\left(\frac{\lambda}{\omega_0}\right)^2\sqrt{N_0\left(N_0+1\right)}\right), \tag{123}$$

where $I_n\left(z\right)$ is the nth Bessel function of the complex argument.

APPENDIX D

AN EXACTLY SOLVABLE MODEL

We examine the simple case of a single-resonant quantum dot, which is an idealistic model with spin-degenerate, non-interacting level, and coupled to two leads. According to Ref.[11], the generalized current formula can be obtained by

$$I = \frac{e}{h}\int d\omega \frac{\Gamma^L(\omega)\Gamma^R(\omega)}{\Gamma^L(\omega)+\Gamma^R(\omega)}\left[f_\alpha^<(\omega)-f_{\bar{\alpha}}^<(\omega)\right]A(\omega), \tag{124}$$

$$A(\omega) = \frac{\Gamma(\omega)}{(\omega-\varepsilon_0)^2+(\Gamma(\omega)/2)^2}. \tag{125}$$

Considering the wide-band limit of $\Gamma^\alpha(\omega)\to\Gamma^\alpha$, Eq.(124) can be solved as

$$\begin{aligned} I = {} & \frac{e}{h}\frac{\Gamma^L\Gamma^R}{\Gamma^L+\Gamma^R}\mathrm{Im}\left\{\psi\left(\frac{1}{2}+\frac{1}{4\pi k_BT}+i\frac{\omega-\mu_L}{2\pi k_BT}\right)\right. \\ & \left.-\psi\left(\frac{1}{2}+\frac{1}{4\pi k_BT}+i\frac{\omega-\mu_R}{2\pi k_BT}\right)\right\}, \end{aligned} \tag{126}$$

where the relation of $\mathrm{Im}\,\psi(z)=\frac{\pi}{2}\tanh(\pi z)$ has been used, and $\psi(z)$ denotes the digamma function. In order to understand the effects of the resonant tunneling processes, we consider the lowest order contributions. This can be solved by expanding Eq.(126) in orders of Γ, which gives

$$\begin{aligned} I = {} & \frac{e}{h}\frac{\Gamma^L\Gamma^R}{\Gamma^L+\Gamma^R}\left[f_L^<(\varepsilon_0)-f_R^<(\varepsilon_0)\right] \\ & +\frac{e}{h}\frac{\beta}{2\pi}\Gamma^L\Gamma^R\mathrm{Im}\left\{\psi'\left(\frac{1}{2}+\frac{1}{4\pi k_BT}+i\frac{\omega-\mu_L}{2\pi k_BT}\right)\right. \\ & \left.-\psi'\left(\frac{1}{2}+\frac{1}{4\pi k_BT}+i\frac{\omega-\mu_R}{2\pi k_BT}\right)\right\}+... \end{aligned} \tag{127}$$

where the first term corresponds to the sequential tunneling current and the second term reflects the co-tunneling current. The detailed discussion can be referred to Ref.[40].

APPENDIX E

THE CALCULATION OF ZERO-FREQUENCY NOISE $S_{\alpha\alpha'}(0)$

Here we study the noise for a single-level quantum dot coupled to a vibronic degrees of freedom.

$$\begin{aligned} S_{\alpha\alpha'}(t,t') &= \left\langle \left\{ \delta I_\alpha(t), \delta I_{\alpha'}(t') \right\} \right\rangle \\ &= \left\langle \left[I_\alpha(t) - J_\alpha \right] \left[I_{\alpha'}(t') - J_{\alpha'} \right] + \left[I_{\alpha'}(t') - J_{\alpha'} \right] \left[I_\alpha(t) - J_\alpha \right] \right\rangle \\ &= \left\langle I_\alpha(t) I_{\alpha'}(t') \right\rangle + \left\langle I_{\alpha'}(t') I_\alpha(t) \right\rangle \\ &\quad -2 \left\langle I_\alpha(t) \right\rangle J_{\alpha'} - 2J_\alpha \left\langle I_{\alpha'}(t') \right\rangle + 2J_\alpha J_{\alpha'}. \end{aligned} \tag{128}$$

Note that in the stationary state $\langle I_\alpha(t) \rangle = \langle I_\alpha(t') \rangle = J_\alpha$, and $J_\alpha = J_{\alpha'} = J$. Thus the noise function becomes

$$S_{\alpha\alpha'}(t,t') = \left\langle I_\alpha(t) I_{\alpha'}(t') \right\rangle + \left\langle I_{\alpha'}(t') I_\alpha(t) \right\rangle - 2J^2. \tag{129}$$

Using the current definition of

$$I_\alpha(t) = \frac{ie}{\hbar} \sum_{k\alpha} \left[V_{k\alpha} c_{k\alpha}^+(t) d(t) - V_{k\alpha} d^+(t) c_{k\alpha}(t) \right], \tag{130}$$

Eq.(129) can be found as

$$\begin{aligned} S_{\alpha\alpha'}(t,t') &= -\frac{e^2}{\hbar^2} \sum_{k\alpha,k\alpha'} \left[V_{k\alpha} V_{k\alpha'} \left\langle c_{k\alpha}^+(t) d(t) c_{k\alpha'}^+(t') d(t') \right\rangle - \right. \\ &\quad V_{k\alpha} V_{k\alpha'}^* \left\langle c_{k\alpha}^+(t) d(t) d^+(t') c_{k\alpha'}(t') \right\rangle \\ &\quad V_{k\alpha}^* V_{k\alpha'} \left\langle d^+(t) c_{k\alpha}(t) c_{k\alpha'}^+(t') d(t') \right\rangle \\ &\quad \left. V_{k\alpha}^* V_{k\alpha'} \left\langle d^+(t) c_{k\alpha}(t) d^+(t') c_{k\alpha'}(t') \right\rangle + h.c. - 2J^2 \right]. \end{aligned} \tag{131}$$

Each $\langle ... \rangle$ in Eq.(131) denotes the two-particle Green's functions. In the non-equilibrium case, these functions are evolving in the contour plane, and they are defined as

$$G^{(2)}_{1(cd)}\left(\tau,\tau'\right) = i^2\left\langle T_c c^+_{k\alpha}\left(\tau\right) d\left(\tau\right) X\left(\tau\right) c^+_{k\alpha'}\left(\tau'\right) d\left(\tau'\right) X\left(\tau'\right)\right\rangle, \quad (132)$$

$$G^{(2)}_{2(cd)}\left(\tau,\tau'\right) = i^2\left\langle T_c c^+_{k\alpha}\left(\tau\right) d\left(\tau\right) X\left(\tau\right) d^+\left(\tau'\right) X^+\left(\tau'\right) c_{k\alpha'}\left(\tau'\right)\right\rangle, \quad (133)$$

$$G^{(2)}_{3(cd)}\left(\tau,\tau'\right) = i^2\left\langle T_c d^+\left(\tau\right) X^+\left(\tau\right) c_{k\alpha}\left(\tau\right) c^+_{k\alpha'}\left(\tau'\right) d\left(\tau'\right) X\left(\tau'\right)\right\rangle, \quad (134)$$

$$G^{(2)}_{4(cd)}\left(\tau,\tau'\right) = i^2\left\langle T_c d^+\left(\tau\right) X^+\left(\tau\right) c_{k\alpha}\left(\tau\right) d^+\left(\tau'\right) X^+\left(\tau'\right) c_{k\alpha'}\left(\tau'\right)\right\rangle, \quad (135)$$

and Eq.(131) equals

$$S_{\alpha\alpha'}\left(t,t'\right) = -\frac{e^2}{\hbar^2}\sum_{k\alpha,k\alpha'}\Big[V_{k\alpha}V_{k\alpha'}G^{(2)>}_{1(cd)}\left(\tau,\tau'\right) - V_{k\alpha}V^*_{k\alpha'}G^{(2)>}_{2(cd)}\left(\tau,\tau'\right) + V^*_{k\alpha}V_{k\alpha'}G^{(2)>}_{3(cd)}\left(\tau,\tau'\right) - V^*_{k\alpha}V_{k\alpha'}G^{(2)>}_{4(cd)}\left(\tau,\tau'\right) + h.c. - 2J_L^2\Big]. \quad (136)$$

Next we need an expression for $G^{(2)}_{1,2,3,4}\left(\tau,\tau'\right)$.The Dyson equation for $G^{(2)}_1\left(\tau,\tau'\right)$ gives

$$\begin{aligned} G^{(2)}_{1(cd)}\left(\tau,\tau'\right) &= -\int_{c1}d\tau_1\int_{c2}d\tau_2\sum_{k_1,k_2}V_{k_1}V^*_{k_2}\left[\left\langle T_c c^+_{k\alpha}\left(\tau\right) c^+_{k\alpha'}\left(\tau'\right) c_{k_1}\left(\tau_1\right) c_{k_2}\left(\tau_2\right)\right\rangle\right. \\ &\quad \left.\left\langle T_c d\left(\tau\right) X\left(\tau\right) d\left(\tau'\right) X\left(\tau'\right) d^+\left(\tau_1\right) X^+\left(\tau_1\right) d^+\left(\tau_2\right) X^+\left(\tau_2\right)\right\rangle\right] \\ &= \int_{c1}d\tau_1\int_{c2}d\tau_2\sum_{k_1,k_2}V_{k_1}V^*_{k_2}\Big[\delta_{k_1k\alpha}\delta_{k_2k\alpha'}g_{k\alpha}\left(\tau_1,\tau\right)g_{k\alpha'}\left(\tau_1,\tau\right) \\ &\quad -\delta_{k_1k\alpha}\delta_{k_2k\alpha'}g_{k\alpha'}\left(\tau_1,\tau\right)g_{k\alpha}\left(\tau_1,\tau\right)\Big] \\ &\quad \left\langle T_c d\left(\tau\right) X\left(\tau\right) d\left(\tau'\right) X\left(\tau'\right) d^+\left(\tau_1\right) X^+\left(\tau_1\right) d^+\left(\tau_2\right) X^+\left(\tau_2\right)\right\rangle\Big]. \\ &= -V_{k_1}V^*_{k_2}\int_{c1}d\tau_1\int_{c2}d\tau_2 g_{k_L}\left(\tau_1,\tau\right)g_{k'_L}\left(\tau_2,\tau'\right)G^{(2)}_{1(dd)}\left(\tau,\tau',\tau_1,\tau_2\right) \end{aligned} \quad (137)$$

and

$$G^{(2)}_{4(cd)}\left(\tau,\tau'\right) = -V_{k_1}V^*_{k_2}\int_{c1}d\tau_1\int_{c2}d\tau_2 g_{k\alpha}\left(\tau,\tau_1\right)g_{k\alpha'}\left(\tau',\tau_2\right)G^{(2)}_{4(dd)}\left(\tau,\tau',\tau_1,\tau_2\right) \quad (138)$$

The performance of the second order Dyson equation on Eq.(133) and Eq.(134) gives

$$\begin{aligned} G^{(2)}_{2(cd)}\left(\tau,\tau'\right) &= -\delta_{k\alpha k\alpha'} g_{k\alpha}\left(\tau',\tau\right) G^{(0)}\left(\tau,\tau'\right) - \int_{c1} d\tau_1 \int_{c2} d\tau_2 \\ &\quad \sum_{k_1,k_2} V_{k_1} V^*_{k_2} \Big[\delta_{k_1 k\alpha'} \delta_{k_L k_2} g_{k'_L}\left(\tau',\tau_1\right) g_{k_L}\left(\tau_2,\tau_1\right) - \\ &\quad - \delta_{k_1 k'_L} \delta_{k_L k_2} g_{k_L}\left(\tau',\tau\right) g_{k_L}\left(\tau_2,\tau_1\right)\Big] \\ &\quad \left\langle T_c d\left(\tau\right) X\left(\tau\right) d^+\left(\tau'\right) X^+\left(\tau'\right) d\left(\tau_1\right) X\left(\tau_1\right) d^+\left(\tau_2\right) X^+\left(\tau_2\right)\right\rangle \qquad (139) \\ &\approx -\delta_{k_L k'_L} g_{k_L}\left(\tau',\tau\right) G\left(\tau,\tau'\right) - \sum_{k_1,k_2} V_{k\alpha} V^*_{k\alpha'} \int_{c1} d\tau_1 \int_{c2} d\tau_2 \qquad (140) \\ &\quad g_{k'_L}\left(\tau',\tau_1\right) g_{k_L}\left(\tau_2,\tau\right) G^{(2)}_{4(dd)}\left(\tau,\tau',\tau_1,\tau_2\right), \end{aligned}$$

where we combine the first term of Eq.(139) together with the second term in the integral, yielding a formal Green's function $G\left(\tau,\tau'\right)$. Similarly, the function $G^{(2)}_{3(cd)}\left(\tau,\tau'\right)$ in Eq.(134) reads

$$\begin{aligned} G^{(2)}_{3(cd)}\left(\tau,\tau'\right) &= -\delta_{k\alpha k\alpha'} g_{k\alpha}\left(\tau',\tau\right) G\left(\tau',\tau\right) - \sum_{k_1,k_2} V_{k\alpha} V^*_{k\alpha'} \int_{c1} d\tau_1 \int_{c2} d\tau_2 \\ &\quad g_{k\alpha}\left(\tau,\tau_1\right) g_{k\alpha'}\left(\tau_2,\tau'\right) G^{(2)}_{3(dd)}\left(\tau,\tau',\tau_1,\tau_2\right). \qquad (141) \end{aligned}$$

Here

$$\begin{aligned} G^{(2)}_{1(dd)}\left(\tau,\tau',\tau_1,\tau_2\right) &= i^2 \left\langle T_c d\left(\tau\right) X\left(\tau\right) d^+\left(\tau_1\right) X^+\left(\tau_1\right) d^+\left(\tau_2\right) X^+\left(\tau_2\right) d\left(\tau'\right) X\left(\tau'\right)\right\rangle \qquad (142) \\ G^{(2)}_{2(dd)}\left(\tau,\tau',\tau_1,\tau_2\right) &= i^2 \left\langle T_c d\left(\tau\right) X\left(\tau\right) d\left(\tau_1\right) X\left(\tau_1\right) d^+\left(\tau_2\right) X^+\left(\tau_2\right) d^+\left(\tau'\right) X^+\left(\tau'\right)\right\rangle \qquad (143) \\ G^{(2)}_{3(dd)}\left(\tau,\tau',\tau_1,\tau_2\right) &= i^2 \left\langle T_c d\left(\tau\right) X\left(\tau\right) d\left(\tau_1\right) X\left(\tau_1\right) d^+\left(\tau_2\right) X^+\left(\tau_2\right) d^+\left(\tau'\right) X^+\left(\tau'\right)\right\rangle \qquad (144) \\ G^{(2)}_{4(dd)}\left(\tau,\tau',\tau_1,\tau_2\right) &= i^2 \left\langle T_c d\left(\tau\right) X\left(\tau\right) d^+\left(\tau_1\right) X^+\left(\tau_1\right) d^+\left(\tau_2\right) X^+\left(\tau_2\right) d\left(\tau'\right) X\left(\tau'\right)\right\rangle \qquad (145) \end{aligned}$$

The noise function now can be concluded as

$$\begin{aligned} S_{\alpha\alpha'}\left(\tau,\tau'\right) &= \frac{e^2}{\hbar^2}\left\{\sum_{k\alpha}\left|V_{k\alpha}\right|^2\left[g_{k\alpha}\left(\tau',\tau\right)G\left(\tau,\tau'\right)+g_{k\alpha}\left(\tau,\tau'\right)G\left(\tau',\tau\right)\right]\right. \\ &+\sum_{k\alpha,k\alpha'}\left|V_{k\alpha}\right|^2\left|V_{k\alpha'}\right|^2\int_{c1}d\tau_1\int_{c2}d\tau_2\times \\ &\Big[-g_{k\alpha}\left(\tau_1,\tau\right)g_{k\alpha'}\left(\tau_2,\tau'\right)G^{(2)}_{1(dd)}\left(\tau,\tau',\tau_1,\tau_2\right) \\ &+g_{k\alpha}\left(\tau_2,\tau\right)g_{k\alpha'}\left(\tau',\tau_1\right)G^{(2)}_{2(dd)}\left(\tau,\tau',\tau_1,\tau_2\right) \\ &-g_{k\alpha}\left(\tau,\tau_1\right)g_{k\alpha'}\left(\tau_2,\tau'\right)G^{(2)}_{3(dd)}\left(\tau,\tau',\tau_1,\tau_2\right) \\ &\left.-g_{k\alpha}\left(\tau,\tau_1\right)g_{k\alpha'}\left(\tau',\tau_2\right)G^{(2)}_{4(dd)}\left(\tau,\tau',\tau_1,\tau_2\right)\Big]\right\}+h.c. \end{aligned} \tag{146}$$

So far only the Wick's theorem has been applied for decoupling a non-interacting electron Green's function in the leads. Next, we need to determine two-particle dot Green's functions, as shown in Eq.(142)~Eq.(145). However, it is not trivial to calculate these functions since they contain interactions. As a result, we need to import a method to simplify our calculation. Usually, the Hatree-Fock approximation is one of the candidates to solve the problem since it admits a direct decomposition of many-body Green's function into pairs of single-particle Green's function. Therefore, the two-particle Green's functions are approximately described as:

$$G^{(2)}_{1(dd)}\left(\tau,\tau',\tau_1,\tau_2\right) \approx \left[G\left(\tau,\tau_2\right)G\left(\tau',\tau_1\right)-G\left(\tau,\tau_1\right)G\left(\tau',\tau_2\right)\right]F^{(2)}_1\left(\tau,\tau',\tau_1,\tau_2\right) \tag{147}$$

$$G^{(2)}_{2(dd)}\left(\tau,\tau',\tau_1,\tau_2\right) \approx \left[G\left(\tau,\tau'\right)G\left(\tau_1,\tau_2\right)-G\left(\tau,\tau_2\right)G\left(\tau_1,\tau'\right)\right]F^{(3)}_2\left(\tau,\tau',\tau_1,\tau_2\right) \tag{148}$$

$$G^{(2)}_{3(dd)}\left(\tau,\tau',\tau_1,\tau_2\right) \approx \left[G\left(\tau_1,\tau\right)G\left(\tau',\tau_2\right)-G\left(\tau',\tau\right)G\left(\tau_1,\tau_2\right)\right]F^{(3)}_3\left(\tau,\tau',\tau_1,\tau_2\right) \tag{149}$$

$$G^{(2)}_{4(dd)}\left(\tau,\tau',\tau_1,\tau_2\right) \approx \left[G\left(\tau_2,\tau\right)G\left(\tau_1,\tau'\right)-G\left(\tau_1,\tau\right)G\left(\tau_2,\tau'\right)\right]F^{(4)}_4\left(\tau,\tau',\tau_1,\tau_2\right) \tag{150}$$

and the vibron correlation functions can be further calculated as

$$\begin{aligned} F^{(2)}_1\left(\tau,\tau',\tau_1,\tau_2\right) &= \left\langle T_c X\left(\tau\right)X^+\left(\tau_1\right)X^+\left(\tau_2\right)X\left(\tau'\right)\right\rangle \\ &= \left\langle T_c X\left(\tau\right)X^+\left(\tau_1\right)\right\rangle\left\langle T_c X^+\left(\tau_2\right)X\left(\tau'\right)\right\rangle+ \\ &\quad \left\langle T_c X\left(\tau\right)X^+\left(\tau_2\right)\right\rangle\left\langle T_c X^+\left(\tau_1\right)X\left(\tau'\right)\right\rangle+ \\ &\quad \left\langle T_c X\left(\tau\right)X\left(\tau'\right)\right\rangle\left\langle T_c X^+\left(\tau_1\right)X^+\left(\tau_2\right)\right\rangle \\ &\approx F\left(\tau,\tau_1\right)F^+\left(\tau',\tau_2\right)+F\left(\tau,\tau_2\right)F^+\left(\tau',\tau_1\right), \end{aligned} \tag{151}$$

and

$$F_2^{(2)}\left(\tau,\tau',\tau_1,\tau_2\right) = F\left(\tau,\tau_2\right)F\left(\tau_1,\tau'\right)+F\left(\tau_1,\tau_2\right)F\left(\tau,\tau'\right), \tag{152}$$

$$F_3^{(2)}\left(\tau,\tau',\tau_1,\tau_2\right) = F\left(\tau,\tau_2\right)F\left(\tau_1,\tau'\right)+F\left(\tau,\tau'\right)F\left(\tau_1,\tau_2\right), \tag{153}$$

$$F_3^{(2)}\left(\tau,\tau',\tau_1,\tau_2\right) = F\left(\tau,\tau_1\right)F^{+}\left(\tau',\tau_2\right)+F\left(\tau,\tau_2\right)F^{+}\left(\tau_1,\tau_2\right), \tag{154}$$

where we omit terms like $\left\langle T_c X^{(+)}\left(\tau\right)X^{(+)}\left(\tau'\right)\right\rangle$ in the stationary state. For further calculation, however, we include only the boson lines connected to the tunneling lines, and consequently we have

$$\begin{aligned} G_{1(dd)}^{(2)}\left(\tau,\tau',\tau_1,\tau_2\right) \approx & \left[G\left(\tau,\tau_2\right)G\left(\tau',\tau_1\right)F\left(\tau,\tau_2\right)F\left(\tau',\tau_1\right)\right. \\ & \left.-G\left(\tau,\tau_1\right)G\left(\tau',\tau_2\right)F\left(\tau,\tau_1\right)F\left(\tau',\tau_2\right)\right], \end{aligned} \tag{155}$$

$$\begin{aligned} G_{2(dd)}^{(2)}\left(\tau,\tau',\tau_1,\tau_2\right) \approx & \left[G\left(\tau,\tau'\right)G\left(\tau_1,\tau_2\right)F\left(\tau,\tau'\right)F\left(\tau_1,\tau_2\right)\right. \\ & \left.-G\left(\tau,\tau_2\right)G\left(\tau_1,\tau'\right)F\left(\tau,\tau_2\right)F\left(\tau_1,\tau'\right)\right], \end{aligned} \tag{156}$$

$$\begin{aligned} G_{3(dd)}^{(2)}\left(\tau,\tau',\tau_1,\tau_2\right) \approx & \left[G\left(\tau_1,\tau\right)G\left(\tau',\tau_2\right)F\left(\tau_1,\tau\right)F\left(\tau',\tau_2\right)\right. \\ & \left.-G\left(\tau',\tau\right)G\left(\tau_1,\tau_2\right)F\left(\tau',\tau\right)F\left(\tau_1,\tau_2\right)\right], \end{aligned} \tag{157}$$

$$\begin{aligned} G_{4(dd)}^{(2)}\left(\tau,\tau',\tau_1,\tau_2\right) \approx & \left[G\left(\tau_2,\tau\right)G\left(\tau_1,\tau'\right)F\left(\tau_2,\tau\right)F\left(\tau_1,\tau'\right)\right. \\ & \left.-G\left(\tau_1,\tau\right)G\left(\tau_2,\tau'\right)F\left(\tau_1,\tau\right)F\left(\tau_2,\tau'\right)\right]. \end{aligned} \tag{158}$$

Substituting Eq.(155)~Eq.(158) into Eq.(146), we obtain

$$\begin{aligned} S_{\alpha\alpha'}^{dis}\left(\tau,\tau'\right) = & \frac{e^2}{\hbar^2}\left\{\sum_{k\alpha,k\alpha'}\left|V_{k\alpha}\right|^2\left|V_{k\alpha'}\right|^2\int_{c1}d\tau_1\int_{c2}d\tau_2\right. \\ & \left[g_{k\alpha}\left(\tau_1,\tau\right)g_{k\alpha'}\left(\tau_2,\tau'\right)G\left(\tau,\tau_1\right)G\left(\tau',\tau_2\right)F\left(\tau,\tau_1\right)F\left(\tau',\tau_2\right)\right. \\ & -g_{k\alpha}\left(\tau_2,\tau\right)g_{k\alpha'}\left(\tau',\tau_1\right)G\left(\tau,\tau_2\right)G\left(\tau_1,\tau'\right)F\left(\tau,\tau_2\right)F\left(\tau_1,\tau'\right) \\ & -g_{k\alpha}\left(\tau,\tau_1\right)g_{k\alpha'}\left(\tau_2,\tau'\right)G\left(\tau_1,\tau\right)G\left(\tau',\tau_2\right)F\left(\tau_1,\tau\right)F\left(\tau',\tau_2\right) \\ & \left.\left.-g_{k\alpha}\left(\tau,\tau_1\right)g_{k\alpha'}\left(\tau',\tau_2\right)G\left(\tau_1,\tau\right)G\left(\tau_2,\tau'\right)F\left(\tau_1,\tau\right)F\left(\tau_2,\tau'\right)\right]\right\}+h.c.. \end{aligned} \tag{159}$$

and

$$
\begin{aligned}
S_{\alpha\alpha'}^{con}\left(\tau,\tau'\right) &= \frac{e^2}{\hbar^2}\left\{\sum_{k\alpha}\left|V_{k\alpha}\right|^2\left[g_{k\alpha}\left(\tau',\tau\right)G\left(\tau,\tau'\right)+g_{k\alpha}\left(\tau,\tau'\right)G\left(\tau',\tau\right)\right]\right. \qquad (160)\\
&+\int_{c1}d\tau_1\int_{c2}d\tau_2\times\\
&\left[-\Sigma_{k\alpha}\left(\tau_1,\tau\right)\Sigma_{k\alpha'}\left(\tau_2,\tau'\right)G\left(\tau,\tau_2\right)G\left(\tau',\tau_1\right)F\left(\tau,\tau_2\right)F\left(\tau',\tau_1\right)\right.\\
&+\Sigma_{k\alpha}\left(\tau_2,\tau\right)\Sigma_{k\alpha'}\left(\tau',\tau_1\right)G\left(\tau,\tau'\right)G\left(\tau_1,\tau_2\right)F\left(\tau,\tau'\right)F\left(\tau_1,\tau_2\right)\\
&-\Sigma_{k\alpha}\left(\tau,\tau_1\right)\Sigma_{k\alpha'}\left(\tau_2,\tau'\right)G\left(\tau',\tau\right)G\left(\tau_1,\tau_2\right)F\left(\tau',\tau\right)F\left(\tau_1,\tau_2\right)\\
&\left.\left.-\Sigma_{k\alpha}\left(\tau,\tau_1\right)\Sigma_{k\alpha'}\left(\tau',\tau_2\right)G\left(\tau_2,\tau\right)G\left(\tau_1,\tau'\right)F\left(\tau_2,\tau\right)F\left(\tau_1,\tau'\right)\right]\right\}+h.c,
\end{aligned}
$$

with $\Sigma_{k\alpha}\left(\tau,\tau'\right)=\sum_{k\alpha}\left|V_{k\alpha}\right|^2 g_{k\alpha}\left(\tau,\tau'\right)$. Note that $S_{\alpha\alpha'}^{dis}\left(\tau,\tau'\right)$ does not contribute to the noise. When applying the Langreth rule on Eq.(159), we find

$$
\begin{aligned}
S_{\alpha\alpha'}^{dis>}\left(\tau,\tau'\right) &= \frac{e^2}{\hbar^2}\left\{\sum_{k\alpha,k\alpha'}\left|V_{k\alpha}\right|^2\left|V_{k\alpha'}\right|^2\int_{c1}d\tau_1\int_{c2}d\tau_2\right. \qquad (161)\\
&\left\{\left[g_{k\alpha}\left(\tau_1,\tau\right)g_{k\alpha'}\left(\tau_2,\tau'\right)G\left(\tau,\tau_1\right)G\left(\tau',\tau_2\right)F\left(\tau,\tau_1\right)F\left(\tau',\tau_2\right)\right]^{>}\right.\\
&-\left[g_{k\alpha}\left(\tau_2,\tau\right)g_{k\alpha'}\left(\tau',\tau_1\right)G\left(\tau,\tau_2\right)G\left(\tau_1,\tau'\right)F\left(\tau,\tau_2\right)F\left(\tau_1,\tau'\right)\right]^{>}\\
&-\left[g_{k\alpha}\left(\tau,\tau_1\right)g_{k\alpha'}\left(\tau_2,\tau'\right)G\left(\tau_1,\tau\right)G\left(\tau',\tau_2\right)F\left(\tau_1,\tau\right)F\left(\tau',\tau_2\right)\right]^{>}\\
&\left.\left.-\left[g_{k\alpha}\left(\tau,\tau_1\right)g_{k\alpha'}\left(\tau',\tau_2\right)G\left(\tau_1,\tau\right)G\left(\tau_2,\tau'\right)F\left(\tau_1,\tau\right)F\left(\tau_2,\tau'\right)\right]^{>}\right\}\right\}+h.c.,
\end{aligned}
$$

where the first term with double integrations is solved with

$$
\begin{aligned}
&\left[V_{k\alpha}\int_{c1}d\tau_1 g_{k\alpha}\left(\tau_1,\tau\right)G\left(\tau,\tau_1\right)F\left(\tau,\tau_1\right)\cdot V_{k\alpha'}\int_{c2}d\tau_2 g_{k\alpha'}\left(\tau_2,\tau'\right)G\left(\tau',\tau_2\right)F\left(\tau',\tau_2\right)\right]^{>}\\
&= G_{d,k\alpha}^{>}\left(\tau,\tau\right)G_{d,k\alpha}^{>}\left(\tau',\tau'\right). \qquad (162)
\end{aligned}
$$

The remaining terms in Eq.(161) can be analyzed accordingly. When substituting Eq.(162)

and the disconnected terms into Eq.(161), we obtain

$$\begin{aligned} S_{\alpha\alpha'}^{dis}\left(t,t'\right) &= \frac{e^2}{\hbar^2}\sum_{k\alpha,k\alpha'}\Big[V_{k\alpha}V_{k\alpha'}G_{d,k\alpha}^{>}\left(\tau,\tau\right)G_{d,k\alpha}^{>}\left(\tau',\tau'\right) \\ &\quad -V_{k\alpha}V_{k\alpha'}^{*}G_{d,k\alpha}^{>}\left(\tau,\tau\right)G_{d,k\alpha'}^{>}\left(\tau',\tau'\right) \\ &\quad -V_{k\alpha}V_{k\alpha'}^{*}G_{d,k\alpha}^{>}\left(\tau,\tau\right)G_{d,k\alpha'}^{>}\left(\tau',\tau'\right) \\ &\quad +V_{k\alpha}V_{k\alpha'}^{*}G_{d,k\alpha}^{>}\left(\tau,\tau\right)G_{d,k\alpha'}^{>}\left(\tau',\tau'\right)\Big]+h.c. \\ &= 2\frac{e^2}{\hbar^2}\sum_{k\alpha,k\alpha'}\Big[V_{k\alpha}G_{d,k\alpha}^{>}\left(\tau,\tau\right)-V_{k\alpha}^{*}G_{d,k\alpha}^{>}\left(\tau,\tau\right)\Big] \\ &\quad \times\Big[V_{k\alpha'}G_{d,k\alpha'}^{>}\left(\tau',\tau'\right)-V_{k\alpha'}^{*}G_{d,k\alpha'}^{>}\left(\tau',\tau'\right)\Big] \\ &= 2J^2, \end{aligned}$$

which exactly cancels $2J^2$ in Eq.(128).

The appliance of the Langreth theorem on $S_{\alpha\alpha'}^{con}\left(\tau,\tau'\right)$ results in

$$\begin{aligned} S_{\alpha\alpha'}^{con>}\left(\tau,\tau'\right) &= \left(\frac{e}{\hbar}\right)^2\Big\{\left[\Sigma_{k\alpha}\left(\tau',\tau\right)G\left(\tau,\tau'\right)F\left(\tau,\tau'\right)+\Sigma_{k\alpha}\left(\tau,\tau'\right)G\left(\tau',\tau\right)F\left(\tau',\tau\right)\right]^{>} \\ &\quad +\int_c d\tau_1\int_c d\tau_2\times \\ &\quad \Big\{-\Sigma_{k\alpha}\left(\tau_1,\tau\right)\Sigma_{k\alpha'}\left(\tau_2,\tau'\right)G\left(\tau,\tau_1\right)G\left(\tau',\tau_2\right)F\left(\tau,\tau_1\right)F\left(\tau',\tau_2\right) \\ &\quad +\Sigma_{k\alpha}\left(\tau_1,\tau'\right)\Sigma_{k\alpha'}\left(\tau_2,\tau\right)G\left(\tau_1,\tau'\right)G\left(\tau,\tau_2\right)F\left(\tau_1,\tau'\right)F\left(\tau,\tau_2\right) \\ &\quad +\Sigma_{k\alpha}\left(\tau,\tau_1\right)\Sigma_{k\alpha'}\left(\tau_2,\tau'\right)G\left(\tau_1,\tau\right)G\left(\tau',\tau_2\right)F\left(\tau_1,\tau'\right)F\left(\tau,\tau_2\right) \\ &\quad -\Sigma_{k\alpha}\left(\tau,\tau_1\right)\Sigma_{k\alpha'}\left(\tau_2,\tau'\right)G\left(\tau_1,\tau\right)G\left(\tau_2,\tau'\right)F\left(\tau_1,\tau'\right)F\left(\tau,\tau_2\right)\Big\}^{>}+(163) \end{aligned}$$

where the first term in Eq.(163) gives

$$\begin{aligned} &\left[\Sigma_{k\alpha}\left(\tau',\tau\right)G\left(\tau,\tau'\right)F\left(\tau,\tau'\right)+\Sigma_{k\alpha}\left(\tau,\tau'\right)G\left(\tau',\tau\right)F\left(\tau',\tau\right)\right]^{>} \qquad (164) \\ &=\Sigma_{k\alpha}^{<}\left(t',t\right)G^{>}\left(t,t'\right)F^{>}\left(t,t'\right)+\Sigma_{k\alpha}^{>}\left(t,t'\right)G^{<}\left(t',t\right)F^{<}\left(t',t\right). \end{aligned}$$

The terms with the double integrations are

$$\int d\tau_1 \left[G\left(\tau',\tau_1\right)F\left(\tau',\tau_1\right)\Sigma_{k\alpha}\left(\tau_1,\tau\right)\right]^{<}\cdot\int d\tau_2\left[G\left(\tau,\tau_2\right)F\left(\tau,\tau_2\right)\Sigma_{k\alpha'}\left(\tau_2,\tau'\right)\right]^{>}$$
$$=\int dt_1\left\{\left[G\left(\tau',\tau_1\right)F\left(\tau',\tau_1\right)\right]^{r}\Sigma^{<}_{k\alpha}\left(t_1,t\right)+\left[G\left(\tau',\tau_1\right)F\left(\tau',\tau_1\right)\right]^{<}\Sigma^{a}_{k\alpha}\left(t',t_1\right)\right\}\times$$
$$\int dt_2\left\{\left[G\left(\tau,\tau_2\right)F\left(\tau,\tau_2\right)\right]^{r}\Sigma^{>}_{k\alpha}\left(t_2,t'\right)+\left[G\left(\tau,\tau_2\right)F\left(\tau,\tau_2\right)\right]^{>}\Sigma^{a}_{k\alpha}\left(t_2,t'\right)\right\}, \tag{165}$$

and

$$\left[G\left(\tau,\tau'\right)\int d\tau_2\int d\tau_1\Sigma_{k\alpha'}\left(\tau',\tau_1\right)G\left(\tau_1,\tau_2\right)F\left(\tau_1,\tau_2\right)\Sigma^{+}_{L'}\left(\tau_2,\tau'\right)\right]$$
$$=G\left(\tau,\tau'\right)\int dt_1\int dt_2\begin{pmatrix}\Sigma^{r}_{k\alpha'}\left(t',t_1\right)\left[G\left(\tau_1,\tau_2\right)F\left(\tau_1,\tau_2\right)\right]^{r}\Sigma^{+<}_{k\alpha'}\left(t_2,t\right)+\\ \Sigma^{r}_{k\alpha'}\left(t',t_1\right)\left[G\left(\tau_1,\tau_2\right)F\left(\tau_1,\tau_2\right)\right]^{<}\Sigma^{+<}_{k\alpha'}\left(t_2,t\right)+\\ \Sigma^{<}_{k\alpha'}\left(t',t_1\right)\left[G\left(\tau_1,\tau_2\right)F\left(\tau_1,\tau_2\right)\right]^{a}\Sigma^{+a}_{k\alpha'}\left(t_2,t\right)\end{pmatrix}. \tag{166}$$

The remaining terms in Eq.(163) are treated in the same way. We could study the finite frequency noise by taking the Fourier transform, then function $S\left(\omega\right)$ reads

$$S_{\alpha\alpha'}\left(\omega\right) = S_1^{\alpha\alpha'}\left(\omega\right)+S_2^{\alpha\alpha'}\left(\omega\right) \tag{167}$$
$$S_1^{\alpha\alpha'}\left(\omega\right) = 2(\frac{e}{\hbar})^2\int\frac{d\omega'}{2\pi}\left\{[GF]^{<}\left(\omega+\omega'\right)\cdot\Sigma^{>}_{k\alpha}\left(\omega'\right)+\Sigma^{<}_{k\alpha}\left(\omega'\right)\cdot[GF]^{>}\left(\omega+\omega'\right)+c.c.\right\} \tag{168}$$
$$\begin{aligned}S_2^{\alpha\alpha'}\left(\omega\right) = {} & 2(\frac{e}{\hbar})^2\int\frac{d\omega'}{2\pi}\left\{\left([GF]^{r}\left(\omega+\omega'\right)\Sigma^{>}_{k\alpha}\left(\omega+\omega'\right)+\right.\right.\\ & [GF]^{>}\left(\omega+\omega'\right)\Sigma^{a}_{k\alpha}\left(\omega+\omega'\right)\big)\times\\ & \left([GF]^{r}\left(\omega'\right)\Sigma^{<}_{k\alpha}\left(\omega'\right)+[GF]^{<}\left(\omega'\right)\Sigma^{a}_{k\alpha}\left(\omega'\right)\right)+\\ & [GF]^{>}\left(\omega+\omega'\right)\left[\Sigma^{r}_{k\alpha}\left(\omega'\right)G^{r}\left(\omega'\right)\Sigma^{<}_{k\alpha}\left(\omega'\right)\right.\\ & \Sigma^{r}_{k\alpha}\left(\omega'\right)[GF]^{<}\left(\omega'\right)\Sigma^{a}_{k\alpha}\left(\omega'\right)\\ & \left.\left.\Sigma^{<}_{k\alpha}\left(\omega'\right)[GF]^{a}\left(\omega'\right)\Sigma^{a}_{k\alpha}\left(\omega'\right)\right]+c.c.\right\}.\end{aligned} \tag{169}$$

where

$$[AB]^{\lessgtr}\left(\omega\right) = A^{\lessgtr}\left(\omega\right)B^{a}\left(\omega\right)+A^{r}\left(\omega\right)B^{\lessgtr}\left(\omega\right), \tag{170}$$
$$[AB]^{r,a}\left(\omega\right) = \int d\omega'\left\{\frac{A^{>}\left(\omega-\omega'\right)B^{>}\left(\omega'\right)}{\omega-\omega'+i\delta^{+}}-\frac{A^{<}\left(\omega-\omega'\right)B^{<}\left(\omega'\right)}{\omega-\omega'+i\delta^{+}}\right\}. \tag{171}$$

In this paper, we focus on the calculation of the zero-frequency noise $\omega\to 0$, thus the S_1

and S_2 are

$$S_1(\omega \to 0) = 2(\frac{e}{\hbar})^2 \int \frac{d\omega}{2\pi} [GF]^< (\omega) \Sigma^>_{k\alpha}(\omega) + \Sigma^<_{k\alpha}(\omega) [GF]^> (\omega), \quad (172)$$

$$S_2(\omega \to 0) = -2(\frac{e}{\hbar})^2 \int \frac{d\omega}{2\pi} \left[2 |[GF]^r(\omega)|^2 \Sigma^>_{k\alpha}(\omega) \Sigma^<_{k\alpha}(\omega) + J^2_\alpha(\omega)\right] \quad (173)$$

where

$$\begin{aligned} J_\alpha(\omega) &= \left[\widetilde{G}^r(\omega) - \widetilde{G}^a(\omega)\right] \Sigma^<_{k\alpha}(\omega) - \widetilde{G}^<(\omega) \left[\Sigma^>_{k\alpha}(\omega) - \Sigma^<_{k\alpha}(\omega)\right] \\ &= \widetilde{G}^>(\omega) \Sigma^<_{k\alpha}(\omega) - \widetilde{G}^<(\omega) \Sigma^>_{k\alpha}(\omega). \end{aligned}$$

APPENDIX F

STRONG ELECTRON-VIBRON COUPLING CALCULATION

Based on NEGF, the current formula is given by

$$J_\alpha = \frac{e}{\hbar}\int \frac{d\omega}{2\pi}\left[\widetilde{\Sigma}^{<}_{k\alpha}(\omega)\,G^{>}(\omega) - \widetilde{\Sigma}^{>}_{k\alpha}(\omega)\,G^{<}(\omega)\right]$$

Note that $\widetilde{\Sigma}_{k\alpha}(\omega) = \sum_{k\alpha}|V_{k\alpha}|^2\, g_{k\alpha}(\omega)$ is the Keldysh self-energy due to coupling to the leads and $\widetilde{\Sigma}^{\lessgtr}_{k\alpha}(\omega)$ are given by

$$\widetilde{\Sigma}^{\lessgtr}_{k\alpha}(\omega) = \pm i f^{\lessgtr}_{\alpha}(\omega)\,\Gamma^{\alpha}(\omega).$$

The Keldysh Green's function for the vibrating system is defined by

$$G(\tau,\tau') = -i\left\langle T_c d(\tau)\, X(\tau)\, d^{+}(\tau')\, X^{+}(\tau')\right\rangle$$

. Via the Langreth rule, lesser (greater) Green's function are found as

$$G^{\lessgtr}(\tau,\tau') = \widetilde{G}^{\lessgtr}(\tau,\tau')\,F^{\lessgtr}(\tau,\tau').$$

Here the electron lesser (greater) Green's function and the vibron lesser (greater) Green's function are respectively defined by

$$G^{\lessgtr}(\tau,\tau') = -i\left\langle T_c d(\tau)\, d^{+}(\tau')\right\rangle \tag{174}$$

$$F^{\lessgtr}(\tau,\tau') = \left\langle T_c X(\tau)\, X^{+}(\tau')\right\rangle \tag{175}$$

Since $X \equiv e^{\lambda\left(b-b^{+}\right)}$, via the Taylor expansion, $F^{\lessgtr}(\tau,\tau')$ can be retained up to the second order, and rewritten by

$$F^{\lessgtr}(\tau,\tau') = e^{\lambda^2\left[iD^{\lessgtr}(\tau,\tau') - \left\langle P^2\right\rangle\right]}$$

where $D(\tau,\tau') = -i\left\langle T_c P(\tau)\, P(\tau')\right\rangle$, and $P = -i\left(b-b^{+}\right)$. The reaming procedure is to determine $\widetilde{G}^{\lessgtr}(\tau,\tau')$ and $D^{\lessgtr}(\tau,\tau')$.

The Dyson equation for the electron Green's function and the vibron Green's function are found as

$$\widetilde{G}_d\left(\tau,\tau'\right) = \widetilde{g}_d\left(\tau,\tau'\right) + \int_c d\tau_1 \int_c d_2 \widetilde{g}_d\left(\tau,\tau_1\right) \Sigma_k\left(\tau_1,\tau_2\right) \widetilde{G}_d\left(\tau_2,\tau'\right), \tag{176}$$

$$\widetilde{D}\left(\tau,\tau'\right) = \widetilde{d}\left(\tau,\tau'\right) + \int_c d\tau_1 \int_c d_2 \widetilde{d}\left(\tau,\tau_1\right) \Pi\left(\tau_1,\tau_2\right) \widetilde{D}\left(\tau_2,\tau'\right), \tag{177}$$

where the functions $\Sigma_k\left(\tau_1,\tau_2\right)$ and $\Pi\left(\tau_1,\tau_2\right)$ are given by

$$\Sigma_k\left(\tau_1,\tau_2\right) = \widetilde{\Sigma}_{k\alpha}\left(\tau_1,\tau_2\right) F^{+}\left(\tau_1,\tau_2\right), \tag{178}$$

$$\begin{aligned}\Pi\left(\tau_1,\tau_2\right) = & -i\lambda^2 \Big\{ \widetilde{\Sigma}_{k\alpha}\left(\tau_1,\tau_2\right) \cdot \widetilde{G}^{+}\left(\tau_1,\tau_2\right) F^{+}\left(\tau_1,\tau_2\right) \\ & \widetilde{\Sigma}^{+}_{k\alpha}\left(\tau_1,\tau_2\right) \cdot \widetilde{G}\left(\tau_1,\tau_2\right) F\left(\tau_1,\tau_2\right) \Big\}\end{aligned} \tag{179}$$

The application of the Keldysh rule on Eq.(176) and Eq.(177) leads to

$$\begin{aligned}\widetilde{G}^{\lessgtr}_d\left(\omega\right) &= \left|\widetilde{G}^{r}_d\right|^2\left(\omega\right) \Sigma^{\lessgtr}_k\left(\omega\right) \\ &= \frac{\Sigma^{\lessgtr}_k\left(\omega\right)}{\left[\omega - \varepsilon_d - \mathrm{Re}\,\Sigma^{r}_k\left(\omega\right)\right]^2 + \left[\mathrm{Im}\,\Sigma^{r}_k\left(\omega\right)\right]^2},\end{aligned} \tag{180}$$

$$\begin{aligned}\widetilde{D}^{\lessgtr}\left(\omega\right) &= \left|\widetilde{D}^{r}\right|^2\left(\omega\right) \Pi^{\lessgtr}\left(\omega\right) \\ &= \frac{\Pi^{\lessgtr}\left(\omega\right)}{\left[\left(\omega^2 - \omega_0^2\right)/2\omega_0 - \mathrm{Re}\,\Pi^{r}\left(\omega\right)\right]^2 + \left[\mathrm{Im}\,\Pi^{r}\left(\omega\right)\right]^2}.\end{aligned} \tag{181}$$

The remaining task is to determine $\Sigma^{r,>,<}_k\left(\omega\right)$ and $\Pi^{r,>,<}\left(\omega\right)$.

From Eq.(178) and Eq.(179), we understand that

$$\Sigma^{r}_k\left(t,t'\right) = \theta\left(t-t'\right)\left[\Sigma^{>}_k\left(t,t'\right) - \Sigma^{<}_k\left(t,t'\right)\right], \tag{182}$$

which denotes the retarded self-energy of the interacting quantum dot and the function $\Pi^{r}\left(t,t'\right)$ represents for the retarded vibron Green's function

$$\Pi^{r}\left(t,t'\right) = \theta\left(t-t'\right)\left[\Pi^{>}\left(t,t'\right) - \Pi^{<}\left(t,t'\right)\right] \tag{183}$$

In energy space, Eq.(182) and Eq.(183) can be expressed as

$$\begin{aligned}
\Sigma_k^{\lessgtr}(\omega) &= \int d\omega' \widetilde{\Sigma}_k^{\lessgtr}(\omega-\omega') F^{+\lessgtr}(\omega') \\
&= \pm i \sum_\alpha \int d\omega' \Gamma_\alpha^{\lessgtr}(\omega-\omega') F^{+\lessgtr}(\omega') \qquad (184) \\
\Pi^{\lessgtr}(\omega) &= -i\lambda^2 \int d\omega' \int d\omega'' \Big\{ \widetilde{\Sigma}_k^{\lessgtr}(\omega-\omega') \cdot \widetilde{G}_d^{+\lessgtr}(\omega'-\omega'') F^{+\lessgtr}(\omega'') \\
&\quad + \widetilde{\Sigma}_k^{+\lessgtr}(\omega-\omega') \cdot \widetilde{G}_d^{\lessgtr}(\omega'-\omega'') F^{\lessgtr}(\omega'') \Big\}, \qquad (185)
\end{aligned}$$

and the retarded self-energies appearing in Eq.(180) are

$$\begin{aligned}
\Sigma_k^r(\omega) &= \sum_\alpha \int d\omega' \left[\frac{V_{k\alpha}^* V_{k\alpha} f_\alpha^<(\varepsilon_{k\alpha}) F^{+<}(\omega')}{\omega-\omega'-\varepsilon_{k\alpha}+i\delta} \right. \\
&\quad \left. + \frac{V_{k\alpha}^* V_{k\alpha} f_\alpha^>(\varepsilon_{k\alpha}) F^{+>}(\omega')}{\omega-\omega'-\varepsilon_{k\alpha}+i\delta} \right], \qquad (186) \\
\Pi^r(\omega) &= -i\lambda^2 \int d\omega' \int d\omega'' \left\{ \frac{V_{k\alpha}^* V_{k\alpha} f_\alpha^<(\varepsilon_{k\alpha}) \cdot \widetilde{G}_d^{+<}(\omega'-\omega'') F^{+<}(\omega'')}{\omega-\omega'-\varepsilon_{k\alpha}+i\delta} \right. \qquad (187) \\
&\quad + \frac{V_{k\alpha}^* V_{k\alpha} f_\alpha^{+<}(\varepsilon_{k\alpha}) \cdot \widetilde{G}_d^<(\omega'-\omega'') F^<(\omega'')}{\omega-\omega'-\varepsilon_{k\alpha}+i\delta} \\
&\quad - \frac{V_{k\alpha}^* V_{k\alpha} f_\alpha^>(\varepsilon_{k\alpha}) \cdot \widetilde{G}_d^{+>}(\omega'-\omega'') F^{+>}(\omega'')}{\omega-\omega'-\varepsilon_{k\alpha}+i\delta} \\
&\quad \left. - \frac{V_{k\alpha}^* V_{k\alpha} f_\alpha^{+>}(\varepsilon_{k\alpha}) \cdot \widetilde{G}_d^>(\omega'-\omega'') F^>(\omega'')}{\omega-\omega'-\varepsilon_{k\alpha}+i\delta} \right\}.
\end{aligned}$$

This is a self-consistent procedure to solve strong electron-vibron coupling molecule. We can see that the vibron Green's function is strongly affected by the bias-dependent electron Green's function, such that the boson modes are nonuniformly broadening.